Nanoscale

REVIEW

View Article Online
View Journal | View Issue

Cite this: *Nanoscale*, 2022, **14**, 14858

Applications, fluid mechanics, and colloidal science of carbon-nanotube-based 3D printable inks

Beihan Zhao,[a] Vishal Sankar Sivasankar,[a] Swarup Kumar Subudhi,[a] Shayandev Sinha,[b] Abhijit Dasgupta[a] and Siddhartha Das *[a]

Additive manufacturing, also known as 3D printing (3DP), is a novel and developing technology, which has a wide range of industrial and scientific applications. This technology has continuously progressed over the past several decades, with improvement in productivity, resolution of the printed features, achievement of more and more complex shapes and topographies, scalability of the printed components and devices, and discovery of new printing materials with multi-functional capabilities. Among these newly developed printing materials, carbon-nanotubes (CNT) based inks, with their remarkable mechanical, electrical, and thermal properties, have emerged as an extremely attractive option. Various formulae of CNT-based ink have been developed, including CNT-nano-particle inks, CNT–polymer inks, and CNT-based non-nanocomposite inks (*i.e.*, CNT ink that is not in a form where CNT particles are suspended in a polymer matrix). Various types of sensors as well as soft and smart electronic devices with a multitude of applications have been fabricated with CNT-based inks by employing different 3DP methods including syringe printing (SP), aerosol-jet printing (AJP), fused deposition modeling (FDM), and stereolithography (SLA). Despite such progress, there is inadequate literature on the various fluid mechanics and colloidal science aspects associated with the printability and property-tunability of nanoparticulate inks, specifically CNT-based inks. This review article, therefore, will focus on the formulation, dispersion, and the associated fluid mechanics and the colloidal science of 3D printable CNT-based inks. This article will first focus on the different examples where 3DP has been employed for printing CNT-based inks for a multitude of applications. Following that, we shall highlight the various key fluid mechanics and colloidal science issues that are central and vital to printing with such inks. Finally, the article will point out the open existing challenges and scope of future work on this topic.

Received 28th July 2021,
Accepted 16th September 2022

DOI: 10.1039/d1nr04912g

rsc.li/nanoscale

A. Introduction

Additive manufacturing (AM), or 3D-printing (3DP), as it is popularly known, is a manufacturing process that builds an object in a "bottom-up" layer-by-layer fashion as opposed to a subtractive process where the final complex net form of a product is achieved by removal of material from a larger raw precursor of simpler shape. Numerous 3DP technologies have been developed, including fused deposition modeling (FDM), direct ink writing (DIW), stereolithography (SLA), selective laser sintering (SLS), two-photon polymerization (TPP), electrohydrodynamic (EHD) 3D printing, and many more. The various corresponding raw materials that are compatible with different 3D printing technologies have been widely investigated, including polymers and resins (mostly for FDM, and UV-3DP), metals powders (usually with SLS), ceramics (usually fabricated with DIW method), carbon-based materials (compatible with FDM, IJP, AJP, SP, *etc.*), and many others.[1–22] Among these materials, 3D-printable carbon inks, which consist of volatile solutions with carbon-based materials in different forms as fillers, have emerged extremely popular due to their multi-functional capabilities as well as outstanding chemical stability and electrical and mechanical properties. Commercial 3D-printable carbon inks that utilize graphene-based materials,[14,18] carbon-fiber,[12,16,17] and carbon-nanotube based materials[11,23–25] have been widely used for a multitude of 3DP applications, such as robotics,[10] fabrication of soft and wearable electronics[11,22] and energy-related devices (such as batteries, heaters, and those with lighting applications),[13,19] surgical and biomedical applications,[2,3,8] and many more.

One such example of carbon-based inks is the ink based on dispersed carbon nanotubes (CNTs). Components and devices printed with such CNT-based inks showcase outstanding elec-

[a]*Department of Mechanical Engineering, University of Maryland, College Park, MD 20742, USA. E-mail: sidd@umd.edu*
[b]*Defect Metrology Group, Logic Technology Development, Intel Corporation, Hillsboro, OR 97124, USA*

trical and mechanical performances. This has made CNT-based inks one of the most promising inks with wide range of potential applications. 3D printable CNT-based inks have been extensively used in fabrication of multi-purpose sensors (including helical liquid sensor, strain sensors, vapor or gas sensors, temperature sensors, *etc.*).[26–30] For example, Xiang *et al.* used FDM (fused deposition modeling) to 3D print strain sensors with CNT-AgNP (AgNP: silver nanoparticle) ink,[26] Alshammari *et al.* developed a gas sensor by inkjet printing polymer-MWCNT inks (MWCNT: multi-walled CNT),[27] Liu *et al.* fabricated hydrogen sensors using platinum (Pt) decorated SWCNTs (SWCNT: single-walled CNT) by employing aerosol-jet printing,[28] Qin *et al.* inkjet-printed pH sensors for electrochemical monitoring using functionalized SWCNTs,[29] and Zhao *et al.* printed temperature sensors using CNT–GO ink (GO: graphene oxide) that operated by leveraging the negative temperature coefficient of resistance of the CNTs.[30] CNT-based inks have also been employed to fabricate conductive patterns, capacitors, transistors, RF devices, circuit patterns, and parts of wearable electronics.[31–43] Furthermore, researchers have investigated the application of CNT-based ink in fabricating energy-related devices including heaters, batteries, and lighting devices[13] as well as several biomedical devices (*e.g.*, devices involving the handling of the human neuroblastoma cells[44] and antioxidant assays in blood bags[45]).

Optimizations of the functionalities and thermofluidic properties of the CNT-based inks, which in turn dictate the performances of the components printed with these inks, necessitate a thorough understanding of the fluid mechanics and the colloidal science aspects of CNT based inks. Printability, homogeneity of the printed traces, and functionalities of the components printed with the CNT-based inks can be significantly improved by understanding and tailoring the viscous and viscoelastic behaviors of the ink, nature and mechanism of colloidal deposition and the resulting pattern formation (*e.g.*, formation or prevention of 'coffee-stain'), and curing. Many researchers have studied the rheological behavior (*e.g.*, shear-thinning effect) or pattern formation behavior (*e.g.* 'coffee-stain' formation) of CNT-based suspensions and inks.[46–57] Despite that, there are only a handful of studies that have comprehensively reviewed both the current research status of CNT-based inks (in terms of their applications) and the associated issues of thermofluidics and colloid science.

In this review article, we fill this void and discuss different CNT-based inks, their applications, the related governing thermofluidics and colloidal science issues dictating their printing, and the possible directions for future research studies. Our goal is to provide a clear picture of the link between the nanoscale properties of CNT-based inks and the performance indicators that determine the quality of the print achieved using the CNT-based inks [examples of these performance indicators include: printability/jettability, wettability (surface tension), deposition pattern (coffee stain), *etc.*]. In order to achieve that, we have: (1) identified the material characteristics that influence the performance indicators (*i.e.*, the material characteristics that make the ink suitable for 3D printing), (2) identified the nanoscale properties (such as the nanoparticle size, nanoparticle shape/aspect ratio, solvent interactions, surface functionalization, *etc.*) which affect various characteristics of the ink (such as rheology, surface tension, dispersibility/stability, and coffee stain effect), and (3) provided a link between each of the nanoscale properties and the ink material rheological properties. First, in section B, we discuss two types of CNT-based inks, those that contain a polymer matrix carrier (termed CNT-nanocomposite here) and those that do not (termed CNT non-nanocomposite here), their compositions, the additive manufacturing methods employed to print with these inks, and their applications. Following that, detailed aspects of the fluid mechanics and colloidal science related properties and effects of the CNT based inks are discussed in section C. Finally, recent advances and current challenges in CNT-based ink manufacturing and printing processes, like CNT material dispersion in solvents, product defects control, and surface tension and viscosity controls while printing are discussed in section D.

Table 1 provides a list of acronyms (along with their meaning) that are used in this paper.

B. 3D-printing with CNT-based inks

Extensive research has been focused on formulations of 3D printable CNT-based nanocomposites, and several review papers on generic nanoparticulate inks as well as CNT-based inks have provided an overview of the CNT-based materials, their applications, properties, manufacturing methods, and suitability for additive manufacturing and printing environments.[22–25] Fig. 1 summarizes some of the most important applications/devices where CNT-based inks have been used. Nayak *et al.*, for example, reviewed different CNT-based inks as well as other types of nanoparticulate inks for printing electronic devices (*e.g.*, integrated circuits, transistors, sensors, capacitors) using inkjet printing. Additionally, they studied the physical properties of the inkjet-generated droplets and the interactions of these droplets with the substrate that eventually controlled the printing process.[22] In another review article, Miyashiro *et al.* focused on the cellulose/nanocellulose – CNT mixed materials and discussed their possible applications in printing sensors, batteries, capacitors, and electromagnetic shielding devices.[23] Ghoshal *et al.* extensively reviewed the additive manufacturing of polymer/CNT based nanocomposite inks: they summarized the use of different kinds of polymers, the existing printing methods for the CNT-based nanocomposites, the limit of 3DP CNT–polymer matrix inks, and their different applications.[24] Eshkalak *et al.* in their review article focused specifically on the inkjet-printing method and the different kinds of CNT-based inks that can be additively manufactured using this method.[25] Wang *et al.* reviewed general material and method options for additively manufacturing polymer matrix, in which CNT–polymer matrix was also included.[5] Agarwala *et al.* evaluated the 3D printing of CNT/polymer matrix and emphasized the electrical performances of

Table 1 A list of different acronyms (and their meanings) used in this paper

Acronyms	Meanings
3DP	3D-printing
ABS	Acrylonitrile butadiene styrene
AgNP	Silver nanoparticle
AJP	Aerosol-jet printing
AM	Additive manufacturing
BSA	Bovine serum albumin
CAD	Computer-aided design
CCD	Charged coupled device
CHP	Cyclohexyl-pyrrolidone
CNF	Cellulose nano fibers
CNT/MWCNT/ SWCNT	Carbon-nanotubes/multi-walled carbon-nanotubes/single-walled carbon-nanotubes
CTAB	Cetrimonium bromide
CV	Crystal violate
DCE	1,2-Dichloroethane
DCM	Dichloromethane
DI	Deionized
DLP	Direct light processing
DLVO	Derjaguin–Landau–Verwey–Overbeek
DMF	Dimethylformamide
DNA	Deoxyribonucleic acid
DOD	Drop-on-demand
DSC	Differential scanning calorimetry
DTAB	Dodecyltrimethylammonium bromide
DW/DIW	Direct writing/direct ink writing
EG	Ethylene glycol
EHD	Electrohydrodynamic
FDM	Fused deposition modeling
FET	Field-effect transistors
FTIR	Fourier-transform infrared spectroscopy
GA	Gum Arabic
GelMA	Gelatin methacryloyl
GO/GNP	Graphene oxide/graphene nanoplatelets
HA	Hyaluronic acid
IC	Indigo carmine
IJP	Inkjet printing
IPA	Isopropyl alcohol
LDM	Liquid deposition modeling
LDS	Lithium dodecyl sulfate
LFP	Lithium iron phosphate ($LiFePo_4$)
LIRF	Local-induced radio frequency
LTO	Lithium–titanium ($Li_4Ti_5O_{12}$)
NMP	*N*-Methyl-2-pyrrolidone
NP	Nanoparticle
NP-10	Nonylphenol ethoxylate surfactant
Oh	Ohnesorge number
PA	Polyacrylamide
PABS	Polyaminobenzene sulfonic acid
PBT	Polybutylene terephthalate
PCA	Phosphino-carboxylic acid
PEDOT:PSS	Poly(3,4-ethylenedioxythiophene) polystyrene sulfonate
PEG	Poly(ethylene glycol)
PEGDA/ PEGMEMA	Poly(ethylene glycol) diacrylate/poly(ethylene glycol) methyl ether methacrylate
PFOA	Perfluorooctanoic acid
PLA	Polylactic acid, or polylactide
PMAS	Poly(2-methoxyaniline-5-sulfonic acid)
PES	Powder/polyether sulfone
PVP	Polyvinylpyrrolidone
RAM	Radar absorbing materials
Re	Reynolds number
RF	Radio frequency
rGO	Reduced graphene oxide
SC	Sodium cholate
SDBS/NaDDBS	Sodium dodecylbenzene sulfonate
SDS	Sodium dodecyl sulfate
SDSA	Sodium dodecane sulphonic acid
SF	Silk fibroin
SLA	Stereolithography
SLS	Selective laser sintering
SP	Syringe printing
TCF	Transparent conductive film
TFT	Thin-film transistors
TGA	Thermogravimetric analysis
TPCL	Three-phase contact line
TPP	Two-photon polymerization
TPU	Thermoplastic polyurethane
TTAB	Tetradecyltrimethylammonium bromide
UV-3DP	Ultraviolet 3D printing
vdW	Van-der Waals
VOC	Volatile organic compounds
WAXS	Wide-angle X-Ray scattering
XHC	Xylan hydrate crystal
We	Weber number

CNT/polymer matrix.[58] Moreover, Goh *et al.* conducted an in-depth review on the mechanism, methods, and challenges for achieving on-demand CNT alignment during 3D printing. They also introduced the applications with aligned CNT network and explained how the alignment can eventually enhance the performances of the final printed product.[11]

These CNT-based inks are often characterized by low viscosities and reversible shear-thinning properties, making them compatible with multiple 3D printing methods. The additive manufacturing techniques that have been employed to print such CNT-based inks include direct ink writing [DIW, which normally includes inkjet printing (IJP), aerosol jet printing (AJP), and syringe printing (SP)],[27,28,30,33–41,43–45,59–64] stereolithography (SLA),[65] fused deposition modeling (FDM),[26,66–68] digital light processing (DLP),[69] liquid deposition modeling (LDM),[47] and many other non-traditional methods.

From previous research, we can classify the CNT-based inks into two broad categories: (i) CNT-based nanocomposites (NC) ink, and (ii). CNT-based non-nanocomposite inks. For the first category, the ink, which is a combination of CNT and polymers or resins, such as CNT-PLA (PLA: polylactic acid), CNT–resin, and CNT-PVP (PVP: polyvinylpyrrolidone), is employed to fabricate nanocomposite structures. Such inks are characterized as a multiphase material with one phase (solid phase) being of micro- or nano-scale dimensions.[27,34,47,60,61,65–70] Fig. 2 provides several example structures printed with CNT-based NC inks, showing the resolution they can achieve.

Meanwhile, the CNT-based non-nanocomposite ink does not manifest such multiphasic characteristics. In this case, the ink consists of functionalized CNTs or CNTs in combination with other carbon materials in a solvent with appropriate dispersion agents. For such inks, a detailed understanding of the solvent properties, mechanism of the dispersants, and methods to ensure the printability and optimization of the functionality of ink become important. Accordingly, research endeavors have focused on the self-assembly mechanisms, CNT-weight-fraction dictate the hydrodynamic properties of this ink, and the effects of substrates, printing conditions, and ink concentrations.[32,59] Examples of such non-nanocomposite

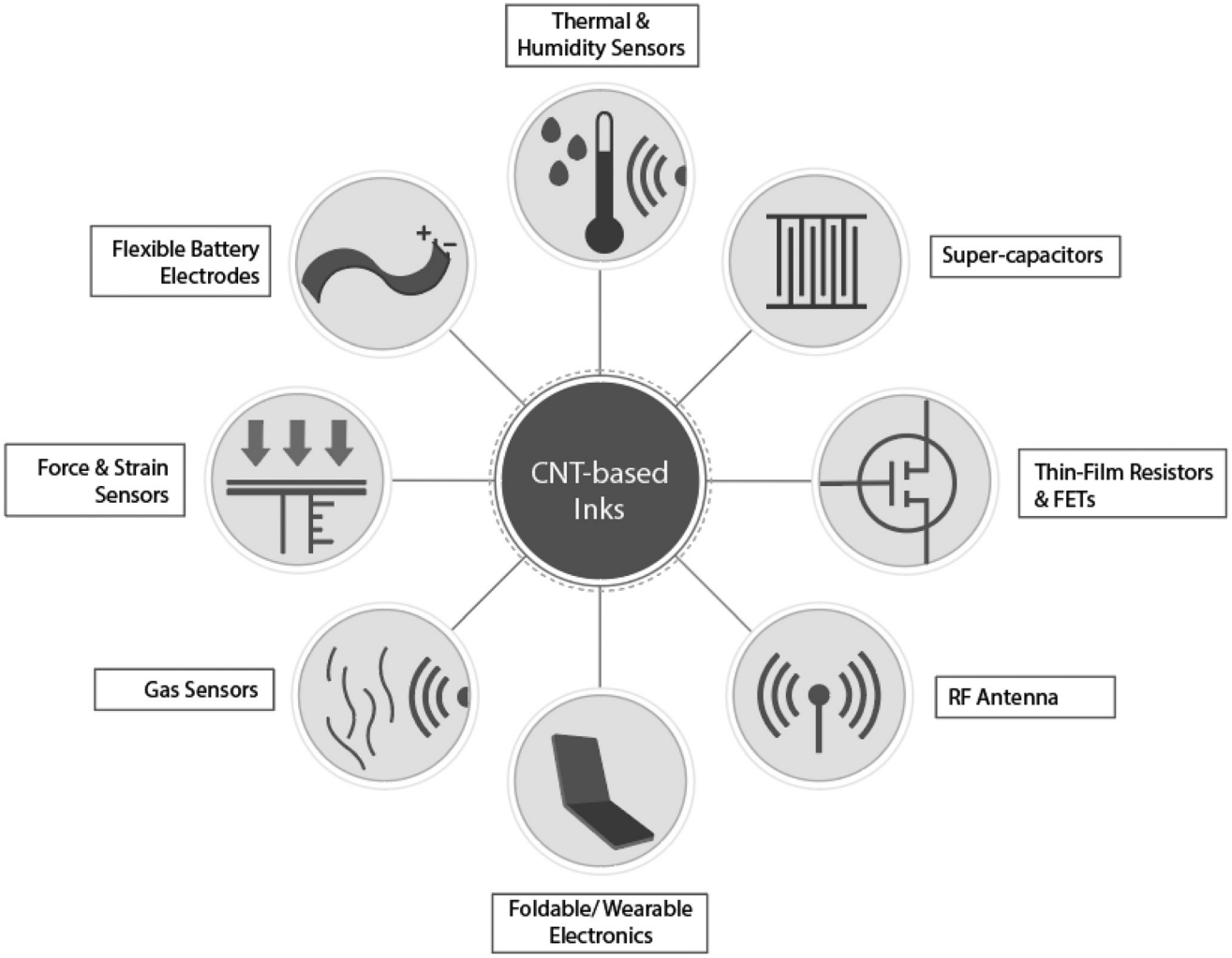

Fig. 1 Schematic summarizing the important applications/devices where CNT-based inks are used.

CNT inks mainly include combinations of CNT and other carbon based materials, such as CNT/graphene oxide (GO) or reduced graphene oxide (rGO) inks,[30,38] or CNTs and (functionalized) CNTs simply mixed with solvents and some surfactants,[29,32,33,35,36,39–41,45,48,59,62] or CNTs decorated with metal nanoparticles (like silver nanoparticles[37,63] and platinum[28]), or combination of CNT and nano-fibers.[44]

Given the extensive number of existing review articles discussing the 3D printing of CNT-based and related materials, in the remainder of this section, we shall simply summarize through Tables 2 and 3 the materials, the printing techniques, and the targeted applications for 3D printing of CNT-based nanocomposite and non-nanocomposite inks.

C. Fluid mechanics and colloidal science of CNT inks

While there are several review articles on 3D printing of CNT inks,[24,76,77] most of them have primarily focused on the aspects of materials or printing techniques with much less attention on the fluid mechanics and the related colloidal science issues dictating the 3D printing of CNT inks. Like any other micro-nanoparticulate ink, the fluid properties and the colloidal science aspects of the CNT ink significantly influence its printability, the quality of the printed structures, printing-speed limit, effectiveness in achieving desired shape and geometries, and the functionalities (*e.g.*, electrical conductivity, sensitivity, and mechanical strength) of the printed components.[22,46,78] This is the most important section of this review article. This section will first discuss the colloidal science and fluid mechanics issues that dictate the printability of a generic nanoparticle-based ink. With that background, we shall subsequently discuss in separate subsections the shear thinning behavior, the surface tension and wetting properties, the sintering behavior, the colloidal stability, and the colloidal properties (and the associated coffee-ring formation) of the CNT-laden inks. Understanding these properties of the CNT-laden inks is critical in dictating the printability of the ink as well as the properties of the printed components.

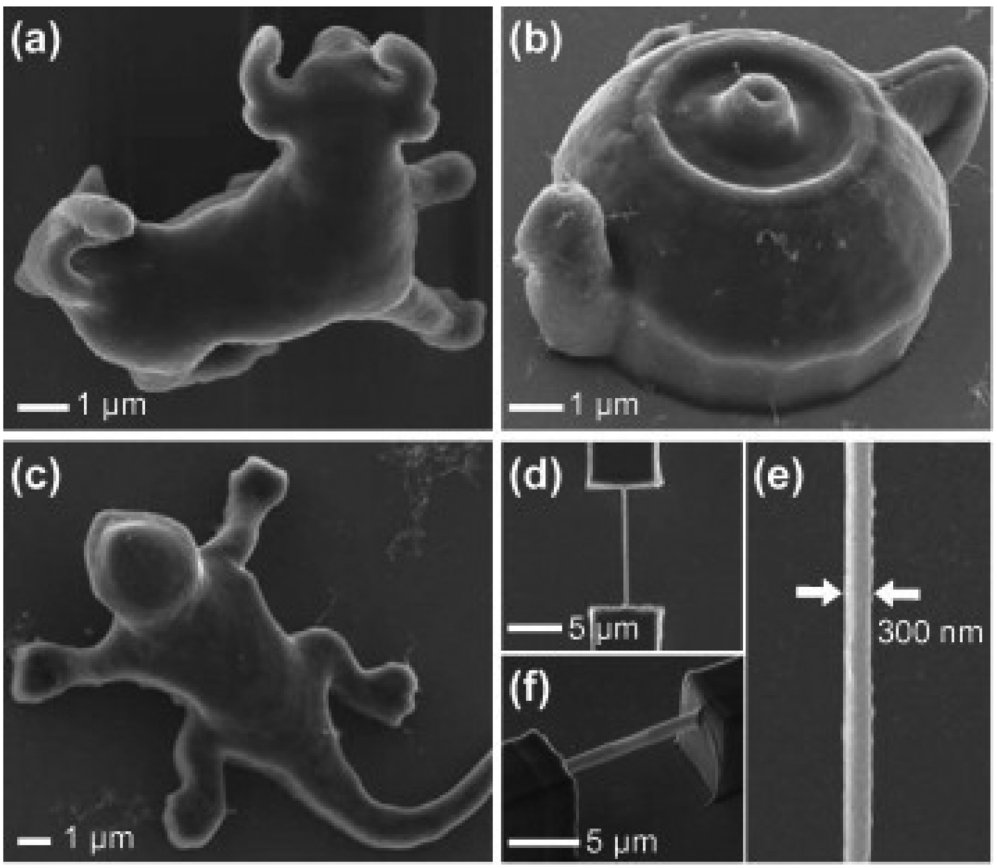

Fig. 2 Examples of structures printed with CNT-nanocomposite inks. (a–f) High-resolution micro-/nano-structures printed using SWCNT/polymer composites through TPP method. All parts of this figure have been reproduced from ref. 70 with permission from Elsevier, copyright 2013.

In the following subsection, we provide a general discussion on how the macroscale ink properties affect the printability and jettability of nanoparticle-based ink, and how these macroscale properties get regulated by the nanoscale properties of the ink properties. In Fig. 3, we provide a schematic representation of all the factors that affect the macroscopic properties of the nanoparticle-based ink.

C.1. Colloidal science and fluid mechanics of generic printable liquids

C.1.1. Printability and jettability for generalized printable inks. Several studies have probed the methods for quantifying the viscosity[79] and printability[80] of various liquids used as inks in inkjet printing. For Newtonian liquids, Ohnesorge number ($\mathrm{Oh} = \frac{\mu}{\sqrt{\rho\sigma L}}$, where μ, ρ, and σ are the dynamic viscosity, density, and surface tension of the liquid, and L is the characteristic length scale) could serve as an indicator of the jettability of the liquids.[80] Several studies have linked the fluid properties of the ink to the droplet formation through the Ohnesorge number (Oh) and have predicted or analyzed the appropriate Z values (Z = 1/Oh quantifies the ink printability) for printing applications corresponding to different types of solvents as well as the sizes and materials of the particulate matter for the case the particle-laden inks.[81–83] $1 < Z < 10$ is the range of Z values for which a liquid is often considered printable (therefore, here the Z value is serving as an indicator of the merit or performance of the ink in terms of its printability); this range in Z values was obtained by correlating the findings of several experimental studies on different suspension systems.[21,83] In a research study by Jang *et al.*, fluids with different Z values (*i.e.*, the inverse of the Ohnesorge numbers) were compared and the drop formation driven by a pulse generating system was captured under a charge-coupled-device (CCD) camera.[84] In the range of Z values between 2 and 17, it was found that the case with the largest Z value led to the formation of a tail of separated droplets, while for the cases of other Z values, the transient satellite drops successfully merged with the primary droplets after a certain elapsed time and formed a continuous filament.[84] This is yet another example where the Z value is serving as a merit or performance indicator, highlighting its effect on the drop generation performance. A detailed comparison of the length of this continuous filament between the cases with different Z values, the time scale associated with the trajectory of the filament tail, the merging and the formation of a single droplet, the generation of the satellite drops, *etc.* have been shown in Fig. 4. In this study, the authors concluded that the printable ink for a

Table 2 Examples of CNT-based nanocomposites (NC) 3D printable inks used in various applications

Ref.	Ink materials	Application and additional features	Printing technique
26	CNT–polymer-AgNPs	Strain sensor	Fused deposition modeling
27	(PEDOT:PSS) wrapped CNT	Gas sensor	Inkjet printing
31	PLA-MWCNT	Helical liquid sensor	Solvent-cast 3D printing
34	Polyacrylamide (PA)-CNT	Amperometric sensors	Inkjet-printing
43	Polymer wrapped SWCNT	Field-effect transistors	Inkjet-printing
47	PLA-MWCNTs	Conductive structures	Liquid deposition modeling
60	Polyvinylpyrrolidone (PVP)-wrapped MWNT	Conductive structures	Meniscus-guided printing
61	(Functionalized) SWCNT-PMAS	Transparent and conductive gas sensor	Inkjet printing
65	CNT-photopolymer	Structures with radar absorbing features	Sterolithography (SLA)
66	CNT-PBT	Conductive structures	Fused deposition modeling
67	CNT-PLA	Conductive structures	(i). Fused deposition modeling for 3D printing; (ii). Local-induced RF (LIRF) for welding to enhance strength
68	PLA/MWCNT/GNP	Conductive structures	Fused deposition modeling
69	PEDGA/PEGMEMA-MWCNTs	Conductive structures	Digital light processing
70	SWCNT-dispersed photo resin/SWCMT-polymer composites	High resolution conductive structures	Two-photon polymerization (TPP) lithography
71	CNT-TPU	Elastic strain sensors	Fused deposition modeling
72	CNT-TPU	Multiaxial force and strain sensors	Fused deposition modeling
73	MWNT-PVP composites	Strain sensors	Meniscus-guided printing

Table 3 Examples of CNT-based non-nanocomposite (nNC) 3D printable inks used in various applications

Ref.	Ink materials	Application and additional features	Printing technique
28	Platinum (Pt) decorated SWCNTs	Hydrogen sensors	Aerosol jet printing
29	Functionalized SWCNT inks	pH sensor	Inkjet-printing
30	GO–CNT	Temperature sensors	Syringe printing
32	MWCNTs in an aqueous suspension	Electrode patterns	Inkjet printing
33	MWCNT	RF devices	Inkjet printing
35	Functionalized SWCNTs	Field-effect transistors	Inkjet printing
36	Purified SWCNTs using DMF as solvent	Thin-film transistors	Inkjet printing
37	CNT + AgNP (solvent: sodium dodecylbenzene sulfonate (SDBS) solution)	Supercapacitors	Direct ink writing
38	CNT/rGO	Wearable thermoresponsive supercapacitors	Direct ink writing
39	SWCMT-DMF	Thin-film transistors	Inkjet printing
40	MWCNT	Conductive patterns	Inkjet printing
41	Functionalized MWCNT aqueous solution	Conductive patterns	Inkjet printing
45	Functionalized CNT	Amperometric sensors	Inkjet-printing
58	CNT, dispersion agent (TNADIS), isopropyl (IPA), and ethylene glycol (EG)	Micro-capacitors	Syringe printing
62	AgNP-CNTs	Conductive patterns	Aerosol-jet printing (AJP)
74	SWCNT inks	Transparent conductive films	Inkjet printing
75	CNT-DMF inks	Micro-supercapacitors	Syringe printing (a self-built extrusion system)

drop-on-demand (DOD) inkjet printing system should have a Z value between 4 and 14.[84] Again, this is an example where the Z value is acting as a performance indicator: it helps to identify the conditions where the DOD inkjet printing system is most effective as a printer.

It has also been reported that the shear-thinning liquids are suitable for inkjet printing as they successfully suppress the formation of satellite drops.[85] In the review article by Guo *et al.*, the liquid properties and printing performances were linked.[80] Guo *et al.* also discussed the significance of the factors such as the shear thinning properties and viscoelasticity in regulating the printability of non-Newtonian liquid inks. Meanwhile, several studies investigated the flow behavior by correlating the process-related shear stress to the shear rate.[86,87]

Other than the fluid properties, the process parameters such as drop ejection velocity (which determines the Weber number, or the ratio of inertial force to surface tension force, expressed as $\mathrm{We} = \frac{\rho v^2 r}{\sigma}$, where ρ is the density of the fluid, v is the fluid velocity, r is the drop radius, and σ is the liquid surface tension) also affect the printability of the ink. Duineveld *et al*. found that the minimum Weber number for a droplet to overcome the surface tension and to be ejected out of the nozzle was 4.[88] On the other hand, the maximum Weber number that can prevent splashing can be expressed in the

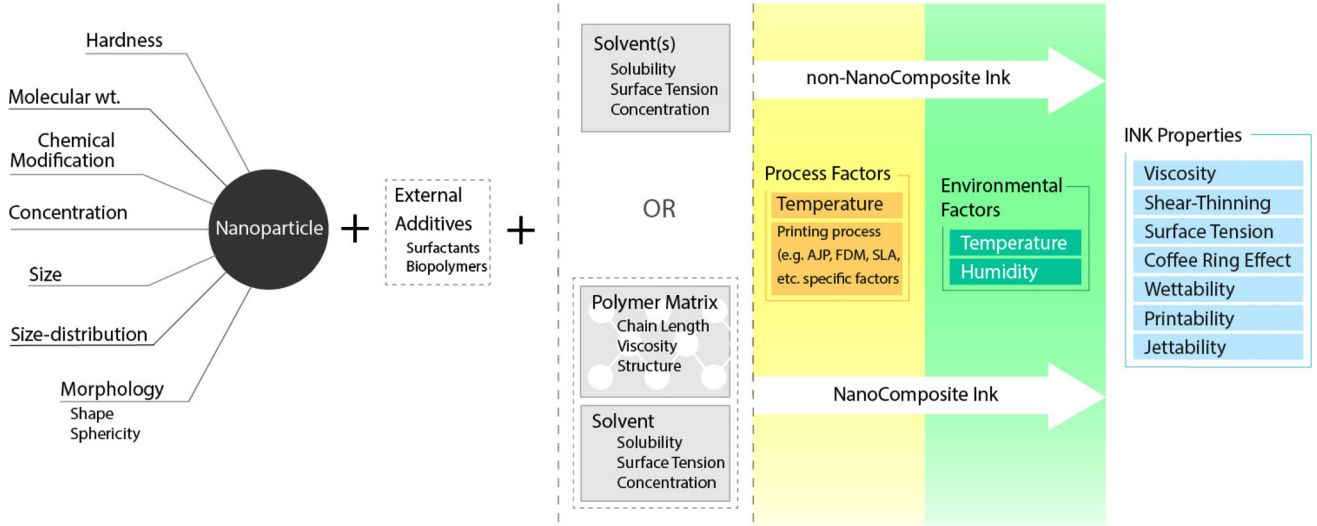

Fig. 3 Schematic representation of the properties of the materials used as well as the process and environmental factors that affect the resultant ink properties.

form of $We^{\frac{1}{2}}Re^{\frac{1}{4}} = K(r)$, as pointed out by Stow and Hadfield.[89] In a review paper by Abdolmaleki, the different conditions that led to non-printable situations were discussed: these conditions included splashing, excessively large viscosity, and the formation of satellite drops. Based on these, the printable region and the boundaries between the printable and the non-printable regions were highlighted (also shown in the schematic below in Fig. 5).[90] Therefore, these Weber number and Reynolds number values also serve as another set of performance indicators as they determine the phase space that demarcate between printable and non-printable conditions.

In other droplet-based printing processes like aerosol jet printing (AJP) process, the droplets are created using the process of atomization prior to ejection through nozzle. The droplet formation through atomization significantly affects the printing process. Commonly used atomization techniques are ultrasonic and pneumatic atomization.[91,92] Both the atomization processes depend on the ink properties such as viscosity, surface tension, as well as the external conditions such as gas flow rate (pneumatic atomization), and vibration frequency (ultrasonic atomization).

In ultrasonic atomization, high frequency vibration is used to break a thin film of liquid to form fine droplets.[93] Various ink properties such as the ink viscosity, surface tension, and process parameters like vibration frequency, and input flow rate (in the atomization chamber) affect the ultrasonic atomization process.

Firstly, the effect of ink viscosity on droplet formation can be explained by the capillary wave hypothesis based on Rayleigh–Taylor instability. Avvaru *et al.* reported a decrease in the droplet size with an increase in viscosity. They reported that the capillary wave formation got retarded by the increase in viscosity, which ensured that the growth rate of the surface disturbance decreased.[93] Such a decrease led to the availability of a lower volume of atomizing liquid at the peaks and crests of the capillary wave at the time of shearing, resulting in a smaller droplet size.[93–95]

The effect of surface tension on droplet formation was reported in a study by Dalmoro *et al.*[96] They explained that a decrease in surface tension increased the number of capillary waves per unit area, which resulted in an increase in the number of droplets produced. At the same time, an increase in the number of droplets for liquid films at the same flow rate decreased the size of droplets. Similarly, an increase in the vibration frequency also increased the number of capillary waves leading to a decrease in the droplet size.

Avvaru *et al.* also studied the effect of the input flow rate of the ink (in the atomization chamber) and reported an increase in droplet size with an increase in flow rate above a critical value of flow rate (Q_{crit}). They hypothesized that with the increase in the film thickness (in the vibrating atomization chamber) due to an increase in the flow rate, it is easier for the droplets to detach from the surface as other forces like gravitational forces become significant compared to surface tension forces.[93] Many researchers proposed an empirical relation for droplet size based on modified non-dimensional parameters such as Ohnesorge number, Weber number and intensity number.[93,97,98] These non-dimensional parameters were modified to account for the frequency and the amplitude of ultrasonic vibrations.

In pneumatic atomization, the atomization process involves shearing of the ink by using a high-velocity carrier gas.[91,99] Pneumatic atomizer is commonly used due to its capability of accommodating liquids of wide range of viscosities (1–1000 cp).[91] There are not many studies that investigate the effect of ink properties such as viscosity, surface tension, *etc.* on the pneumatic atomization process within the AJP setup. However, a few papers have studied the pneumatic atomization process (independent of the AJP) separately.[100,101] Kumar *et al.*, for example, provided an extensive review of pneumatic

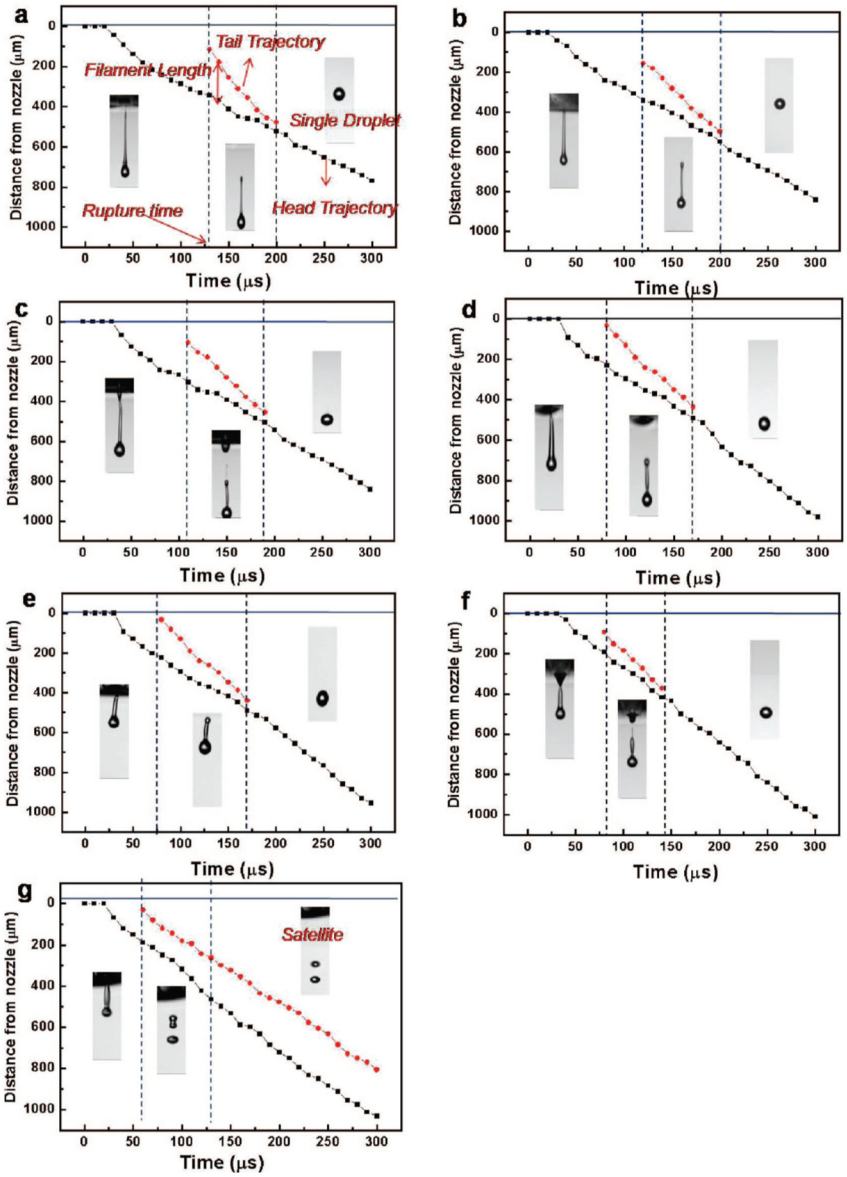

Fig. 4 Influence of Z value (related to viscous force, inertial force, and surface tension) on drop formation and trajectories of the ejected droplets for (a) Z = 2.17; (b) Z = 3.57; (c) Z = 4.08; (d) Z = 6.57; (e) Z = 7.32; (f) Z = 13.68; (g). Z = 17.32. All the parts of this figure have been reproduced from ref. 84 with permission from American Chemical Society, copyright 2009.

atomization, especially the effects of ink properties on the drop size distribution.[100] In their experimental investigation using glycine-water and glycine-alcohol solutions, they reported an increase in the droplet size with viscosity owing to the increase in the viscous force, which in turn increased the resistance to detachment. They also reported an increase in the drop size with an increase in the surface tension. They attributed this increase to the jet size at the point of drop formation. It was reported that the drop size decreased with a decrease in flow rate, as the decrease in flow rate decreased the total force driving the detachment of the drop.

In electrohydrodynamic (EHD) jet printing, the parameter that affects the jettability has been widely researched because of the capability of EHD to print objects with very high resolution (up to the order of tens of nanometers).[102–104] EHD printing uses electrostatic force to create droplets. With the application of electric field, conducting liquids forms a cone-shaped interface (from its usual spherical interface) called Taylor-cone due to the rearrangement of charges in the liquid. At a sufficiently large electric field, electrostatic stresses overcome the surface tension to form droplets.[102,105] The droplet formation and the fluid motion inside the Taylor cone depends on various ink properties such as surface tension, dielectric constant, ink viscosity, electrical conductivity, *etc.*[103,106] Mu *et al.* investigated the effect of dielectric constant on the printability of various inks.[107] They observed that the inks whose dielectric constant was below 7 were not printable using the EHD jet printing even when a DC voltage as high as

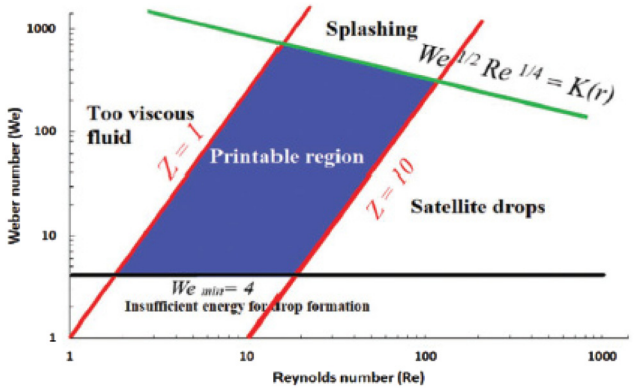

Fig. 5 Identification of the inkjet printable region and demarcation of the printable and non-printable regions as functions of the corresponding Weber number and Reynolds number values. This figure has been reproduced from ref. 90 with permission from John Wiley and Sons, copyright 2021.

1000 V was used. This dielectric constant value, therefore, serves as a merit indicator determining the condition of printing using EHD jet printing. They also observed that the jetting voltage (voltage applied to form jet) is lower for inks of higher dielectric constant for solvents with similar surface tension values. Such dependence of the jetting voltage on the surface tension of the fluid stemmed from the fact that the jet formation became possible only when the applied electrostatic force (resulting from the applied voltage) was large enough to overcome the surface tension force. Many studies have probed the scaling of the droplet size produced by electro-spraying (the mechanism of droplet formation during EHD jet printing).[108–110] These studies reported the following scaling for the droplet size (d): $d \sim (\varepsilon_0 \varepsilon' Q/K)^{1/3}$, where ε_0 is the permittivity of free space, ε' is the dielectric constant of the ink, Q is the flow rate, and K is the electrical conductivity of the ink. As it has been pointed out above, surface tension (γ) of the ink is critical in determining the jetting behavior in EHD jet printing: the applied electrostatic force, resulting from the applied voltage, must overcome the surface tension at the meniscus of the fluid to deform and form jet or microdroplets (based on the jetting mode). To understand the significance of surface tension on the EHD jetting process, Bae *et al.* studied the jetting mode formation for solvents of different surface tension values (see Fig. 6).[111] They demonstrated that irrespective of other parameters, liquid surface tension significantly affected the ability to form jets using EHD. They also reported the absence of jet formation when the surface tension of the liquid was greater than 43 dyne per cm when a 1.2 kV voltage was applied. Interestingly, increasing the electric field may not result in a stable cone-jet for liquids with higher surface tension. This is because the electric field required to overcome the surface tension may result in an electric breakdown in the gas that surrounds the jet.[112,113]

The effect of viscosity on EHD jetting and the drop size distribution were studied by a number of researchers.[114,115] For example, Jayasinghe *et al.* studied drop formation using the EHD process for a variety of liquids whose Newtonian viscosity ranged from 1 mPa s to 1340 mPa s and reported a significant influence of viscosity on the drop size.[114] By maintaining other properties like conductivity constant, they reported an increase in the size of the droplets with an increase in the viscosity values. In another study, Yu *et al.* studied the effect of viscosity and elastic properties of a viscoelastic drop on the stability of the Taylor cones.[115]

The effect of conductivity is one of the most important properties that determines the jetting behavior: this stems from the fact that conductivity determines the stability of electrospray given by Rayleigh limit.[112–116] The lower limit of the conductivity to ensure the formation of a stable jet has been reported by many studies: they identify this lower limit of the conductivity to be in the range of 10^{-8} S m^{-1} to 10^{-11} S m^{-1}. However, there are studies which report EHD printing using dielectric liquids of much lower conductivity of 10^{-13} S m^{-1}.[117] Electrical conductivity not only affects the stability of droplet formation but also plays an important role in determining size

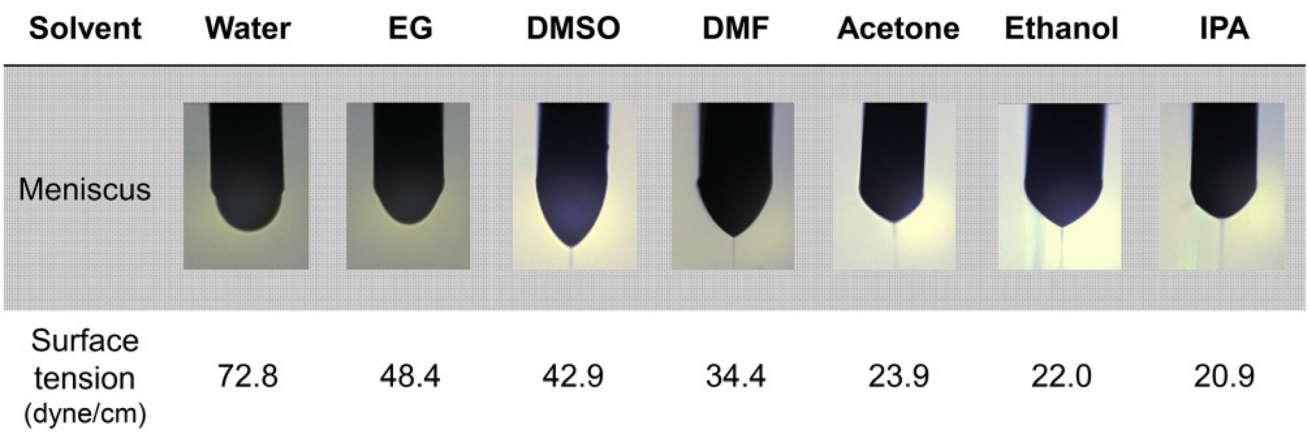

Fig. 6 Effect of surface tension on the jetting behavior. This figure has been reproduced from ref. 111 with permission from John Wiley and Sons, copyright 2017.

of the droplets produced. In a study by Tang *et al.*,[112] the authors reported a monotonic decrease in the droplet size with an increase in the electrical conductivity of the ink for various flow rates: this is a finding that is consistent with scaling reported in several other research studies.

Apart from the ink properties, the printing conditions like the flow rate, applied voltage, *etc*. also determine the jetting modes. For example, Lee *et al.* showed various jetting regimes based on the type of jet ejected from the Taylor-cone.[118] They reported the following six different jetting regimes observed for various combinations of applied voltage and flow rate: dripping, pulsating, cone-jet, tilted-jet, twin-jet, and multi-jet (see Fig. 7).

C.1.2. Rheological properties of generic particle-laden inks. Nanoparticle (NP) based inks and suspensions, which constitute the most important class of particle-laden inks and suspensions, are mostly non-Newtonian liquids. One of the most important factors that will dictate if such NP-laden inks will be printable or not will be the "shear-thinning" properties of these inks. Shear-thinning liquids are a class of non-Newtonian liquids, which are characterized by their reversible decrease in viscosity with an increase in the shear rate. The shear-thinning characteristic makes a liquid 3D-printable as this characteristic ensures that the viscosity of the liquid is smaller when it passes through the print head, thereby avoiding any clogging of the printing nozzle.[46] At the same time, as the liquid detaches from the nozzle and is no longer under an applied shear, its viscosity increases, which in turn allows the deposited liquid to remain in place on the printing substrate without flowing (and thereby hold its shape). The shear-thinning property of a liquid is often used to determine the printability window and the printing speed limit for a particular liquid.[46,47,80] Furthermore, this behavior can minimize the generation of satellite droplets during printing, which in turn enhances the resolution of the printed components. This was identified by Hoath *et al.*, who conducted printing using aqueous PEDOT:PSS ink.[85,119] On the contrary, 'shear-thickening' liquids are the liquids for which the viscosity increases with the shear rate: these liquids will clog the printing nozzle during the extrusion/deposition process and hence are less favorable for application as 3D printable inks.[120,121] Several studies have focused on maintaining the desired ink viscosity, and accordingly, have considered using suspensions based on graphene or graphene oxide and carbon-black or CNTs.[51,52,54–56,122–125] Fu *et al.* tested the apparent viscosity of their different fabricated GO-based printable inks as a function of the shear rate and noticed a shear-thinning behavior in all of them.[126] Such shear-thinning behavior has also been observed in other types of nanoparticulate inks, such as GO, GO/$LiFe_4PO_4$ (LFP), and GO/$Li_4Ti_5O_{12}$ (LTO) inks.[13]

Nanoparticle concentration, size, shape, hardness, molecular weight, surface functionalization, surfactant chemistry, and interactions with the solvent as well as the printing and environmental conditions (*e.g.*, melt viscosity for FDM printing inks) are some of the factors that impact the viscosity and the shear-thinning behavior of the ink. In Fig. 8, we show the relationship between the various nanoscale properties and ink viscosity.

Several research studies on formulation of inks for additive manufacturing focus on obtaining desired rheological properties by controlling the nanoparticle concentration (or solid fraction) of the nanoparticles in the solvent. For instance, An *et al.* studied the viscosity of two kinds of liquid–solid suspension systems [(i) oil-paraffin and ABS plastic system and (ii). Fe–2.4%C melt during solidification] by considering the effects of their solid fraction and solid particle shape (*i.e.*, the

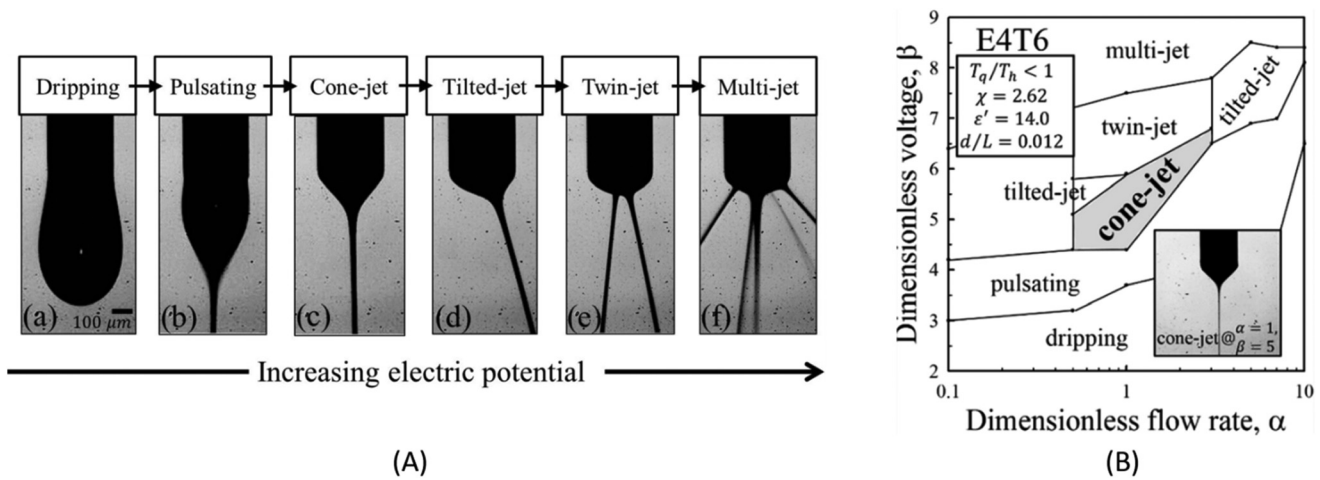

Fig. 7 (A) Jetting regimes observed in the electrohydrodynamic jet printing, (B) Jetting maps as a function of dimensionless flow rate $\left[\alpha = \frac{Q}{\left(\frac{\gamma\varepsilon_0\varepsilon'}{\rho K}\right)}\right]$ and dimensionless applied voltage $\left[\beta = \frac{V}{\sqrt{\frac{\gamma d}{\varepsilon_0}}}\right]$. Here, Q is the supplied flow rate, γ is the surface tension of the ink, ε_0 is the permittivity of free space, ε' is the dielectric constant of the ink, ρ is the mass density of the ink, K is the electrical conductivity, V is the applied voltage, and D is the nozzle diameter. Both the parts of this figure have been reproduced from ref. 118 with permission from American Chemical Society, copyright 2013.

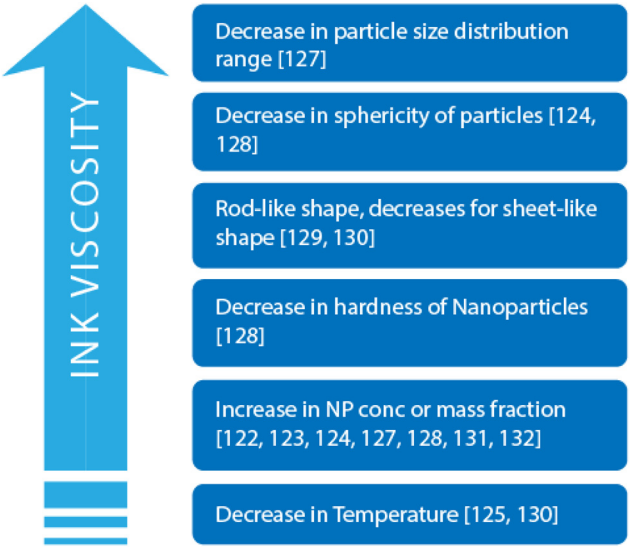

Fig. 8 Relation of nanoscale properties to macro-scale ink viscosity for generic inks.

sphericity of the particles).[128] They noticed that with less than 15% of solid fraction, the system behaves as Newtonian fluid, while it behaves like a non-Newtonian fluid when the solid fraction becomes higher than 15%. The suspension viscosity increased with the increase in particle fraction. Naficy *et al.* studied the viscoelastic properties of graphene oxide (GO) dispersions, controlled the rheological properties of GO dispersion by adjusting the GO concentrations, and developed a practical guideline for achieving rheology that is conducive for printing 2D-materials (like GO) based inks.[122] Vallés *et al.* studied and compared the rheological behaviors of GO in aqueous system, GO in polymer matrix system, and an aqueous dispersion of oxidized CNTs. They found that both GO and CNT systems behaved as thixotropic materials. Moreover, different dynamic behaviors were observed in GO systems: these systems respectively showed weak (strong), transitional, and strong (weak) gel-like (fluid-like) behaviors when the volume concentrations of GO were smaller than 0.03%, between 0.03% and 1.2%, and greater than 1.2%, respectively.[123] Ma *et al.*[51] and Hobbie *et al.*[52] studied the rheological behaviors of the CNT suspensions consisting of different CNT concentrations and solvents. Hobbie *et al.* showed that the viscosity of the MWCNT suspension, at a given shear rate, progressively increased as the MWCNT concentration (by mass) increased. They also noticed a more obvious shear-thinning behavior in more concentrated MWCNT suspensions.

On the other hand, Malkin *et al.* focused on the effect of molecular weight on fluid viscosities.[133] In their study, a system of nano-silica with different particle sizes or surface areas in polymer matrix (with polymers of different molecular weights) was studied. They noticed that suspensions consisting of matrix of larger molecular weight polymers can demonstrate viscoelastic properties and exhibit gel-like structures even for overall low volume concentrations (*e.g.*, 7%) of silica nanoparticles.

The NP size distribution plays a crucial role in affecting the ink viscosity. Liu *et al.* experimented on a dispersion of deionized fruit sugar solution and spherical silica particles and reported that the increase in the variance of the particle sizes decreased the relative viscosity of the dispersion significantly irrespective of the shear rates applied to the system.[127] Also, it was reported that higher volume fraction of particles ensured a better shear thinning behavior of the dispersion.

The shape of a NP can significantly affect the interactions with the solvent (for a non-NC ink) or the polymer (for a NC ink). Barrie *et al.* studied the rheology of carbon-black aqueous dispersions and noticed a shear-thinning behavior [see Fig. 9 (a and b)]. Additionally, they observed that the shape of the carbon black particles impacted the viscosity under different

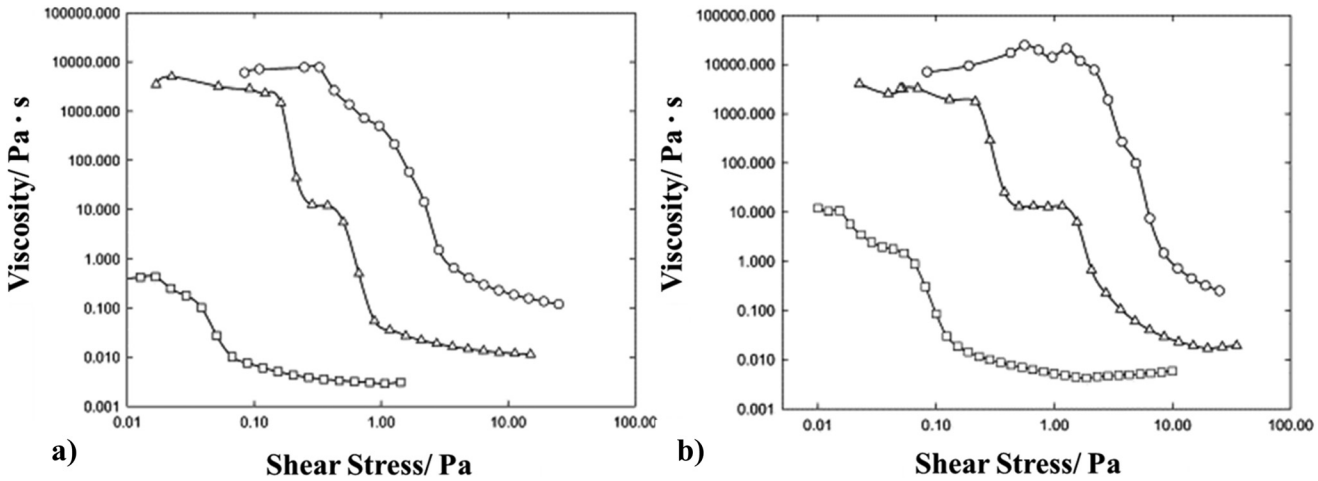

Fig. 9 (a and b) Viscosity–stress curve for carbon black aqueous suspensions with different particle shapes for (a) spherical particles and (b) fractional particles. Both the parts of this figure have been reproduced from ref. 124 with permission from Elsevier, copyright 2004.

polymer concentrations.[124] In general, fractal particles (with an average diameter of 105 nm) exhibited a higher viscosity at smaller shear rates and underwent a more prominent shear-thinning at higher shear rates as compared to spherical particles (with an average diameter of 87 nm). The study of An *et al.* on oil-paraffin and ABS plastic system showed a significant dependence of viscosity on the degree of sphericity of solid particle.[128] For a constant solid fraction, the liquid containing particles with a smaller degree of sphericity exhibited higher apparent viscosities (see Fig. 10), as the friction forces between particles of higher sphericity are smaller. Another interesting observation reported was the dependence of viscosity on particle hardness. Particles with higher hardness are less prone to deformation due to collisions and thus exhibit lower friction forces; therefore, liquid with particles of increased hardness demonstrate a more reduced apparent viscosity. Knauert *et al.* performed MD simulations to understand the effect of NP morphology on the viscosity of NP-polymer system.[129] It was observed that the liquid with rod-like NPs exhibited higher viscosities as compared to liquid with NPs of icosahedron shapes and sheet-like shapes: such an effect was attributed to the phenomenon of 'chain bridging' of polymer networks by the rod-like NPs.

Numerous studies have probed the rheological properties of printable liquids (*e.g.*, homogeneous fluids such as polymeric solutions as well as the particle-laden fluids where the particles are suspended as dispersed phases in a background solvent). Rheological properties of an ink represent its fluidic behavior under certain shear rate and can indicate its printability under certain feed rate and printing speed. Many studies have investigated the applicable shear rates that could be employed for printing and have evaluated the appropriate viscosity values for the inks to extrude without clogging the nozzle during the printing process.[46] It is also noticed that for printing continuous filaments, the ideal ink viscosity values ranges from 10^3 to 10^4 Pa s at the shear rate of 1 s^{-1}, while for traditional inkjet printing the ideal ink viscosity values are around 10^{-3} Pa s at the shear rate of 1 s^{-1}.[58,134,135] Also, the relationship between the fluid properties of the ink and the ink printability for the particle-laden inks has been widely reviewed and investigated for different solvents (such as water or organic solvents) serving as the continuous phase as well as

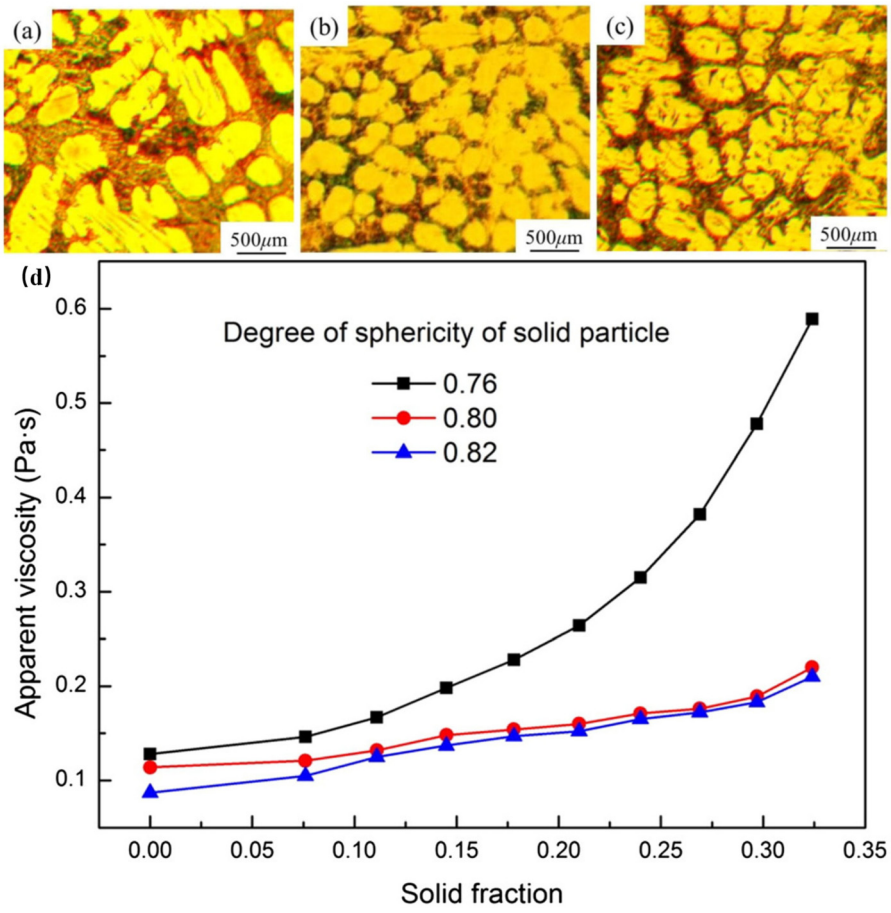

Fig. 10 (a–c): Water-quenched Fe–2.40%C alloy (solid fraction = 0.32) with different microstructures under different processing conditions: (a) sphericity: 0.76 cooling rate: 5 °C min^{-1}, shear rate: 12.7 s^{-1}, (b) sphericity: 0.82; cooling rate: 5 °C min^{-1}, shear rate: 25.4 s^{-1}, (c) sphericity: 0.80; cooling rate: 8 °C min^{-1}, shear rate: 25.4 s^{-1}; (d). viscosity as function of solid fraction for Fe–2.4%C melt with different sphericities. All the parts of this figure have been reproduced from ref. 128 with permission from Elsevier, copyright 2018.

different suspended materials including carbon-based materials and metal nanoparticles (serving as the dispersed phase).[22,46,47]

Ma *et al.* compared chemically-treated CNT suspensions with chemically-untreated ones and observed a significantly larger shear-thinning behavior in the untreated CNT suspensions.[51] Kim *et al.* used acid-treated MWNTs over untreated MWNTs for improving their dispersibility in a solution, and further used PVP polymer to make the ink 3D printable.[60] The effect of the surface functionalization of the NP on the viscosity of the ink is specific to the type of functionalization and its behavior in the given solvent or polymer matrix medium. The mechanisms of these phenomena with respect to CNT inks and their contribution to improving the stability of CNT-based inks have been discussed in section C.2.

It was also observed that for a polymer-nanocomposite system, the relative viscosity of the system increased with an increase in the polymer chain lengths.[129] MD simulations for the system were conducted for different polymer chain lengths N ($10 < N < 40$) at a constant shear rate, and it was observed that the chain friction coefficient increased linearly with N, as longer polymer chains are more prone to entanglements.

In some other cases, additives, or fillers can have impact on the rheological properties of the suspension as well.[136] For example, for cellulose nanofibrils (CNF) suspensions, addition of an acid can impact the entanglement of nanofibril agglomerates, while the stiffness, viscosities, or particle agglomeration behavior can be changed by changing the pH level (*via* the addition of acid). Alves *et al.* studied the properties of TEMPO-treated CNFs maintained at different pH levels (ensured by changing the amount of the added phosphoric acid), and they found that the system demonstrated a higher yield stress and a larger viscosity at low pH values.[136] Some additives have been noticed to reduce the ink viscosity and affect its rheological performance and printability. For example, some commercial polymer-dispersing agents were found to effectively lower the viscosity of graphene-based inks [see Fig. 11(a and b)]. In addition, due to the reduced viscosity caused by the addition of the dispensing agents, the ink was found to become compatible with a wider range of print parameter settings.[125]

Controlling the shear stresses to which the printable ink gets subjected (by using different size of nozzles, which can simultaneously change the volumetric flow and pressure drop during the ink printing process), which interplayed with the shear-thinning behavior of the printable inks (discussed in the following sections), have been used to devise alternative printing strategies for making the ink printable.[137]

Some post treatments, such as thermal or mechanical treatments, can be another method to tune the viscosity of the suspension.[138] For identical material systems, different processing methods, tools, or orders of each step will lead to different final properties of the product. Taking vegetable suspensions as an example, Lopez-Sanchez *et al.* studied the carrot, broccoli, and tomato suspensions, and it was found that for the suspension with the same kind of materials, different thermal and mechanical treatments resulted in different flow viscosities.[138]

Material and environmental conditions, such as ink concentration, pH level, and heating temperature, can induce changes in the ink viscosity and the shear-thinning behavior.[50,54,55] O'Mahony *et al.* reviewed the connection between the rheology and the printability of different carbon-based inks, and found out that several factors such as the temperature, pressure, pH, shape of the particles, and the surface tension impact the ink rheology.[46]

C.1.3. Wetting properties of printable nano-particle laden inks. Ink wettability, or the degree to which an ink wets a particular substrate, is another critical property for the ink to remain stable (on that particular substrate) after being printed/deposited.[84,128,137,139] Smaller ink surface tension means a reduced internal cohesive force between the ink molecules, which in turn will result in a higher wettability and smaller contact angle on a given substrate, and therefore, a larger propensity for the ink to remain stable on the substrate after being printed/deposited. Moreover, in nozzle-based printing processes, especially where a very small volume of liquid is used, it is essential for the ink material to have lower surface

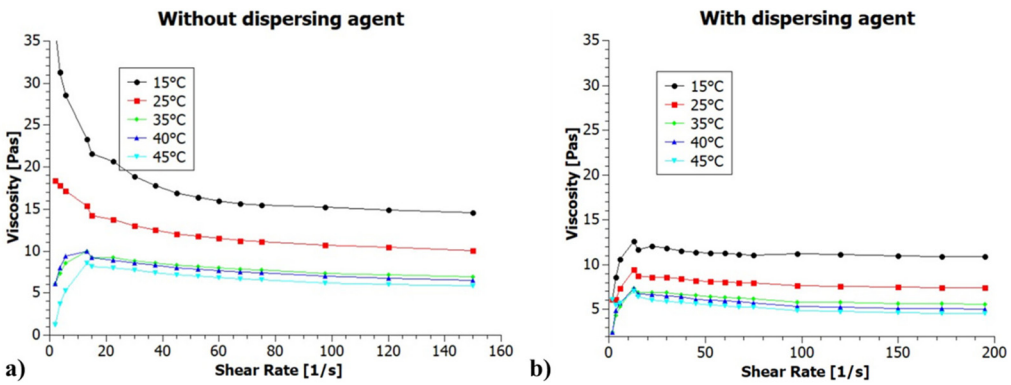

Fig. 11 (a and b) Viscosity of graphene-based inks as a function of shear rates under different temperatures for (a) ink without dispersing agent and (b) ink with functional polymer dispersing agent. Both the parts of this figure have been reproduced from ref. 125.

tension to be able to eject the droplets from the nozzle.[140] Inappropriate surface tension values, combined with oscillatory kinetic energy, tend to generate unstable flow with discontinued droplets (*i.e.*, in the form of satellite drops) during the printing.[84,139]

Surface tension of a nanoparticle-based ink depends on a number of factors including particle concentration, surfactant, type of the binder and filler material, *etc*. The effect of the concentration of the uncharged NP (in the absence of surfactants/filler) on the ink's surface tension can be significant. At dilute NP concentrations, the surface tension seems to be relatively unaffected. This can be attributed to the fact that at low NP concentrations, *i.e.*, dilute solutions, the interaction forces between the particle, namely the van der Waals interactions, would not significantly impact the surface energy of the liquid. On the other hand, at higher NP concentrations, where the particles are much closer to each other, there could be significant van der Waals attractive interactions which could essentially lead to a change in the surface tension of the liquid.[141,142] However, for some combinations of nanoparticle and solvent, the surface tension has been found to decrease with the increase in the NP concentration as shown by Khaleduzzaman *et al.*[143]

The effect of particle size on the surface tension of the NP-based ink has been studied by a number of researchers. These studies show a clear increase in the surface tension with the particle size, which could be attributed to increased van der Waals force with particle radius.[141,142,144] However, it was observed that the surface tension of nanofluids decreased with an increase in temperature and also, with the increase in surfactant concentration.[143,145]

Binder material is also known to have a significant impact on the surface tension of the ink. For example, the inks containing solvent-based binders (*e.g.*, acetone-based) tend to have lower surface tension as compared to inks containing water-based binders.[139] The binder surface tension has a significant influence on the width of the line printed with the ink containing the binder;[133] for example, an ink containing a binder with a larger surface tension will result in smaller printed line width. Moon *et al.* compared the printed line widths obtained with inks containing four different kinds of binders and found the line width to be 800 μm for the ink containing a binder with surface tension of 25 mN m^{-1} and a viscosity of 1.5 mPa s, while the line width was found to be less than 400 μm for the ink containing a binder with a surface tension of 50 mN m^{-1} and a viscosity of greater than 4 mPa s.[139]

C.1.4. Coffee stain effect for generic particle-laden inks. An effect that is intricately related to the drying of any micro-nanoparticulate suspension is the formation of the "coffee stain" or "coffee ring". The drying process caused by the evaporation of the solvent from the deposited drop of the suspension triggers an advective transport within the drop directed towards the three-phase contact line (TPCL). This flow drives the particles inside the drop to get deposited at the TPCL. As a result, once the drop is evaporated, most of the particles are localized at the TPCL and hence gives the impression of a ring-like deposit. Exactly same type of deposits (of the coffee particles) occurs from an evaporating coffee drop and hence the formation of this ring-like deposit is also known as the "coffee stain" or "coffee ring" effect. There have been numerous studies that have exploited the formation of such "coffee ring" for a multitude of applications ranging from self-assembly-driven fabrication of biological devices and fabrication of conductive metal nanoparticle based patterns and CNT-based structures.[30,48,74,146] On the other hand, several studies have pointed out the detrimental effects of the formation of "coffee stain" in the quality of the 3D printed traces, devices, and components and have developed strategies to arrest the coffee stain formation and ensure a uniform evaporation-induced deposition of the particles.[147–150] The presence of "coffee stain" in 3D printed traces, devices, and components is known to cause reduced performance in crystallization and inferior field emission properties,[147] lower adhesion strength in printed NP-based traces,[148] and voids in printed structures.[116] The suppression of the coffee-stain effect can enhance the quality of printed silver NP traces and minimize defects such as the 'trench formation' by the printed traces (*i.e.*, the scenario where more particles are deposited on the edges of the traces than the center of the traces, ensuring that the edges of the traces contain more materials and hence are more raised than the center of the traces).[117]

The coffee-stain phenomena could be affected by multiple parameters including (a) printing process control such as substrate surface roughness,[151,152] porosity and hydrophobicity,[143,145] introducing humidity cycling conditions, vibration or acoustic waves,[153,154] and controlling the Marangoni flow or the interactions on the air-ink interfaces;[155,156] (b) the property of inks including particle concentrations,[22] types of solvents,[157] and the microstructure of ink particles such as their size and shape.[30,158–160]

Zhang *et al.* analyzed the patterns formed from colloidal droplets on different surface roughness.[151] They found that increasing the substrate roughness could make the coffee-ring formation more significant because the rough surfaces could suppress the backflow of the capillary flow and prevent the materials from recirculating to the center of the droplet. Meanwhile, another research study claims that the use of a hydrophobic surface can reduce contact-line pinning and result in a deposition without a coffee-stain.[145] The effect of the environmental conditions on the coffee-ring effect, such as humidity or temperatures have also been studied. For example, Marangoni flow generated by the surface tension gradient on a surface with temperature perturbation can affect the formation of coffee-stain.[154] Ta *et al.* used a laser beam to create a local hot spot, and the Marangoni flow generated by this local temperature gradient ensured a flow directed towards the center of the deposited droplet, which effectively suppressed the coffee-ring effect.[156] Post-processing (*e.g.* sintering) of printed nanoparticulate inks can also induce the formation of such coffee stain effect and has been observed in numerous studies employing different printing techniques and ink materials (*e.g.*, ceramic inks,[21] metal nanoparticles-based inks,[28] carbon-

based inks such as CNT-based inks,[48,74] *etc*.). Zhan *et al.* have conducted a detailed review of inkjet-printed optoelectronics: they discussed the formation of coffee-ring structures by metal-based and CNT-based inks.[161]

On the other hand, several properties of the ink, including its concentration, surfactant and solvent type, and the microstructure of the particulate matter (such as shape and size) present within the ink material, also have a certain impact on the formation of coffee-stain. Shen *et al.* studied the evaporation dynamics of droplets with and without surfactants and proposed a method to suppress coffee-ring formation by controlling the droplet size [see Fig. 12(a)].[160] Yunker *et al.* found the impact of particle shape on the 'coffee-ring' formation. In their case, a uniform deposition was achieved with ellipsoidal particles (aspect ratio = 3.5), in which the shape-dependent capillary interaction became significant, thereby enforcing the ellipsoidal particles to localize at the air–water interface of the evaporating drop and in the process overcome the coffee-stain effect.[158] Oh *et al.* found that adding DMF to water facilitated more uniform patterns in inkjet-printed Al_2O_3 droplets as compared to the patterns obtained using only water as solvent [see Fig. 12(b and c)].[157] In Fig. 13, we have provided a schematic identifying the different factors that affect the coffee-stain formation in NP-based inks.

C.1.5. Sintering of printable inks. Sintering is a post-processing technique (employed after the printing/deposition of the particle-based inks) that can be leveraged to achieve higher quality print with desired trace properties. For example, sintering can be used for accelerating the evaporation of solvents, removing voids, bridging nanoparticles, removing unwanted binders and additives,[90] *etc*. Insufficient sintering will leave gaps between the nanoparticles, and hence hamper the electrical performance of the printed parts.[164]

Thermal sintering, which is one of the most commonly used sintering methods in additive manufacturing for metal-based nanoparticle inks, involves applying a high temperature (150 °C–650 °C)[164] to heat the printed samples and degrade (and evaporate) the binder or surfactants. The sintering

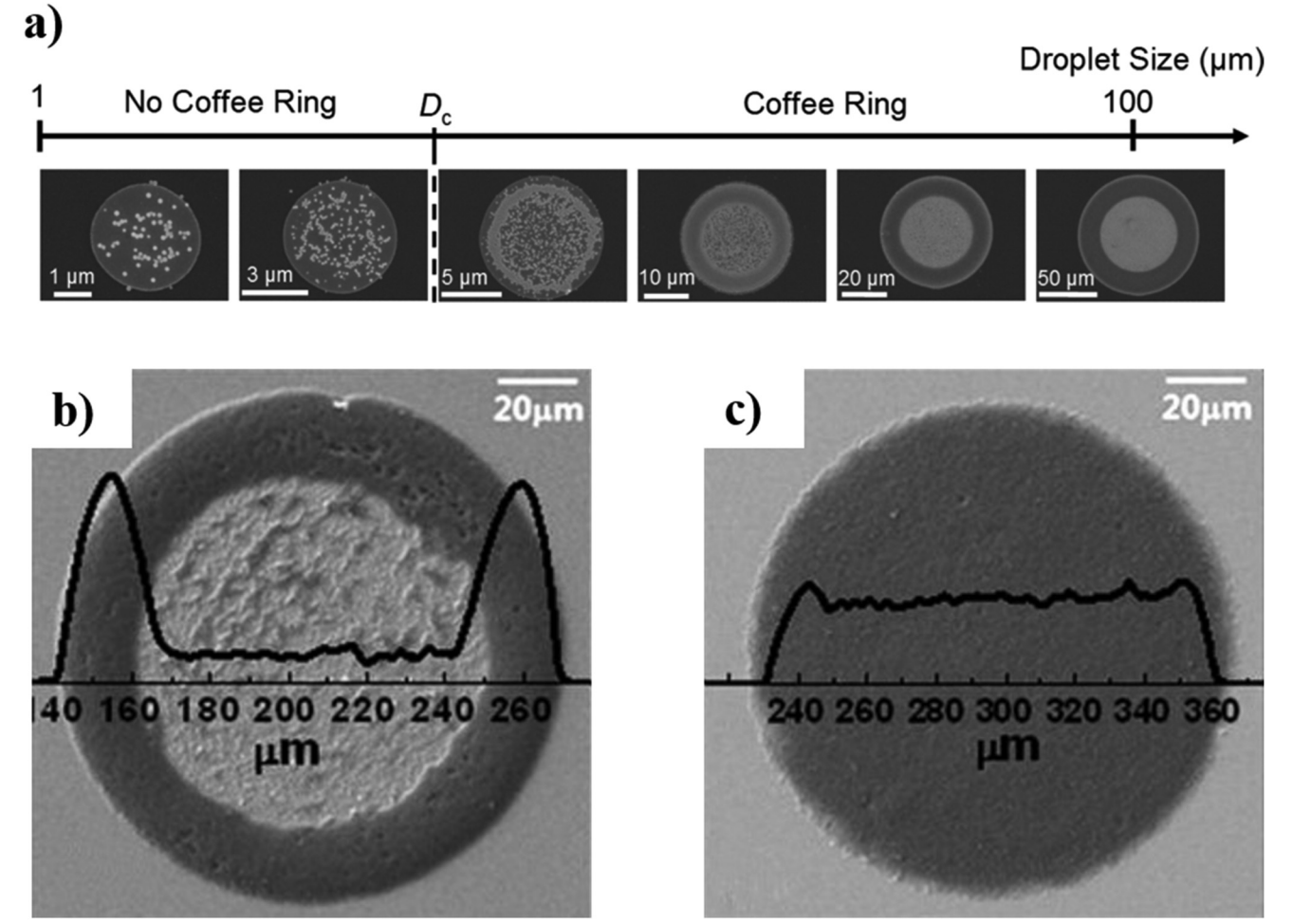

Fig. 12 Examples of suppressing coffee-stain effect by using (a) a smaller droplet diameter (droplet diameters increased from 3 to 100 μm) and (b and c) Al_2O_3 dispersion with different solvent composites (b) water-only solvent (showing coffee-stain effect) and (c) water/DMF mixed solvent (showing no coffee-stain effect). Part (a) this figure has been reproduced from ref. 160 with permission from American Chemical Society, copyright 2010. Parts (b) and (c) of this figure have been reproduced from ref. 157 with permission from Elsevier, copyright 2011.

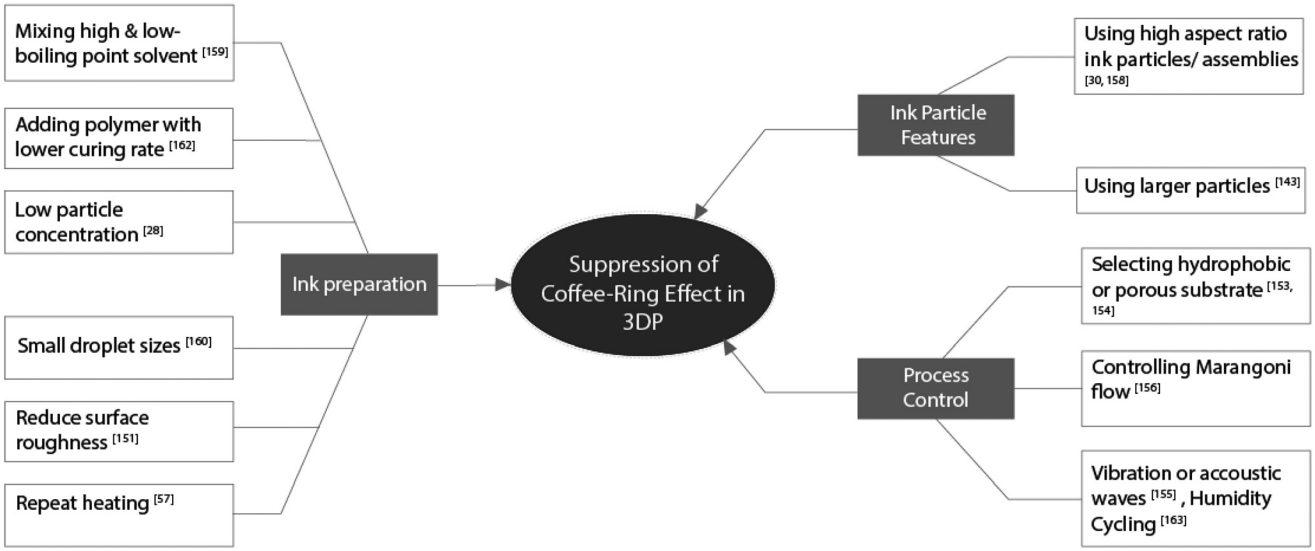

Fig. 13 Schematic identifying the various factors that affect the coffee-ring formation in generic particulate inks during 3D printing.

process is also important to ensure that the metal nanoparticles lose the stabilizing ligands that are grafted on the NP surface and in the process these NPs come in close enough proximity in the dried sample enabling the attainment of a desirable electrical conductivity of the printed traces. However, due to the high temperatures associated with the thermal sintering process, the choices of the substrates (where the conducting traces can be printed) have been limited, and extensive research has been conducted to develop NP-based conductive ink with reduced binder or surfactant content that enables thermal sintering at a reduced temperature.[146,147] One sintering method capable of avoiding the overheating of the material system is photonic sintering, which uses laser or lamps to selectively deliver the energy,[165] and this method has been employed for sintering traces printed with gold nanoparticle inks[166] and silver NP inks.[167] The morphology differences in metal-based nanoparticle inks may require different sintering processes, which in turn may also affect the performances of the printed products. It was noticed that the silver nanoparticles with a higher surface to volume ratio tend to have smaller melting temperatures.[168] The electrical performance of the silver-nanoparticle inks also varies as a function of the NP shapes; for example, Yang *et al.* found that the pattern printed with an ink containing a mixture of silver nanoplates, and nanoparticles have higher conductivity as compared to the pattern printed with an ink containing only spherical silver nanoparticles.[169]

Other alternative sintering approaches that can be used to remove binders or surfactants after printing include microwave sintering,[170] plasma sintering,[171] electrical sintering,[172] *etc*.

The following sections will primarily focus on the shear-thinning property (rheology), the stability, the wettability (or drop contact angle), and the coffee-stain phenomenon of CNT-based liquid drops and CNT-based 3D printable inks. The connection of the fluid properties of the ink to the printability and functionalities of the ink will be discussed in detail. The viscosity range of CNT inks under steady or increased shear rates will be listed, and methods to adjust it will be discussed. Following that, discussions will be provided on the coffee rings (observed in 3D printed CNT composites) and the related characterizations.

C.2. Rheology and stability of CNT-based inks

In this section, we shall discuss the rheological behavior and stability of two categories of CNT-based inks: (i) 3D printable CNT-based NC (nanocomposite) inks, and (ii) 3D printable CNT-based nNC (non-nanocomposite) inks. We provide a schematic representation of all the factors that affect the macroscopic properties of the CNT-based ink in Fig. 14.

C.2.1 Rheology of CNT-based inks. 'Shear-thinning' behavior has been commonly observed in CNT suspensions and has been widely reported in the literature. Hu *et al.* reviewed the appropriate fluidic properties that dictated the fabrication of CNT thin-films using CNT suspensions.[173] They pointed out the range of viscosities of CNT suspensions, methods to adjust the viscosities, and the effect of these viscosity values on thin film fabrication. Hobbie and Fry measured the rheological properties of non-Brownian CNT suspensions with different CNT loadings from 0 to 10% weight ratio. They noticed that under identical shear rates, the viscosity increased by several orders of magnitude for the case when the suspension became more concentrated.[52] Ma *et al.* studied the relationship between the rheological behavior and the CNT agglomerates.[51] They compared the effects of CNT treatment on the viscoelastic properties of CNT dispersions suspended in a Newtonian liquid matrix. They noticed a higher level of viscoelasticity in non-treated CNT dispersions, while the treated-CNT dispersions showed a smaller shear-thinning behavior. They explained their results by *in situ* monitoring of CNT microstructure. Yokozeki *et al.* quantified the microstructure of MWCNT/epoxy

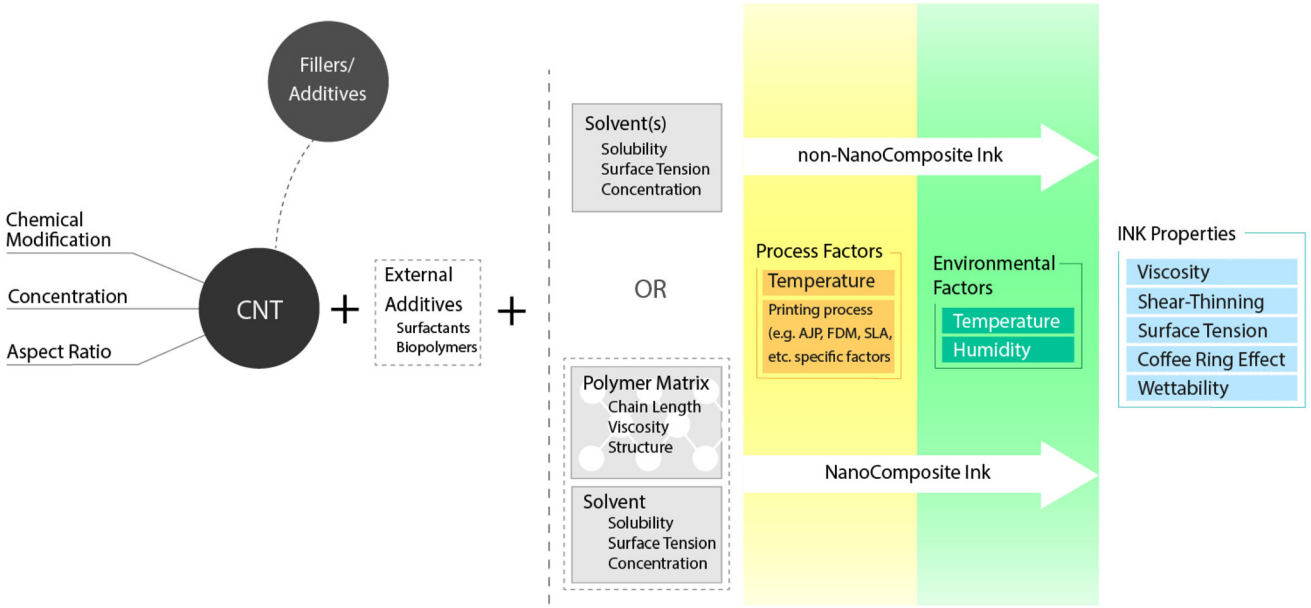

Fig. 14 Schematic representation of the properties of materials used and the process and environmental factors that affect the resultant CNT-ink properties.

suspensions with different MWCNT mass fractions under different temperature and shear rates.[131] They studied the agglomerate formation for the 0.1 wt% suspension of MWCNT at 25 °C and 60 °C and found that the agglomerates are sparser at 60 °C (see Fig. 15).

Shear-thinning behavior has also been widely observed in CNT-based NC inks. A variety of different models have been introduced for determining the printability window and for analyzing the corresponding rheological properties of CNT-based 3D printable NC inks.[47,60] Examples of shear-thinning behavior of CNT-based NC inks are shown in Fig. 16(a and b). For example, studies have related shear-rate to shear-stress using a capillary flow model and have identified a mechanism to estimate the allowable shear stress for 3D-printing process. As already discussed above, the shear-thinning properties of a printing ink ensure the appropriate flowability of the ink

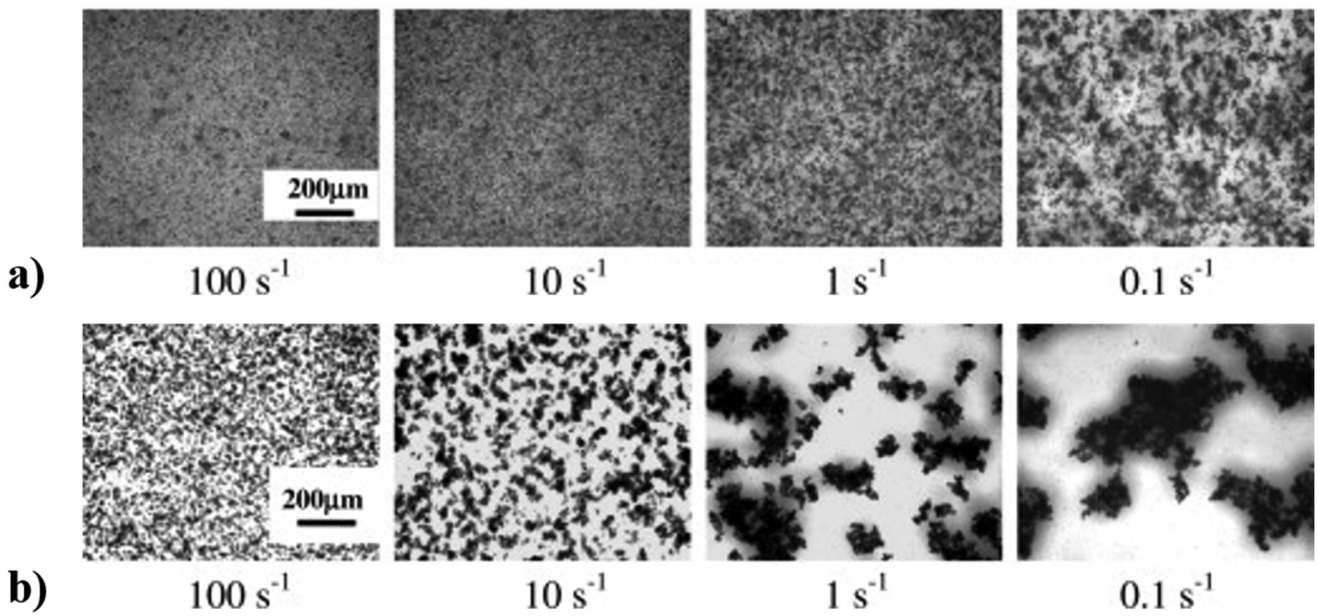

Fig. 15 Microstructure of epoxy–CNT suspension (0.1 wt% MWCNT) under different shear rates at (a) 25 °C and (b) at 60 °C. Both the parts of this figure have been reproduced from ref. 131 with permission from Elsevier, copyright 2012.

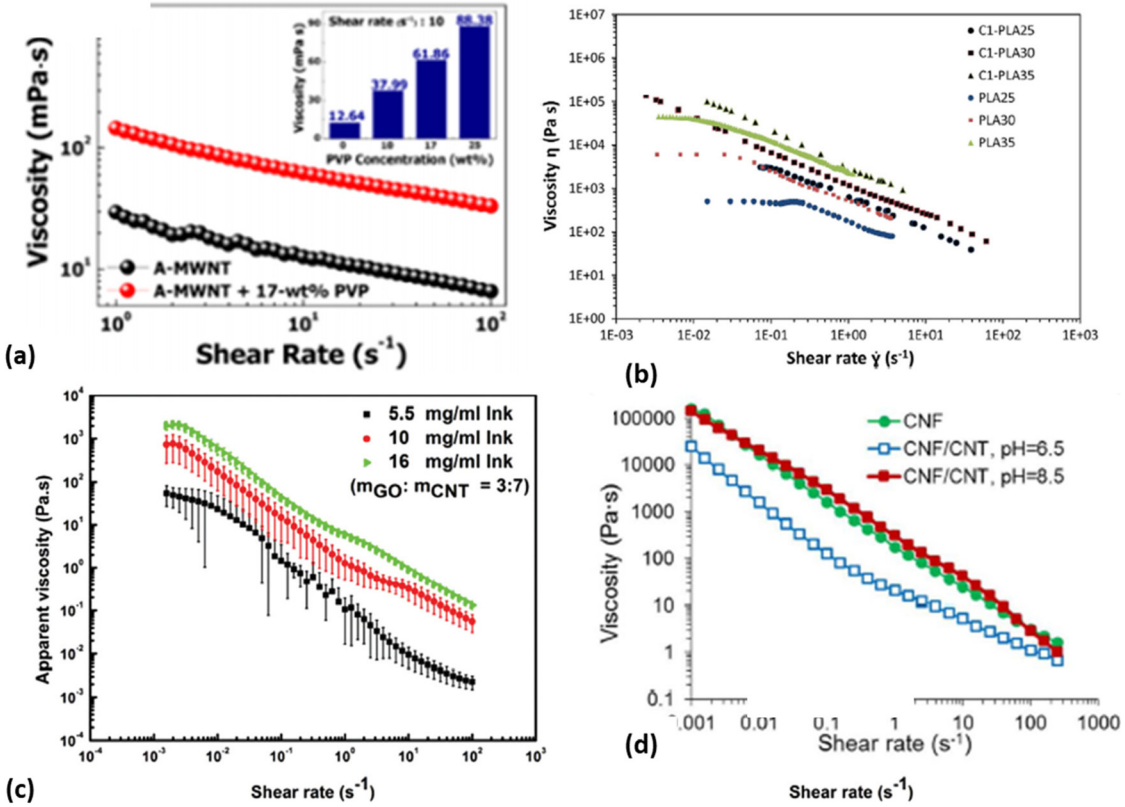

Fig. 16 Examples of CNT-based ink viscosity plot as a function of shear rate for (a) MWCNT-PVP ink, (b) MWCNT-PLA nanocomposite ink with different PLA concentration, (c) CNT–GO inks considering different ink concentrations, (d) CNT/CNF inks under different pH level. Part (a) of this figure has been reproduced from ref. 60 with permission from American Chemical Society, copyright 2016. Part (b) of this figure has been reproduced from ref. 47 with permission from Elsevier, copyright 2015. Part (c) of this figure has been reproduced from ref. 30 with permission from Royal Society of Chemistry, copyright 2019. Part (d) of this figure has been reproduced from ref. 176 with permission from Elsevier, copyright 2018.

during printing at high shear stresses (or high shear rates) and acquiring of a stable, non-flowing structure (by the ink) after extrusion.[80] This 'shear-thinning' fluidic property has been widely tested and measured in the context of the application of 3D printable CNT-based NC inks.

Similar shear-thinning behavior has been observed in CNT-based nNC inks such as CNT-solvent-only inks,[59,75,174] CNT-graphene inks, CNT–GO inks [one example is shown in Fig. 16(c)], CNT–rGO (rGO: reduced GO) inks,[30,38,175] and CNT-nanocellulose ink [see Fig. 16(d)].[176] In Table 4, we have summarized the viscosity values of the CNT-based 3D printable inks, the corresponding shear rate ranges to which the inks have been subjected, and the ink compositions reported in different publications.

As pointed out in section C.1.2, the viscosity of the CNT-based inks can be modified by altering the following aspects of the NP system: NP concentration, polymer concentration (CNT based NC inks), type of solvent, NP aspect ratio, temperature, stabilization methods, fabrication methods.

Firstly, the NP concentration affects the viscosity of the generic particle-laden inks: similar behavior is observed for CNT-based inks. With an increase in the CNT concentration, the viscosity of the ink increases as has been shown in multiple studies.[30,38,59,69,131] Ivanova and Kotsilkova parametrically studied the impact of using CNT or graphene additives on the rheological behavior of 3D printable PLA NC inks.[53] They measured the complex viscosity as a function of the angular frequency for six different weight ratios of CNT or graphene additives and noticed that the addition of MWCNT with a higher aspect ratio resulted in the steady-state viscosity (η) demonstrating a more significant shear-thinning behavior (quantified by smaller values of n in the relationship $\eta = K_0\dot{\gamma}^{n-1}$, where K_0 is the flow consistency index and $\dot{\gamma}$ is the shear rate). It was observed that the complex viscosity increased with the increase in the concentration of MWCNTs (from 1.5% to 12% by weight).

Next, the viscosity of the CNT-based NC inks was found to increase with an increase in the polymer matrix concentration. The MWCNT/PLA NC ink developed by Postiglione *et al.* exhibited a decreasing apparent viscosity as a function of shear rate [see Fig. 16(b)].[47] They related the increasing shear stress to an increasing shear rate for inks having different PLA and MWCNT concentrations. They also determined appropriate process conditions for specific inks by estimating the corresponding shear stress for certain printing speeds with the printing speeds being directly related to the shear-rate. PLA

Table 4 Examples of viscosity testing results of several printable CNT inks under specific testing conditions and printable ink concentrations

Ref.	Ink composite	Shear rate (increasing)	Viscosity (decreasing)
30	CNT–GO	0.001–100 s^{-1}	~100–0.01 Pa s (at 5.5 mg ml^{-1})
38	CNT–rGO	0.1–100 s^{-1}	106.5–0.5 Pa s
42	(1). GelMA/ DNA-MWCNT	0.01–100 s^{-1}	(1). ~1–0.001 Pa s
	(2). HA/DNA-SWCNT		(2). ~10 000–1 Pa s
47	CNT-PLA	0.001–1000 s^{-1}	Viscosity at 10^{-1}–10^{1} s^{-1} shear rate ~5000–200 Pa s (25 wt% PLA); ~8000–800 Pa s (30 wt% PLA); ~30 000–1000 Pa s (35 wt% PLA);
53	MWCNT-PLA	0.05–1000 s^{-1}	~100 000–1 Pa s
59	CNT/IPA/EG	1–100 s^{-1}	~0.125–0.075 Pa s (6 wt% of CNT); ~0.16–0.09 Pa s (7 wt% of CNT); ~0.2–0.1 Pa s (8 wt% of CNT)
60	PVP-MWCNT	1–100 s^{-1}	Viscosity at 10^{-1} s^{-1} shear rate: 12.64 mPa s (0 wt% PVP) 37.99 mPa s (10 wt% PVP) 61.86 mPa s (17 wt% PVP) 88.38 mPa s (25 wt% PVP)
69	(1). PEGDA-CNT	1–100 s^{-1}	Viscosity at 1 s^{-1} shear rate
	(2). PEGDA: PEGMEMA-CNT		(1). 31 Pa s (0 wt% CNT) 2010 Pa s (1.5 wt% CNT)
			(2). 15 Pa s (0 wt% CNT) 1370 Pa s (1.5 wt% CNT)
75	CNT-DMF	1–100 s^{-1}	50–10 mPa s
175	CNT–GO	0.1–1000 s^{-1}	3000–0.25 Pa s
176	SWCNT-CNF	0.001–500 s^{-1}	100 000–1 Pa s
177	MWCNT-PLA: (1). solution-blended	0.05–10 s^{-1}	(1). ~4000–1000 Pa s
	(2). Melt-mixed		(2). ~50 000–1000 Pa s

concentrations of 25%, 30%, and 35% by weight were considered for experiments, and it was observed that the viscosity of the ink increased with an increase in the concentration of the PLA polymer matrix.

The solvent type for CNT-based fluid can also affect the rheological behavior, and based on different material concentrations, it is possible for CNT-based fluids or inks to behave as either Newtonian or non-Newtonian liquids. Chen *et al.*[178] found different rheological behaviors in MWCNTs dispersed separately in water, silicon oil, glycerol, and ethylene glycol, but they claimed Newtonian rheological behavior for each of these cases. However, in a research study by Ruan *et al.*, a shear-thinning behavior of MWCNT dispersions in ethylene glycol was noticed.[179] Pötschke *et al.* studied the fluidic properties of 0.5, 1, 2, and 5 wt% of MWCNT-polycarbonate composites, in which they noticed that the dispersions with CNT concentration larger than 2 wt% exhibited non-Newtonian rheological behaviors.[132]

Another feature of the CNTs is their 1D rod-like geometry, which influences the rheological property of the CNT-laden inks. In reference to the comparison of the NP-polymer composite behavior as shown in a study by Knauert *et al.*,[129] CNT-laden inks exhibit higher viscosities as compared to graphene-sheet laden inks, for a given mass fraction (of the dispersant) and a finite chain length of polymers in the matrix. Based on the differences in tube diameter or length, or different functional groups attached to the tubes, the aspect ratio of the CNTs can cover a large range. As discussed in the previous section C.1, for NP-based fluids, the particle aspect ratio is one of the key parameters that can affect the viscosity or rheological performance of the fluid containing these particles. Omrani *et al.* studied the MWCNT in DI water for different nanotube diameters and lengths (*i.e.*, different aspect ratios ranging from 10 to 3750) and found that for all the cases the dispersion exhibited Newtonian behavior.[130] It was also observed that the dynamic viscosity decreased non-linearly with an increase in the aspect ratio of the CNTs.

Mechanical, physical, and chemical methods that are typically applied to make CNTs more dispersible in various kinds of solvents alter their rheological properties and ink printabilities.[180–186] Ultrasonication process, which is one of the common mechanical methods applied for dispersing CNT-based inks, can alter the rheological behavior of the CNT-based fluids as well as the length of the tubes and their agglomeration sizes. Ruan *et al.*[179] found that the shear-thinning behavior for MWCNT-ethylene glycol fluids varied as a function of the time of ultrasonication to which the fluid was subjected to. For example, the fluid exhibited a more pronounced shear-thinning behavior after being ultrasonicated for 40 minutes, as compared to the case when it was not subjected to any ultrasonication [see Fig. 17(a)]. Specifically, they described the manner in which the agglomeration was reduced by the sonication process in two stages: in the first stage, the CNT agglomerates were loosened, while in the second stage, the entangled CNTs were broken. Moreover, for CNT-based suspensions or inks, they noticed that the length of the CNTs decreased with an increase in the sonication time [see Fig. 17(b)], while the aspect ratio of the CNT tubes decreased in the presence of a greater sonication energy [see Fig. 17(c)]. Surfactants used for the stabilization of CNT inks (section C.2.2 discusses the stabilization of CNT inks in detail) have a significant effect on the rheology of CNT inks.[187–189] For instance, addition of Triton X-100 surfactant to the SWNT-SBDS dispersion increased the zero-shear viscosity by 3 orders of magnitude and increased the high-shear viscosity by nearly 5 times the value in the absence of Triton X-100 surfac-

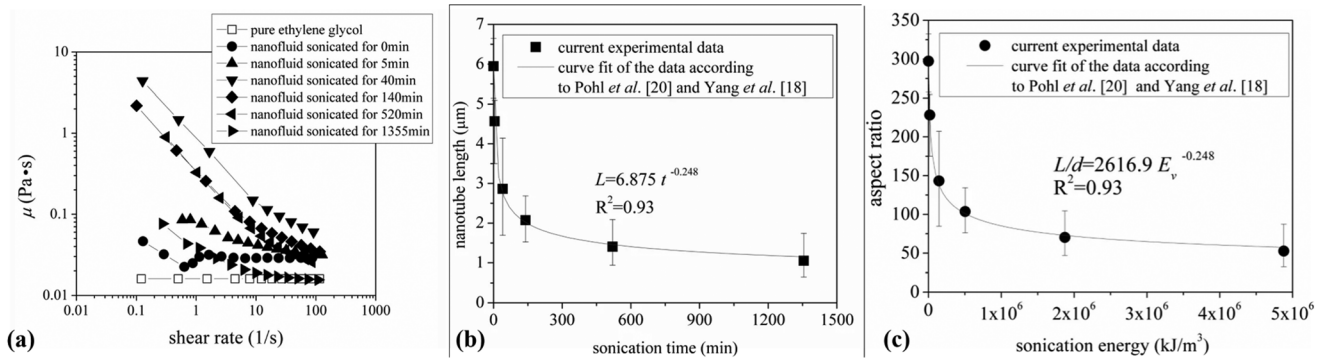

Fig. 17 (a). Shear-thinning properties for CNT-EG fluids as a function of sonication time; (b). nanotube length as a function of sonication time; (c). CNT aspect ratio as a function of sonication energy. All the parts of this figure have been reproduced from ref. 179.

tant. Such a massive increase in the viscosity could be attributed to synergistic association between the surfactants[187] or due to morphological change in the surfactant.[188,189] We have provided a schematic illustrating the role of surfactants on the different properties of the ink, including the viscosity, dispersity, and surface tension in Fig. 18.

Yokozeki *et al.* experimented on MWCNT–epoxy nanocomposite inks of different MWCNT concentrations at ambient temperatures of 25 °C, 40 °C, and 60 °C.[131] They observed that the ink viscosity decreased in all the cases with an increase in temperature. Similar observations were reported by Omrani *et al.* for –COOH functionalized MWCNTs in distilled water.[130]

Furthermore, Spinelli *et al.* compared the rheological behavior of PLA/MWCNT and PLA/GNP printable NC inks fabricated using two separate methods: solution blending and melt mixing. Compared to the Newtonian fluid behavior of pristine PLA, both types of NC inks containing high concentrations of GNP and MWCNT fillers demonstrated distinct shear-thinning behaviors.[177] They also noticed Newtonian viscosity plateau in

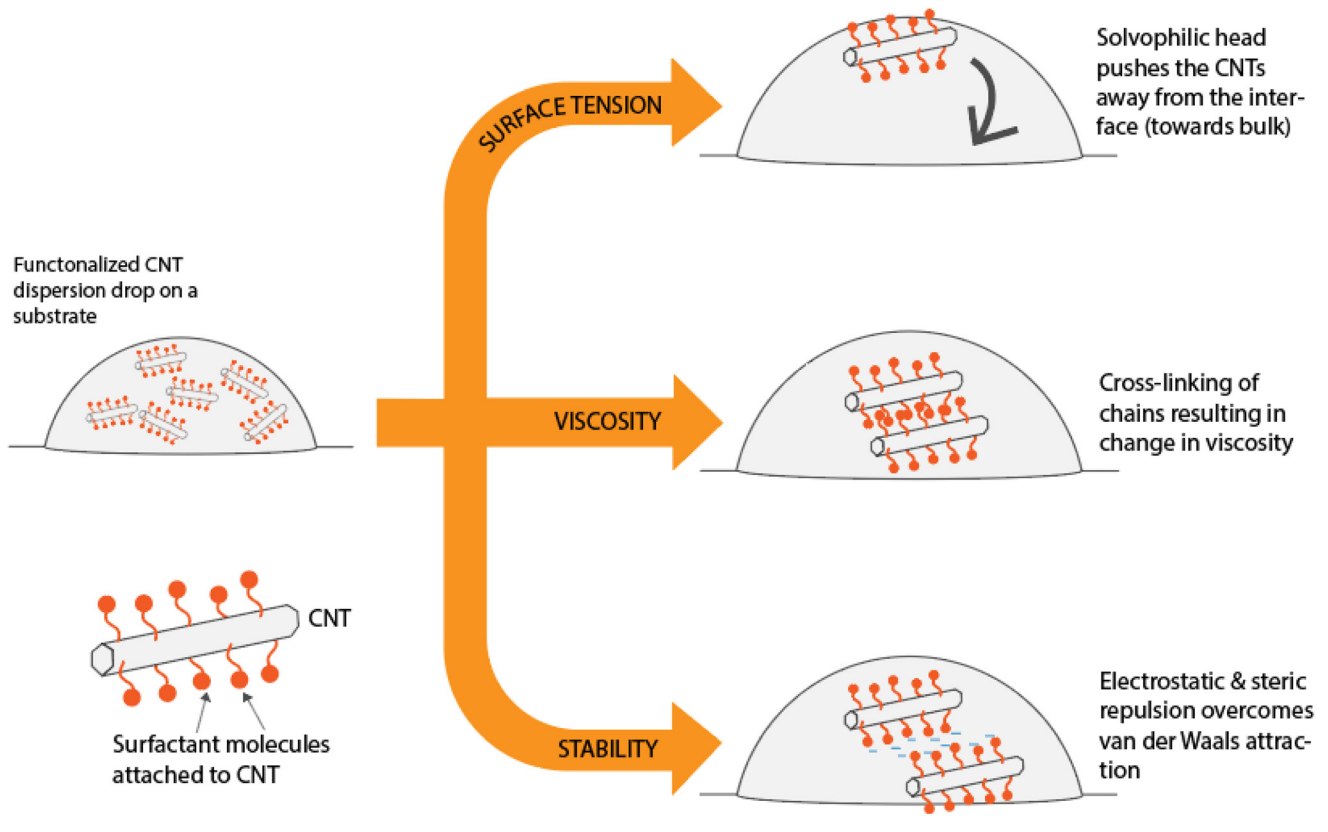

Fig. 18 Schematic illustrating the role of surfactants in modifying the surface tension, viscosity, and stability of CNT-based ink droplets containing functionalized-CNT particles.

GNP/PLA systems under low shear rates, but pseudo-plastic flow behavior in MWCNT/PLA systems under the same shear rates. Different viscosity values were observed in specimens depending on the fabrication method (solution blending or melt mixing). The GNP/PLA NC ink fabricated by the solution blending system exhibited a larger viscosity as compared to the MWCNT/PLA ink having the same filler percentage. On the other hand, a MWCNT/PLA NC ink fabricated using the melt mixing method demonstrated a much larger viscosity. Moreover, under the melt mixing method, the viscosity of MWCNT/PLA ink increased over 10 times with filler content increasing from 1.5% to 6%, while the viscosity for GNP/PLA ink increased less than 5 times under the same filler content change [see Fig. 19(a and b)].[177]

C.2.2 Stabilization of CNT inks. Dispersity of CNT is typically poor in pure solvents (especially water or organic solvents like IPA), or polymer matrices, because of the strong π–π interactions between the CNTs which leads to aggregation of particles into bundles or rope. Such aggregation is undesirable as it results in a non-uniform concentration of CNTs in the ink, thereby affecting the print quality. It also affects the shelf life of the CNT-based inks and also causes blockage in the printing nozzle.[190,191] To avoid aggregation, colloidal stabilization is typically achieved by controlling the interparticle forces (potential) and by providing means of altering the system to overcome the attractive interparticle forces, often described by the Derjaguin–Landau–Verwey–Overbeek (DLVO) theory.[192] Stable colloid suspensions of CNT can be achieved by means of (1) mechanical treatments, (2) dispersion in solvents, (3) covalent functionalization of CNTs, and (4) addition of external surfactants/stimuli.

Firstly, mechanical techniques rely on using mechanical forces to disperse the CNT particles and de-bundle the CNT clusters. Mechanical techniques include ultrasonication which uses ultrasonic transducers, ball-milling, calendaring, stir and melt compounding.[193,194]

Secondly, obtaining stable dispersion of CNTs through dispersing in solvents depends on identifying solvents in which the CNTs are thermodynamically soluble, *i.e.* identifying solvents that when combined with CNT possesses a negative value of free energy of mixing.[195] Some of the commonly used solvents include hexamethylphosphoramide, *N*-methyl-2-pyrrolidone (NMP), dimethylformamide (DMF), cyclopentanone, tetramethylene sulfoxide,[195–197] acids such as cholic acid,[181] taurocholic acid,[182] and deoxycholic acid,[183] super-acids,[198,199] and cyclohexyl-pyrrolidone (CHP).[90,200] However, in many solvents the stability of the dispersed CNTs is observed only for smaller concentrations of CNT.[201]

Thirdly, covalent functionalization of CNTs have been used to stabilize the CNT based inks. Such functionalization works on the principle of modifying the sidewall or the terminal surfaces of the carbon nanotubes by covalent attachment of the functional groups such as –COOH, –OH, –COOR, $–NH_2$, $–SO_3H$,[194,202–209] which in turn improved the solubility of CNT particles in the selected solvent. Typically, such covalent modifications of the CNT walls disturb the π electron configuration, as there is conversion of π (sp^2) to σ (sp^3) which affects the electrical performances of CNTs.[209]

Finally, the most common method used for colloidal stabilization of CNT-based inks is the non-covalent functionalization where external additives (such as polymers and surfactants) are added to the solution. These external additives are categorized into non-ionic surfactants, ionic-surfactants, and biopolymers. These surfactant molecules interact with the CNTs through either adsorption or wrapping and achieve stabilization by altering strong π–π interactions between different CNTs. For non-ionic surfactants, typically steric interactions between the chains of the surfactants prevents the aggregation of the CNTs. For ionic surfactants, the electrostatic repulsion between the adsorbed surfactant molecules, in addition to the steric interactions, prevent the CNT aggregate formation.

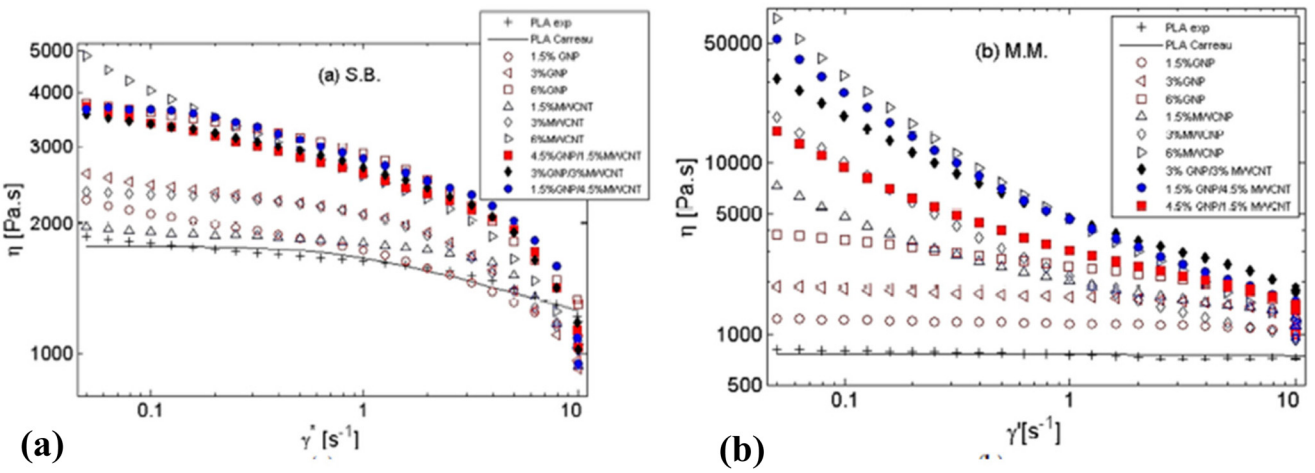

Fig. 19 (a and b) Viscosity *vs.* shear rate for CNT or GNP fillers impregnated PLA and prepared through (a) solution-blended method and (b) melt-mixed method, tested under at 200 °C. Both the parts of this figure have been reproduced from ref. 177.

Other than amphiphilic surfactant molecules or biopolymers, additives such as organic dyes are also sometimes used to improve the stability of the CNTs in the solvent. These organic dyes have strong π–π interactions with the CNT surfaces and hence prevent aggregation. Some of the additives include organic dyes such as crystal violate (CV)[184] and indigo carmine (IC),[185] these additives enhancing the CNT dispersibility in both organic solvents and water. Other external stimulus like irradiation with microwave,[210] electron beam,[211] plasma,[212] and gamma radiation,[213] has also been used to increase the CNT dispersity by modifying the CNT surface *via* the alteration of the C=C bonds.

The dispersity of colloids achieved through surfactants depends on several parameters including surfactant concentration, chain length, size of head group, zeta potential (ionic surfactant), molecular structure (presence or absence of aromatic groups to promote directional stacking), *etc*. For a given initial CNT concentration, the surfactant performance enhances with surfactant concentration (especially for the amphiphilic surfactant molecules), until it reaches an optimal level after which the performance decreases with increase in surfactant concentration. This is because with an increase in the surfactant concentration initially, the dispersity increases as more surface area gets covered with the surfactant. The limited adsorption sites on the CNT surface means that the adsorption becomes saturated at certain surfactant concentration above which reverse micellization occurs. Such reverse micellization promotes aggregation of CNTs: hence the dispersity decreases above such critical surfactant concentration.[201,214] Other studies, found that the agglomeration and the sedimentation could be reduced by increasing the ratio of surfactant to CNTs.[215] Almanassra *et al.* compared the viscosity and stability of CNT-water nanofluids in presence of three types of surfactants [namely, Gum Arabic (GA), sodium dodecyl sulfate (SDS), and polyvinyl pyrrolidone (PVP)] for different CNT weight percentages as well as different CNT to surfactant ratios. The highest suspension stability was found for the case with CNT : SDS-surfactant = 1 : 1 (for different weight percentages of CNT) (shown below in Fig. 20). This behavior seems to be in contrast to what was observed in other studies. Such a behavior could result from the fact that the studied range of concentration was smaller than the critical surfactant concentration before which reverse micellization occurs. Similar non-monotonic agglomeration behavior was shown in a CNT–epoxy composite where PVP was used as a surfactant. The authors reported optimal stability with reduced aggregation at 1.5% wt concentration of PVP, while extensive aggregation was noted at 2.0% wt concentration of PVP.[216]

The length of the surfactant molecule's tail also plays a significant role in the adsorption of the surfactant molecule to the CNT surface and hence the dispersion process. Longer tail ensures larger spatial volume and hence has larger steric hinderance which promotes intermolecular repulsion and hence dispersion.[217] In ionic surfactants, the surfactant molecules adsorbed onto the CNT surface possesses charge on its headgroup, where electric double layer is eventually formed. The extent of charge on the surfactant is quantified by means of zeta potential. For the case of larger zeta potential values, the electrostatic repulsions between the surfactant molecules will be larger leading to better dispersion.[201]

Finally, certain molecular configurations of the surfactants can promote adsorption and hence dispersion. For instance, the surfactant molecules with aromatic groups can adsorb strongly to the CNT surfaces. Benzene ring in the surfactant molecule will interact with the delocalized π-electrons of MWCNTs *via* π–π stacking which will enhance the adsorption of the surfactants.[214,218–228] Many commonly used surfactants molecules such as SDBS, pyrene, anthracene, silk sercin, curcumin ensure very good dispersion of the CNT molecules owing to this reason. The mechanism of interaction of different types of surfactant molecules with CNTs is provided in Table 5.

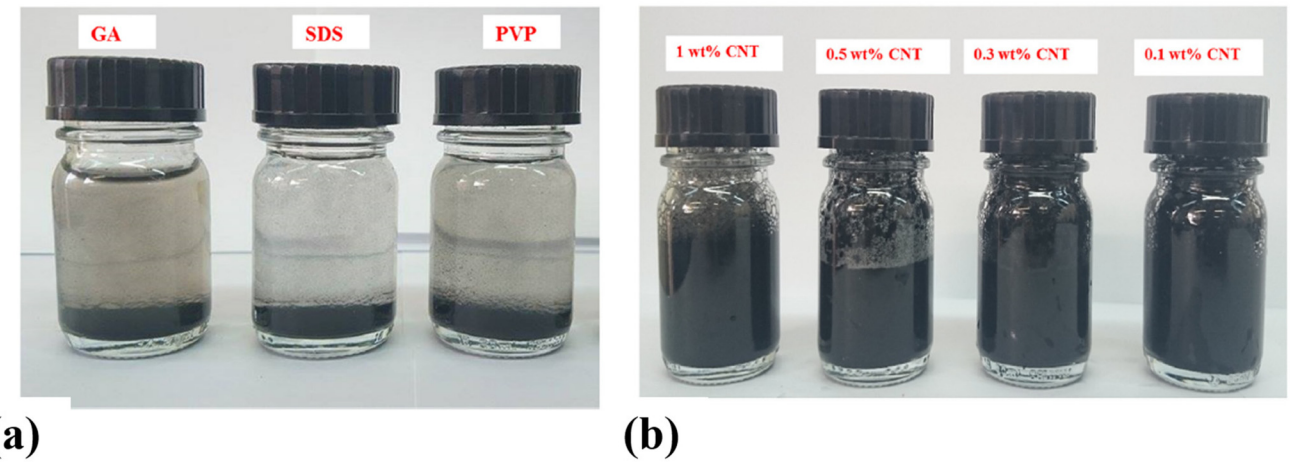

Fig. 20 Stability of CNT-water inks under different conditions. (a) 36 h stability of the CNT-water suspensions with 0.5 wt% CNT and CNT : surfactant = 1 : 0.2; (b) 6-month stability with of the CNT-water suspensions (for different CNT weight percentages) with CNT : SDS-surfactant = 1 : 1. Both the parts of this figure have been reproduced from ref. 215 with permission from Elsevier, copyright 2020.

Table 5 Table of surfactants and their effect on NP-solvent dispersions

Compound	Interaction mechanism	Ref.
Non-ionic surfactant		
PVP	Wrapping of polymer around nanotubes provide steric stabilization	229–232
Pyrene	π–πstacking of benzene ring in the polyaromatic polymer promotes adsorption to CNT	210–220 and 233
Anthracene		219, 221 and 222
Terphenyl		221 and 223
Triton X-100, X-114, X-165, X-304	Adsorption through interaction of the aromatic ring with CNT surface through π-stacking interactions	224–228
Tween-80,60,20	Adsorption through hydrophobic tail – CNT interaction	217, 234 and 235
NP-10		214
Pluronic	Hydrophobic interaction of tail with CNT. Large hydrophobic–hydrophilic component ratio leads to lower driving force for micellization.	236–240
Ionic surfactant		
SDS	Hydrophobic tail consisting of carboxyl groups attaches to the CNT surface and the hydrophilic sulfonic head groups dissolves in water to enhance the dispersity of CNTs.	190, 214, 217, 229 and 241–243
SDBS/NaDDBS	Interaction of the localized π electrons of CNT with benzene ring in the SDBS leading to π–π stacking promoting adsorption of SDBS to CNT.	191, 214 and 244–252
SDSA	Hydrophobic tail – CNT interactions	219 and 253–255
SC		201 and 256–259
LDS	Adsorption through solvatophobic tails and through "cation–π" complex at the CNT surface.	201 and 260–263
PFOA		263 and 264
CTAB	Hydrophobic tail-CNT interactions. Bromide ion shielding of head groups helps adsorption close to each other. Wrapping around CNT at larger CNT diameter.	214, 259 and 265–267
DTAB		267 and 268
TTAB		201 and 269–271
Biopolymers		
Xylan hydrate crystal (XHC)	Carboxymethylization of XHC surface with carboxyls enables the amphiphilic molecule to adsorb to CNT surface and provide stability.	186
Silk fibroin (SF)	Hydrophobic interaction of non-polar moieties in SF with CNT surface	191 and 272–274
Curcumin	Strong π–π interaction between the aromatic groups	223 and 275
Sericin	Strong π–π interaction between the aromatic groups in sericin (in the side chain groups of amino acid residues) and the CNTs prevents aggregation of CNTs. Columbic repulsion due to the negative charges on the silk sericin-CNT (SSCNT) also enhances stabilization.	191, 272 and 276
Bovine serum albumin (BSA)	Positive non-polar patches of protein interaction with hydrophobic CNT surface	191, 277 and 278

C.3. Surface tension of the CNT-laden liquid drops

The wettability of the CNT-based nNC inks has been drawing attention in the context of understanding their printability and the resulting post-printing behavior on different surfaces. For example, Dinh *et al.* inkjet-printed patterns of MWCNTs dispersed in water in the presence of some surfactants and characterized the evaporation driven self-assembly behavior of the MWCNTs.[48] Wang *et al.* studied the interactions between MWCNT droplets and glass substrates (cleaned with ethanol) and found a drop equilibrium contact angle of 10 ± 1° and a drop advancing contact angle of 15 ± 1°.[40] To study the hydrodynamic properties and interaction between the droplet (droplet of this nNC CNT ink) and the substrate, Yu *et al.* tested the ink droplet contact angle with different CNT weight content to indicate the printability: they reported that the contact angle increased from 47.4° to 52.3° on gas-treated basal plane when the CNT content increased from 6 wt% to 8 wt%.[59] Kwon *et al.* inkjet-printed electrode patterns on paper using MWCNT aqueous suspension and continuously monitored the droplet contact angle as a function of time (see Fig. 21).[32]

As discussed before, the wettability of the ink on a specific surface depends on the energy of interaction between the ink and the surface. It is mentioned in the previous section C.2. that the dispersibility of CNT-based inks is usually low in multiple kinds of solvents: the dispersibility of CNTs in those solvents dictates the surface tension and hence the wettability (on different surfaces) of the corresponding CNT-solvent ink. Moreover, different treatments, or the presence of specific functional groups (with different hydrophobic zones) on the CNTs can also affect the wettability of the corresponding CNT-based inks. Also, there are instances where a mixture of solvents has been used to meet the surface tension and viscosity requirements of the CNT-based inks. For example, Lin *et al.* dispersed CNTs into the mixture of glycerol and water (weight ratio 1 : 3) to obtain a desirable surface tension of the ink.[279] Berrada *et al.* compared the surface tension of CNT-based nanofluids in DI water with the surface tension of CNT-based nanofluids dispersed in Tyfocor without any surfactant and identified an opposite relationship between the mass concentration and surface tension in these two cases, which could be attributed to the differences in affinity of functionalized CNTs between DI water and Tyfocor.[280]

Surface tension decreases with an increasing wt% of the functionalized MWCNTs in DI solution as functionalized MWCNTs bear hydrophobic zones due to which affinity with air/water interface is expected to increase, leading to reduction of surface tension with an increase in the concentration of the MWCNTs (see Fig. 22).[280] In case of Tyfocor solution, however, the covering of hydrophobic surfaces of MWCNTs by the

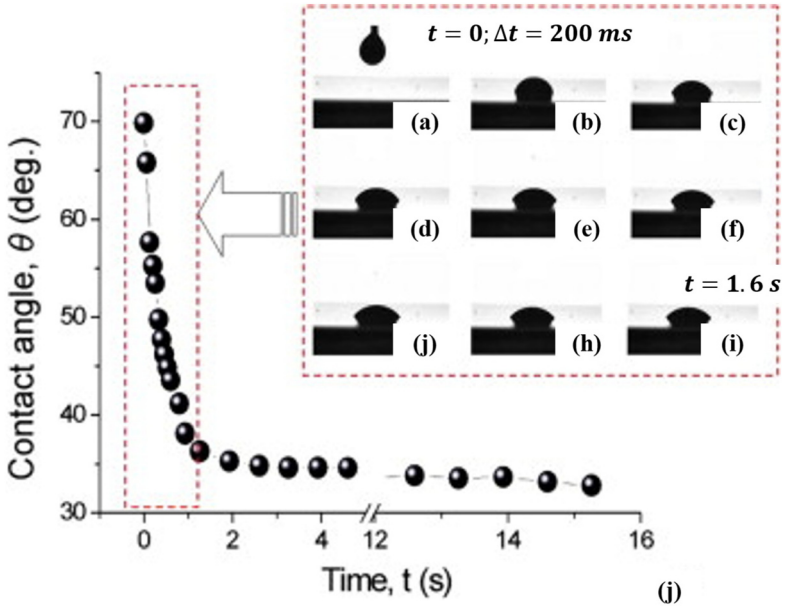

Fig. 21 (a)–(i) Images showing wetting dynamics of a 1 μL MWCNT ink drop on paper as a function of time and (j) measured contact angle. All the parts of this figure have been reproduced from ref. 32 with permission from Elsevier, copyright 2013.

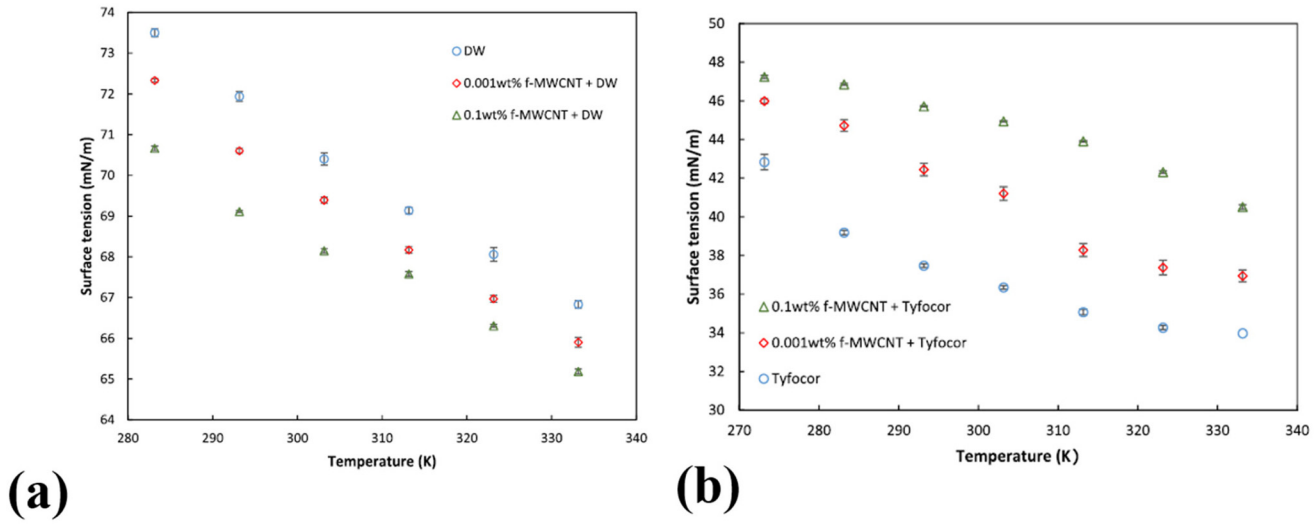

Fig. 22 Surface tension of CNT-based nanofluids using different base fluid: (a). DI water; (b). Tyfocor. Both the parts of this figure have been reproduced from ref. 280 with permission from Elsevier, copyright 2019.

polymer chains of propylene glycol increases the affinity between MWCNTs and Tyfocor leading to an increase in surface tension with the concentration of NPs.

Environmental temperature and particle sizes are among several factors that contribute to the surface tension of CNT-based fluids. For charged nanoparticulate fluids, larger nanoparticle size normally leads to a higher surface tension due to smaller surface charge density.[281] For CNT-based inks, the particle size or the length and diameters of CNTs can be modified through the methods mentioned in the previous section. Meanwhile, it is widely noticed that increasing the temperature can result in decreasing the fluid surface tension.[282–284] Mei *et al.*, for example, showed that the surface tension of CNT-suspended nano-fuels always decreased with an increase in temperature for different values of CNT particle size and mass concentration.[285]

C.4. Sintering and drying of 3D-printed CNT-based inks

For CNT inks, the thermal assisted sintering process is sometimes evitable, but it has been noted in several studies that the

electrical performances of the CNT-based printed products will change after several rounds of thermal cycling.[286] Also there are a few studies probing the behavior of CNT-alloy or CNT-wood plastic composites during selective laser sintering (SLS) 3D printing. Zhang *et al.* 3D printed CNT-wood powder/polyether sulfone (PES) composite using selective laser sintering method, followed by microwave irradiation based post-printing treatment.[287] The authors found that the interfacial bonding between PES and CNT could be enhanced through microwave treatment, and the overall bending strength of the printed component was improved. Qi *et al.* printed CNT coated PA11/$BaTiO_3$ powders using SLS and found those CNT-coated powders have wider sintering window as well as better radiation absorption capabilities, as compared to conventional powders.[288] Duan *et al.* studied the effects of CNT content during microwave sintering on Cu/CNT composite and found that the product with 0.5 wt% of CNTs exhibited optimal properties. They also noticed agglomerations of CNTs (and hence a lesser control on their micro-structures during sintering) when its weight percentage was over 1%.[289] Zhang *et al.* sintered CNT-Al_2O_3 composites under different volume ratio of MWCNTs, and identified that by using pressure-less sintering method it was possible to avoid degradation of CNTs during sintering.[290] Yuan *et al.* employed SLS based 3D printing to print CNT-coated polyamide powders and noticed that the presence of the CNT improved both thermal and mechanical properties of fabricated composites.[291]

For most of the cases in 3D printing CNT-based inks, especially for those applying inkjet or syringe printing methods, evaporation process would be sufficient to provide functional products with acceptable qualities. The main challenge here is to be able to achieve uniform material deposition across the printed patterns. One common phenomenon is the 'coffee-ring' formation after sintering or evaporation-driven curing, and this will be discussed in the following section C.5.

C.5. Coffee-ring formation by the CNT drops

'Coffee-ring' formation after sintering and/or evaporation process can be widely seen in experiments with carbon-based suspensions as well as with printable SWCNT/MWCNT-based inks.[28,30,40,48,57]

In this section, we shall first list the "coffee-stain" phenomenon observed in different kinds of CNT-rich droplets, including CNT-suspensions and CNT-based NC or nNC 3D printable inks. We also provide a schematic that shows the different factors that affect the coffee-stain formation in CNT-based inks in Fig. 23. Second, we shall discuss the different issues and problems associated with the formation of such "coffee-stain" and the directions of utilizing such "coffee stain" effect to achieve desired properties of the printed patterns. Finally, we shall discuss different methods employed to suppress or precisely control the "coffee stain" formation in different kinds of CNT-based ink systems.

Wang *et al.* inkjet-printed MWCNT networks for fabricating conductive films and found that the coffee-stain formation was an important factor that affected the film quality. They studied the manner in which the droplet spacing affects the morphology of printed traces, thereby designing an optimum spacing for uniform 'ring' edge formation after evaporation.[40] Dinh *et al.* noticed the coffee-ring structure of MWCNT patterns and utilized this structure to form the conductive twin lines [see Fig. 24(a–c)].[48] Liu *et al.* found coffee-stain formation in dried SWCNT patterns on silicon substrate.[28] Zhao *et al.* compared the patterns formed by evaporated droplets of CNT, GO, and CNT/GO, and coffee-ring structures were noticed only in CNT-only inks but not in GO suspensions.[30]

In order to improve the product quality and achieve the desired deposited CNT pattern, three methods have been tested to ensure the arrest of such post-printing coffee-stain effect. Wang *et al.* studied coffee-stain formation on substrates maintained at different temperatures and found that the coffee staining formed in MWCNT droplets could be sup-

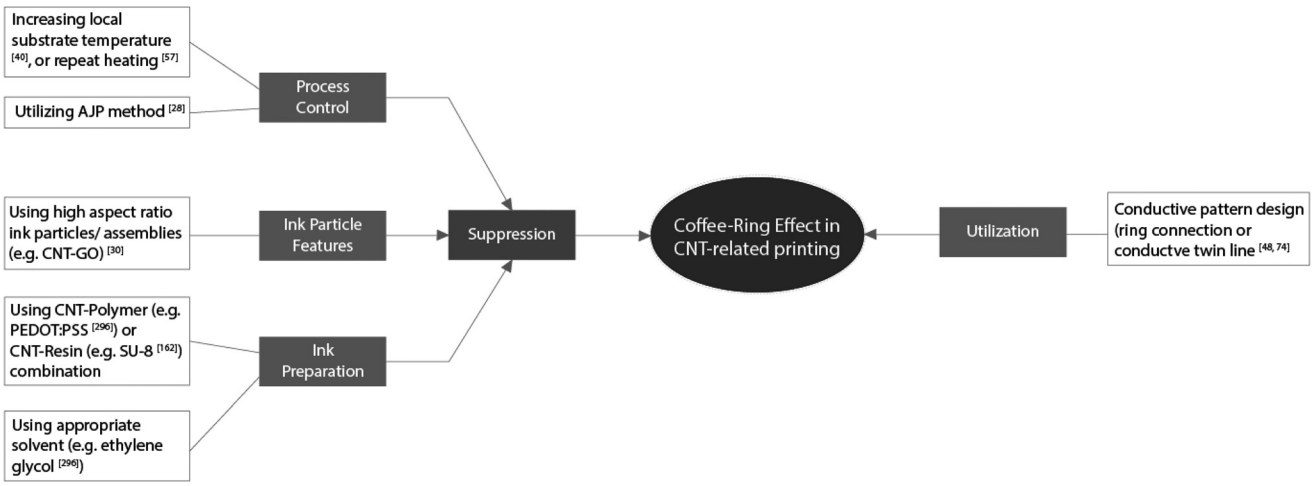

Fig. 23 Schematic of different factors at play that affect the "coffee stain" formation in CNT-based inks.

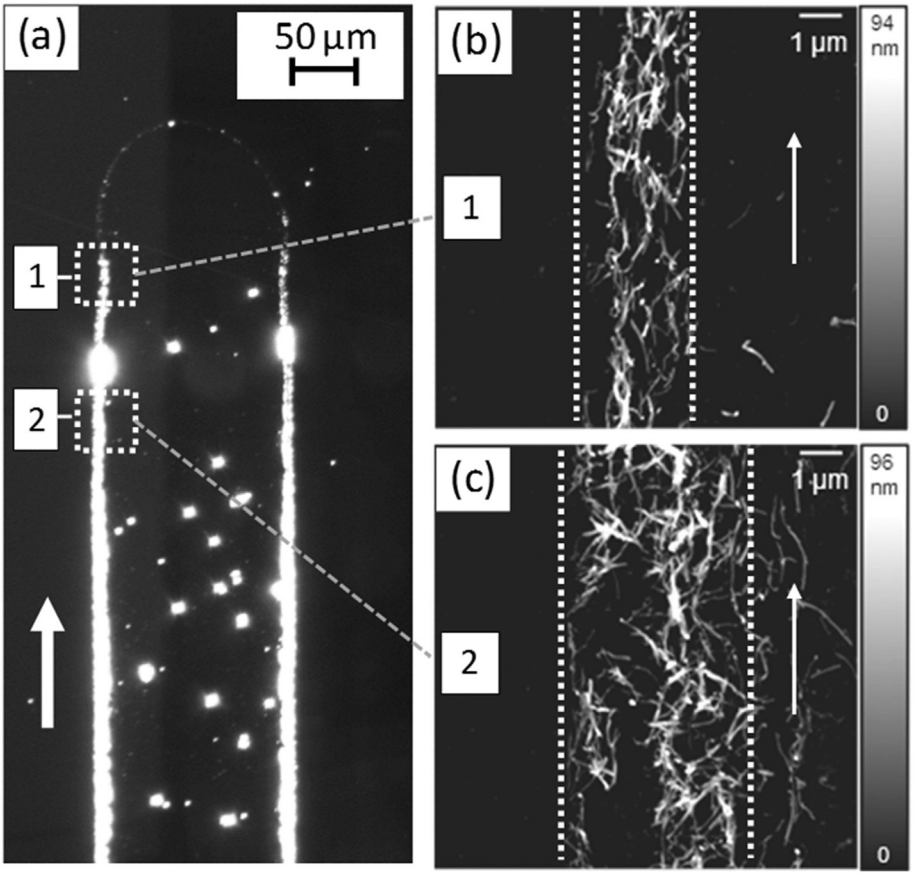

Fig. 24 Characterizations of coffee-stain formed in the MWCNT and SWCNT inks. (a–c) AFM images indicating coffee-stain phenomena in printed MWCNT lines (showing agglomerate position and direction). Both the parts of this figure have been reproduced from ref. 48 with permission from Elsevier, copyright 2016.

pressed by increasing substrate temperature.[40] They considered substrates maintained at room temperature, at 60 °C, and at 70 °C, and found that the most uniform deposition profile was obtained for the case of $T_{substrate}$ = 70 °C. This is not consistent with some other experimental results using polymer solution and it is probably due to the variation in the droplet surface tension caused by a local variation in temperature and droplet composition.[292–296] Results similar to Wang *et al.* were observed in the study by Dinh *et al.*[48] that considered the morphology of MWCNT patterns. This study further optimized those printing parameters (*e.g.*, drop spacing and substrate temperatures) and achieved accurate fabrication of conductive twin-line by leveraging the 'coffee-stain' effect (see Fig. 25). Majumder *et al.* reported coffee-stain formation in dried droplets of SWCNT suspension (with SDBS as solvents). They noticed that a rapid heating method could suppress the formation of the 'coffee-ring'.[57] Liu *et al.* found that for same materials and substrate, the patterns deposited by drop-casting formed coffee-ring structure, while the one deposited through AJP showed less obvious agglomerations. This indicated to the possibility of eliminating coffee-ring formation through different fabrication methods.[28] Dou and Derby hypothesized that substrate porosity might also impact the formation of the coffee-stain and they tested their hypothesis with several types of metal-nanoparticle based inks.[152]

Researchers have also investigated the effect of nanoparticle shape on the evaporation-induced pattern formation and its role in 3D printing. For example, Zhao *et al.* found that an ink formulation containing only CNT and DI water would certainly result in a coffee-stain formation.[30] However, mixing it with other materials, like flake-like graphene-oxide (GO) nanosheets, could ensure a suppression of the coffee stain effect, which was explained by the shape-dependent arrest of the 'coffee-ring' effect introduced earlier.[158] Through microscopy and surface profilometry measurements, this study clearly demonstrated that the ink with only CNT nanoparticles presented the most obvious coffee-ring formation, while the GO solution had no formation of coffee-stain (see Fig. 26). Therefore, an optimized ink formulation, with an appropriate GO : CNT weight percentage combination, simultaneously ensured an improved printability (by the flake-like GO induced arrest of the coffee ring effect) as well as the capability to print temperature sensors that utilized the negative temperature coefficient of resistance property of the CNTs.[30,286]

There are also examples of studies that have actually utilized the coffee-stain effect to fabricate conductive

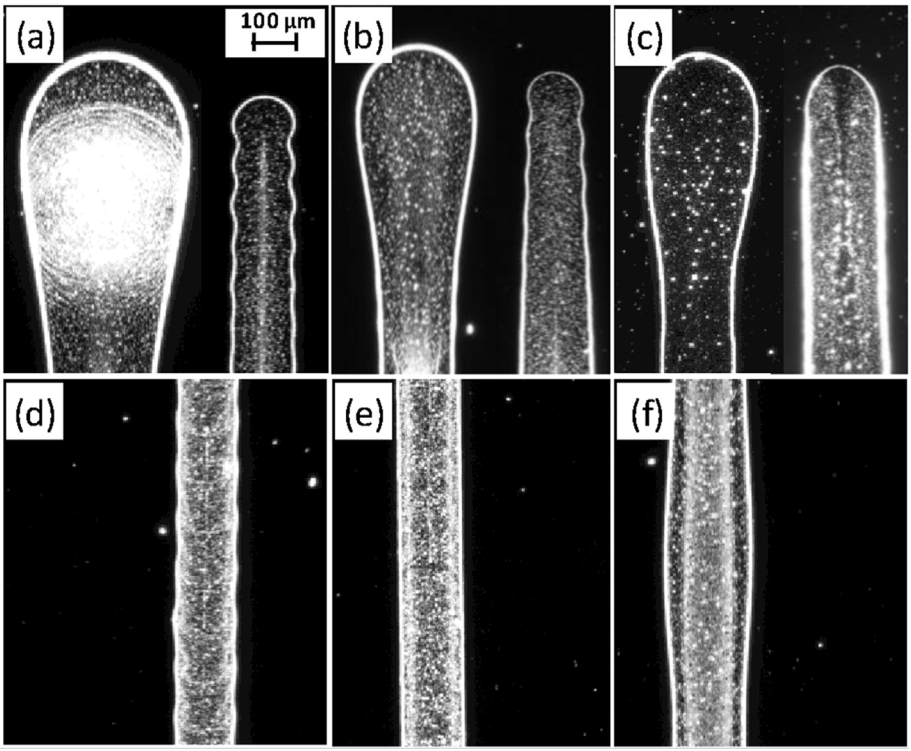

Fig. 25 Optical microscopic images of the 'coffee-ring' formed in printed MWCNT lines at substrate temperatures of (a) 35 °C, (b) 50 °C, and (c) 60 °C and droplet spacing of (d) 110 μm, (e) 90 μm, and (f) 60 μm. All the parts of this figure have been reproduced from ref. 48 with permission from Elsevier, copyright 2016.

patterns.[48,74] Shimoni *et al.*, for example, inkjet-printed SWCNT-based inks on PET substrate for fabricating transparent conductive films. They utilized the features of 'coffee-ring' formation and connected each individual CNT ring by precise deposition to form a conductive pattern. By printing films consisting of 1 to 12 printed CNT layers, they observed an almost-linear relationship between the number of layers printed and the sheet resistance. In their case, a sheet resistance of 156 Ω sq^{-1} and a transparency of 81% were achieved (see Fig. 27).[74] Dinh *et al.* also utilized this structure for printing conductive twin lines, which helped them in the alignment of those conductive twin lines formed by the edges.[48]

Several other studies probed methods for the suppression of the 'coffee-ring' in CNT–polymer or CNT–resin system.[162,292] Denneulin *et al.* compared the inkjet printing results of functional SWCNT aqueous ink and SWCNT-PEDOT:PSS ink and noticed a much more uniform distribution of the CNT particles across the printed traces for the SWCNT-PEDOT:PSS ink (see Fig. 28).[292] They suspected that this effect might be due to the Marangoni flow and the presence of the polymer chain affecting the particle migration. Mionić *et al.* studied a CNT-SU8 epoxy composite ink and found that no coffee-ring structure was formed.[162] They hypothesized that the coffee-stain was eliminated due to the fact that the SU8 epoxy resin cured slower than other solvents and maintained a liquid state for a longer duration of time.

In Table 6, we summarize the different studies that have considered the suppression or utilization of the coffee stain effect for CNT-based inks.

D. Open challenges and questions

One of the major challenges associated with the printing of CNT-based inks is obtaining a uniform dispersion of the CNTs in the solvent. These CNTs tend to attract each other strongly due to the large van der Waals (vdW) forces causing their agglomeration.[297] Agglomeration is highly undesirable as it could result in poor-quality prints by clogging the printing nozzles and causing nonuniform deposition. Various techniques have been employed by researchers to overcome this difficulty, including the use of surfactants and biopolymers in the solvent in which CNTs are dispersed, functionalizing the CNT surfaces, *etc.* (please see section C.2.2. for more discussions). Kim *et al.*, for example, provided an extensive review of the surface modifications of the CNTs that will aid in the dispersion of CNTs in the surrounding liquid medium. A popular technique of surface modification is the functionalization the CNT walls with functional groups such as –OH, –COOH, –COH which enable a proper dispersion of CNTs in various solvents. These surface modifications change the CNT–CNT vdW interactions and prevent the agglomeration and clustering.[298]

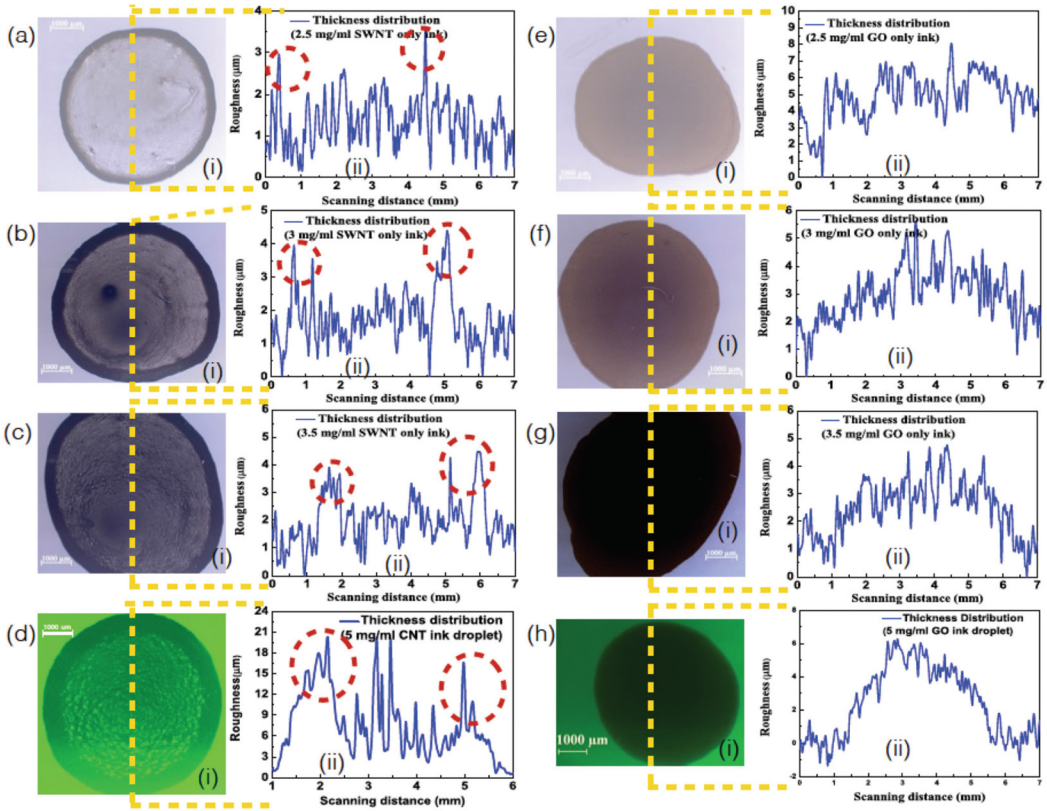

Fig. 26 (a–d, i) Top-view microscopic images of dried pure SWCNT droplets (coffee stain observed): (a–d, ii) surface height profile across the droplet diameter; (e–h, i) top-view microscopic images of dried GO droplets (no coffee stain observed): (a–d, ii) surface height profile across the droplet diameter. All the parts of this figure have been reproduced from ref. 30 with permission from Royal Society of Chemistry, copyright 2019.

Other techniques include dispersing CNTs in organic solvents such as NMP (NMP: *N*-methyl-2-pyrrolidone) and DCE (DCE: 1,2-dichloroethane),[299] or the use of dispersants such as SDS (SDS: sodium dodecyl sulfate)[300] and (NaDDBS: sodium dodecylbenzene sulfonate)[301] in water-based solvents. A continuing topic of active interest is the identification of appropriate functionalizing agents and/or dispersing agents that will simultaneously ensure: (a) most effective dispersion of CNTs in solvents; (b) easy printability of the resulting CNT-based ink with different printing methods; and (c) desirable deposition patterns after sintering.

A critical barrier in CNT-based inkjet printing is the control of the surface tension. Section C.3. has provided extensive discussions on the modification of the surface tension of the CNT-based inks by altering the solvent (in which the CNTs are dispersed), functionalization of the CNT surface, CNT sizes, environmental temperature, *etc*. Surface tension plays an important role in dictating two issues: (1) the droplet release from the tip of the nozzle; and (2) the wetting of the surface. First, at the exit of the nozzle, for the ink to be ejected properly, the surface tension of the liquid has to be low.[140] Surfactants such as SDS, NaDDBS can be used to decrease the surface tension of the ink.[302] Second, a favorable wettability of the ink on the substrate is extremely important to have a high-quality print with robust interfacial adhesion to the substrate. The surface energies of the CNT-based inks and the printing substrate as well as the interactions of the CNT-based ink and the substrate dictate this wettability. Therefore, with a prior knowledge of the substrate on which the printing is to be conducted, one needs to carefully choose the material composition of the ink. Choice of this material combination of the ink also enables a control of the CNT-ink viscosity that plays a very significant role in the printing process. Viscosity of the ink (and the corresponding shear-thinning nature of the ink) has to be maintained within a certain range known as "printability window", as mentioned earlier (please see section C.1). The range is so selected as to prevent excess fluidity on one side and blockage of the printer head (lack of fluidity) on the other end. In addition, the effect of various CNT properties on the surface tension doesn't follow a general trend and is utterly specific to the combined effect of all the factors at play. Such examples have been discussed in section C.3. What can be helpful is a handbook on controlling the surface tension of a fabricated ink.

A big drawback of the existing fabrication approaches for CNT-based inks as well as other general nanoparticulate inks stems from the fact that often these approaches rely on an *ad hoc*, iterative, trial-and-error approaches with regards to the material selection. For example, the vast number of examples discussed in sections from C.2 to C.5 identify the different

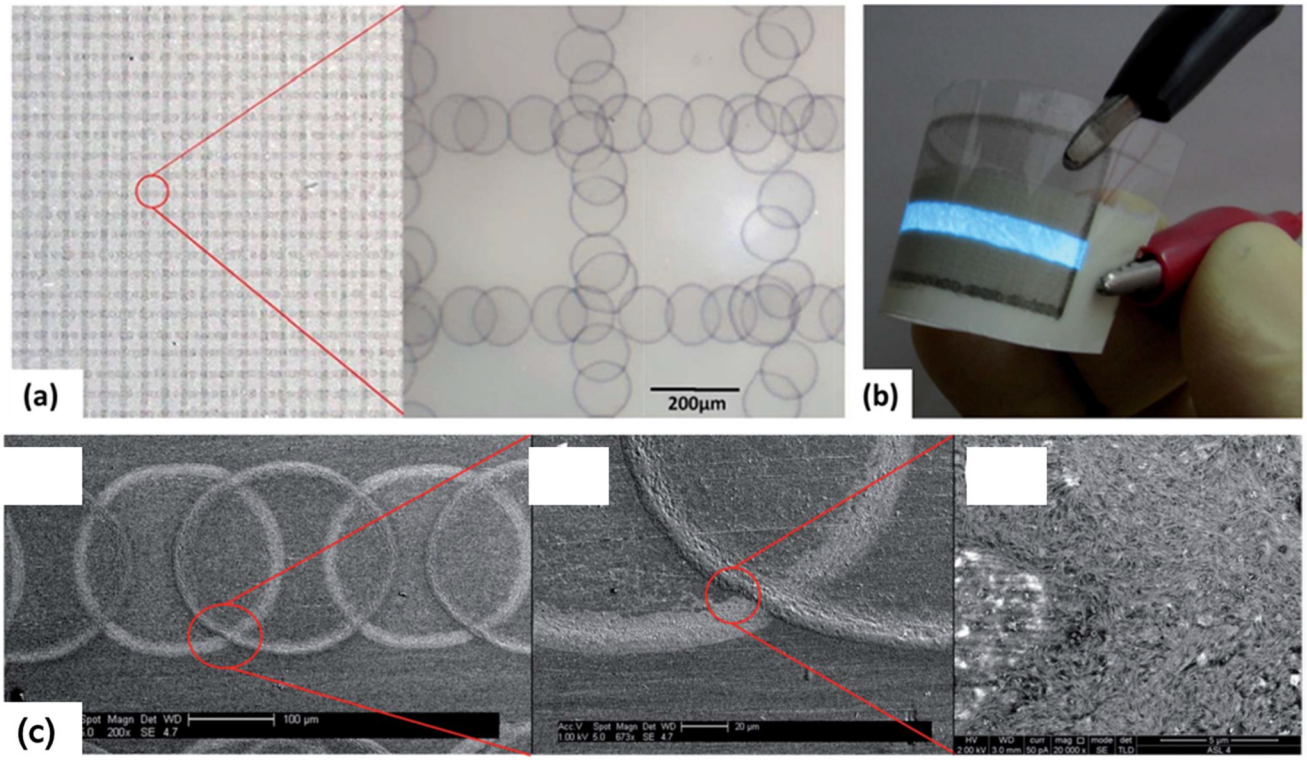

Fig. 27 (a) Printed SWNT conductive patterns. (b) Application of CNT-TCF as electroluminescent (EL) device. (c) SEM images showing the connection between each ring, which performed similar structures in connection between CNTs different rings and connection between CNTs in the same ring. All the parts of this figure have been reproduced from ref. 74 with permission from Royal Society of Chemistry, copyright 2014.

fluid mechanics properties (jettability, printability, rheology), colloidal properties (formation of coffee stain, morphology specific properties), and sintering properties of the CNT-based inks. However, virtually all the studies achieve these specific properties through a trial-and-error method without any mechanistic design-based approach. Under these circumstances, a useful alternative will be to employ sophisticated multiscale simulations to assist the initial predictions of the role of different dispersants and solvents to ensure the best quality prints with CNT-based inks. Such simulations will consist of sophisticated molecular dynamics simulations that quantify the structure of the CNT-dispersant particles (*e.g.*, CNT–GO particles in Zhao *et al.*[30]) in the solvent and use that information in a CFD (computational fluid dynamics) simulation for quantifying the structure of CNT-based printed patterns. These simulations will be easy to run and will help to significantly downsize the choice of materials that could be used with the CNTs to develop CNT-based inks with desired properties.

Besides that, only limited researches focused on the heating assisted sintering process on CNT based inks. Of course, these studies too, employ no design-based approach in optimizing the sintering performance of the CNT-based inks. One of the possible approaches that will be beneficial will be to use multiscale simulations (as identified in the previous paragraph) to identify the effect of sintering on the evaporation profile of the deposited CNT-laden drop and from that quantify (1) the final structure of the CNT-based patterns (with explicit quantification of the position and size of the CNT particles constituting the pattern) and (2) the overall macroscale properties of these patterns by using multi-phase averaging models (*e.g.*, Mori–Tanaka model[303]). Of course, for the simulation efforts described here as well as in the previous paragraph, it will be immensely helpful to obtain the exact shape and size of the CNT particles (or aggregates) within the ink itself by employing sophisticated nanoscale imaging techniques such liquid phase transmission electron microscopy[304] and compare the findings with the predictions (on the size and shape of the CNT particles) made by the MD simulations (please see the previous paragraph).

Throughout the article, we have tried to establish the relation between the nanoscale properties of the materials involved in the fabrication of the ink as well as the process and environmental factors. These relations have been discussed in detail by identifying the various mechanisms dictating the colloidal sciences and fluid mechanics aspects of the CNT-laden ink. However, these are true in a setting where only one of these parameters is varied. In a scenario where multiple parameters are varied, the resultant effect on the ink properties is hard to predict, and as mentioned in the previous paragraph, mostly becomes a trial-and-error approach at achieving the desired ink properties.

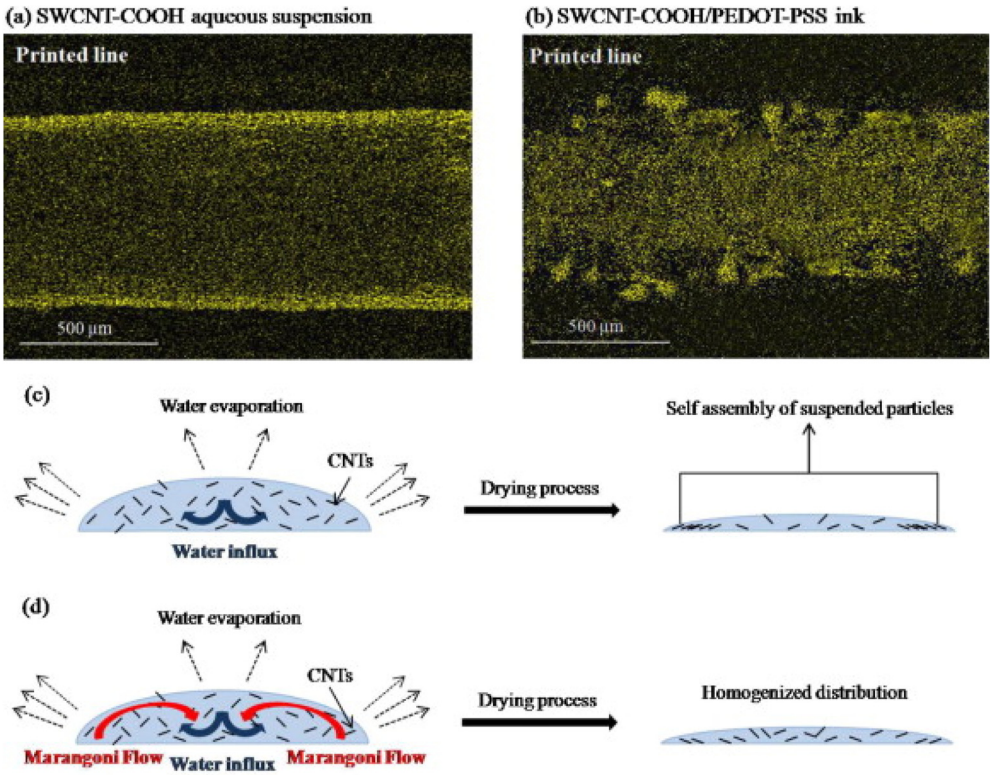

Fig. 28 Coffee stain formation/suppression in inkjet printable (a) SWCNT aqueous ink and (b) SWCNT-polymer ink (*i.e.*, SWCNT-PEDOT:PSS ink). (c) and (d) Schematic demonstration of formation/suppression of coffee-stain for the cases shown in (a) and (b), respectively. All the parts of this figure have been reproduced from ref. 292 with permission from Elsevier, copyright 2011.

Table 6 Examples of suppressions and utilizations of coffee-stain structure in CNT-based inks

Ref.	Ink composites	Methods to suppress or utilize coffee-stain formation
28	Platinum (Pt) decorated SWCNTs	Implied the AJP method to avoid un-expected agglomeration
30	CNT/GO	Suppressed the coffee-stain formation by interplay with particle shape and induce long-range capillary interaction
40	MWCNT	Suppressed coffee-ring formation by increasing substrate temperature
48	MWCNT (with TirtonX-100 as surfactant)	Utilized the coffee-ring structure to form high-resolution of conductive twin lines
74	SWCNT	Utilized coffee-ring structures to connect each droplet and form conductive patterns on transparent PET forms
57	SWCNT	Rapid heating reduced the formation of 'coffee-stain'
162	CNT-SU8 ink	The presence of Su-8 could reduce coffee-stain effect because it remained as a liquid form after solvents being evaporated.
292	PEDOT-PSS/functionalized SWCNT	Reduction in coffee stain effect by: (1). Recirculation flow introduced by ethylene glycol (2). Impeding of migration of CNT by polymer chains (3). Viscosity adjustments

E. Conclusions

3D-printable CNT-based inks have a plethora of applications relevant for a variety of industries. This article reviewed recent progress in development of CNT-based nanocomposite and CNT-based non-nanocomposite inks. Current progress in CNT based ink materials, printing process, and its applications were discussed. Furthermore, fluid mechanics and colloidal science issues of CNT-based inks, which significantly affect the ink printability and pattern formation as well as the properties of the components and devices printed with these CNT-based inks, have been discussed. The printability windows of inks using different printing techniques have been discussed and the suppression or the utilization of the coffee-stain formation and their advantages and disadvantages have been presented.

Conflicts of interest

There are no conflicts to declare.

References

1 Z. Chen, Z. Li, J. Li, C. Liu, C. Lao, Y. Fu, C. Liu, Y. Li, P. Wang and Y. He, *J. Eur. Ceram. Soc.*, 2019, **39**, 661–687.
2 H.-H. Lin, D. Lonic and L.-J. Lo, *J. Formosan Med. Assoc.*, 2018, **117**, 547–558.
3 T. Distler and A. R. Boccaccini, *Acta Biomater.*, 2020, **101**, 1–13.
4 T. D. Ngo, A. Kashani, G. Imbalzano, K. T. Q. Nguyen and D. Hui, *Composites, Part B*, 2018, **143**, 172–196.
5 X. Wang, M. Jiang, Z. Zhou, J. Gou and D. Hui, *Composites, Part B*, 2017, **110**, 442–458.
6 C. Buchanan and L. Gardner, *Eng. Struct.*, 2019, **180**, 332–348.
7 S. Patra and V. Young, *Cell Biochem. Biophys.*, 2016, **74**, 93–98.
8 V. Bagaria, R. Bhansali and P. Pawar, *J. Clin. Orthop. Trauma*, 2018, **9**, 207–212.
9 T. DebRoy, H. L. Wei, J. S. Zuback, T. Mukherjee, J. W. Elmer, J. O. Milewski, A. M. Beese, A. Wilson-Heid, A. De and W. Zhang, *Prog. Mater. Sci.*, 2018, **92**, 112–224.
10 J. Z. Gul, M. Sajid, M. M. Rehman, G. U. Siddiqui, I. Shah, K.-H. Kim, J.-W. Lee and K. H. Choi, *Sci. Technol. Adv. Mater.*, 2018, **19**, 243–262.
11 G. L. Goh, S. Agarwala and W. Y. Yeong, *Adv. Mater. Interfaces*, 2019, **6**, 1801318.
12 P. Parandoush, C. Zhou and D. Lin, *Adv. Eng. Mater.*, 2019, **21**, 1800622.
13 K. Fu, Y. Yao, J. Dai and L. Hu, *Adv. Mater.*, 2017, **29**, 1603486.
14 Q. Zhang, F. Zhang, S. P. Medarametla, H. Li, C. Zhou and D. Lin, *Small*, 2016, **12**, 1702–1708.
15 B. Elder, R. Neupane, E. Tokita, U. Ghosh, S. Hales and Y. L. Kong, *Adv. Mater.*, 2020, **32**, 1907142.
16 L. Yin, X. Tian, Z. Shang, X. Wang and Z. Hou, *Appl. Phys. A*, 2019, **125**, 266.
17 Q. Hu, Y. Duan, H. Zhang, D. Liu, B. Yan and F. Peng, *J. Mater. Sci.*, 2018, **53**, 1887–1898.
18 A. E. Jakus and R. N. Shah, *J. Biomed. Mater. Res., Part A*, 2017, **105**, 274–283.
19 Z. Hao, X. Xu, H. Wang, J. Liu and H. Yan, *Ionics*, 2018, **24**, 951–965.
20 Y. Li, X. Huang, L. Zeng, R. Li, H. Tian, X. Fu, Y. Wang and W.-H. Zhong, *J. Mater. Sci.*, 2019, **54**, 1036–1076.
21 B. Derby, *Engineering*, 2015, **1**, 113–123.
22 L. Nayak, S. Mohanty, S. K. Nayak and A. Ramadoss, *J. Mater. Chem. C*, 2019, **7**, 8771–8795.
23 D. Miyashiro, R. Hamano and K. Umemura, *Nanomaterials*, 2020, **10**, 186.
24 S. Ghoshal, *Fibers*, 2017, **5**, 40.
25 S. K. Eshkalak, A. Chinnappan, W. A. D. M. Jayathilaka, M. Khatibzadeh, E. Kowsari and S. Ramakrishna, *Appl. Mater. Today*, 2017, **9**, 372–386.
26 D. Xiang, X. Zhang, E. Harkin-Jones, W. Zhu, Z. Zhou, Y. Shen, Y. Li, C. Zhao and P. Wang, *Composites, Part A*, 2020, **129**, 105730.
27 A. S. Alshammari, M. R. Alenezi, K. T. Lai and S. R. P. Silva, *Mater. Lett.*, 2017, **189**, 299–302.
28 R. Liu, H. Ding, J. Lin, F. Shen, Z. Cui and T. Zhang, *Nanotechnology*, 2012, **23**, 505301.
29 Y. Qin, H.-J. Kwon, A. Subrahmanyam, M. M. R. Howlader, P. R. Selvaganapathy, A. Adronov and M. J. Deen, *Mater. Lett.*, 2016, **176**, 68–70.
30 B. Zhao, Y. Wang, S. Sinha, C. Chen, D. Liu, A. Dasgupta, L. Hu and S. Das, *Nanoscale*, 2019, **11**, 23402–23415.
31 S. Z. Guo, X. Yang, M. C. Heuzey and D. Therriault, *Nanoscale*, 2015, **7**, 6451–6456.
32 O.-S. Kwon, H. Kim, H. Ko, J. Lee, B. Lee, C.-H. Jung, J.-H. Choi and K. Shin, *Carbon*, 2013, **58**, 116–127.
33 M. Dragoman, E. Flahaut, D. Dragoman, M. al Ahmad and R. Plana, *Nanotechnology*, 2009, **20**, 375203.
34 A. Lesch, F. Cortés-Salazar, V. Amstutz, P. Tacchini and H. H. Girault, *Anal. Chem.*, 2015, **87**, 1026–1033.
35 E. Gracia-Espino, G. Sala, F. Pino, N. Halonen, J. Luomahaara, J. Mäklin, G. Tóth, K. Kordás, H. Jantunen, M. Terrones, P. Helistö, H. Seppá, P. M. Ajayan and R. Vajtai, *ACS Nano*, 2010, **4**, 3318–3324.
36 H. Okimoto, T. Takenobu, K. Yanagi, Y. Miyata, H. Shimotani, H. Kataura and Y. Iwasa, *Adv. Mater.*, 2010, **22**, 3981–3986.
37 X. Guan, L. Cao, Q. Huang, D. Kong, P. Zhang, H. Lin, W. Li, Z. Lin and H. Yuan, *Polymers*, 2019, **11**, 973.
38 Y. Jiang, M. Cheng, R. Shahbazian-Yassar and Y. Pan, *Adv. Mater. Technol.*, 2019, **4**, 1900691.
39 H. Okimoto, T. Takenobu, K. Yanagi, Y. Miyata, H. Kataura, T. Asano and Y. Iwasa, *Jpn. J. Appl. Phys.*, 2009, **48**, 06FF03.
40 T. Wang, M. A. Roberts, I. A. Kinloch and B. Derby, *J. Phys. D: Appl. Phys.*, 2012, **45**, 315304.
41 K. Kordás, T. Mustonen, G. Tóth, H. Jantunen, M. Lajunen, C. Soldano, S. Talapatra, S. Kar, R. Vajtai and P. M. Ajayan, *Small*, 2006, **2**, 1021–1025.
42 S. R. Shin, R. Farzad, A. Tamayol, V. Manoharan, P. Mostafalu, Y. S. Zhang, M. Akbari, S. M. Jung, D. Kim, M. Comotto, N. Annabi, F. E. Al-Hazmi, M. R. Dokmeci and A. Khademhosseini, *Adv. Mater.*, 2016, **28**, 3280–3289.
43 S. G. Bucella, J. M. Salazar-Rios, V. Derenskyi, M. Fritsch, U. Scherf, M. A. Loi and M. Caironi, *Adv. Electron. Mater.*, 2016, **2**, 1600094.
44 M. Bordoni, E. Karabulut, V. Kuzmenko, V. Fantini, O. Pansarasa, C. Cereda and P. Gatenholm, *Cells*, 2020, **9**, 682.
45 A. Lesch, F. Cortés-Salazar, M. Prudent, J. Delobel, S. Rastgar, N. Lion, J.-D. Tissot, P. Tacchini and H. H. Girault, *J. Electroanal. Chem.*, 2014, **717–718**, 61–68.
46 C. O'Mahony, E. Ul Haq, C. Sillien and S. A. M. Tofail, *Micromachines*, 2019, **10**(2), 99.
47 G. Postiglione, G. Natale, G. Griffini, M. Levi and S. Turri, *Composites, Part A*, 2015, **76**, 110–114.
48 N. T. Dinh, E. Sowade, T. Blaudeck, S. Hermann, R. D. Rodriguez, D. R. T. Zahn, S. E. Schulz,

R. R. Baumann and O. Kanoun, *Carbon*, 2016, **96**, 382–393.
49 G. C. Pidcock and M. in het Panhuis, *Adv. Funct. Mater.*, 2012, **22**, 4790–4800.
50 Y. Ding, H. Alias, D. Wen and R. A. Williams, *Int. J. Heat Mass Transfer*, 2006, **49**, 240–250.
51 A. W. K. Ma, M. R. Mackley and F. Chinesta, *Int. J. Mater. Form.*, 2008, **1**, 75–81.
52 E. K. Hobbie and D. J. Fry, *J. Chem. Phys.*, 2007, **126**, 124907.
53 R. Ivanova and R. Kotsilkova, *Appl. Rheol.*, 2018, **28**, 201854014.
54 A. W. K. Ma, F. Chinesta, M. R. Mackley, A. Co, G. L. Leal, R. H. Colby and A. J. Giacomin, in *AIP Conference Proceedings*, AIP, 2008, pp. 752–754.
55 A. Shahsavar and M. Bahiraei, *Powder Technol.*, 2017, **318**, 441–450.
56 T. Gao, Z. Zhou, J. Yu, J. Zhao, G. Wang, D. Cao, B. Ding and Y. Li, *Adv. Energy Mater.*, 2019, **9**, 1802578.
57 M. Majumder, C. Rendall, M. Li, N. Behabtu, J. A. Eukel, R. H. Hauge, H. K. Schmidt and M. Pasquali, *Chem. Eng. Sci.*, 2010, **65**, 2000–2008.
58 S. Agarwala, G. L. Goh, G. D. Goh, V. Dikshit and W. Y. Yeong, in *3D and 4D Printing of Polymer Nanocomposite Materials*, Elsevier, 2020, pp. 297–324.
59 W. Yu, H. Zhou, B. Q. Li and S. Ding, *ACS Appl. Mater. Interfaces*, 2017, **9**, 4597–4604.
60 J. H. Kim, S. Lee, M. Wajahat, H. Jeong, W. S. Chang, H. J. Jeong, J. R. Yang, J. T. Kim and S. K. Seol, *ACS Nano*, 2016, **10**, 8879–8887.
61 W. R. Small and M. in het Panhuis, *Small*, 2007, **3**, 1500–1503.
62 L. Yang, R. Zhang, D. Staiculescu, C. P. Wong and M. M. Tentzeris, *IEEE Antennas Wireless Propag. Lett.*, 2009, **8**, 653–656.
63 D. Zhao, T. Liu, J. G. Park, M. Zhang, J.-M. Chen and B. Wang, *Microelectron. Eng.*, 2012, **96**, 71–75.
64 N. S. Shabanov, A. K. Akhmedov, A. B. Isaev, A. Sh. Asvarov, K. Sh. Rabadanov and K. Kaviyarasu, *Mater. Today: Proc*, 2021, **36**, 263–267.
65 Y. Zhang, H. Li, X. Yang, T. Zhang, K. Zhu, W. Si, Z. Liu and H. Sun, *Polym. Compos.*, 2018, **39**, E671–E676.
66 K. Gnanasekaran, T. Heijmans, S. van Bennekom, H. Woldhuis, S. Wijnia, G. de With and H. Friedrich, *Appl. Mater. Today*, 2017, **9**, 21–28.
67 C. B. Sweeney, B. A. Lackey, M. J. Pospisil, T. C. Achee, V. K. Hicks, A. G. Moran, B. R. Teipel, M. A. Saed and M. J. Green, *Sci. Adv.*, 2017, **3**, e1700262.
68 G. Spinelli, R. Kotsilkova, E. Ivanov, I. Petrova-Doycheva, D. Menseidov, V. Georgiev, R. di Maio and C. Silvestre, *Nanomaterials*, 2019, **10**, 35.
69 G. Gonzalez, A. Chiappone, I. Roppolo, E. Fantino, V. Bertana, F. Perrucci, L. Scaltrito, F. Pirri and M. Sangermano, *Polymer*, 2017, **109**, 246–253.
70 S. Ushiba, S. Shoji, K. Masui, P. Kuray, J. Kono and S. Kawata, *Carbon*, 2013, **59**, 283–288.
71 D. Xiang, X. Zhang, Y. Li, E. Harkin-Jones, Y. Zheng, L. Wang, C. Zhao and P. Wang, *Composites, Part B*, 2019, **176**, 107250.
72 K. Kim, J. Park, J. Suh, M. Kim, Y. Jeong and I. Park, *Sens. Actuators, A*, 2017, **263**, 493–500.
73 M. Wajahat, S. Lee, J. H. Kim, W. S. Chang, J. Pyo, S. H. Cho and S. K. Seol, *ACS Appl. Mater. Interfaces*, 2018, **10**, 19999–20005.
74 A. Shimoni, S. Azoubel and S. Magdassi, *Nanoscale*, 2014, **6**, 11084–11089.
75 W. Yu, B. Q. Li, S. Ding and H. Liu, *J. Micromech. Microeng.*, 2018, **28**, 105014.
76 A. Kamyshny and S. Magdassi, *Chem. Soc. Rev.*, 2019, **48**, 1712–1740.
77 P. Blyweert, V. Nicolas, V. Fierro and A. Celzard, *Carbon*, 2021, **183**, 449–485.
78 S. B. Bakrani, F. Chabert, V. Nassiet and A. Cantarel, *Addit. Manuf.*, 2019, **25**, 112–121.
79 D. S. Udawattha, M. Narayana and U. P. L. Wijayarathne, *J. King Saud Univ., Sci.*, 2019, **31**, 412–426.
80 Y. Guo, H. S. Patanwala, B. Bognet and A. W. K. Ma, *Rapid Prototyp. J.*, 2017, **23**, 562–576.
81 J. E. Fromm, *IBM J. Res. Dev.*, 1984, **28**, 322–333.
82 N. Reis, C. Ainsley and B. Derby, *J. Appl. Phys.*, 2005, **97**, 094903.
83 B. J. de Gans, E. Kazancioglu, W. Meyer and U. S. Schubert, *Macromol. Rapid Commun.*, 2004, **25**, 292–296.
84 D. Jang, D. Kim and J. Moon, *Langmuir*, 2009, **25**, 2629–2635.
85 S. D. Hoath, S. Jung, W.-K. Hsiao and I. M. Hutchings, *Org. Electron.*, 2012, **13**, 3259–3262.
86 M. Wei, F. Zhang, W. Wang, P. Alexandridis, C. Zhou and G. Wu, *J. Power Sources*, 2017, **354**, 134–147.
87 J. Liang, K. Tong and Q. Pei, *Adv. Mater.*, 2016, **28**, 5986–5996.
88 P. C. Duineveld, M. M. de Kok, M. Buechel, A. Sempel, K. A. H. Mutsaers, P. van de Weijer, I. G. J. Camps, T. van de Biggelaar, J.-E. J. M. Rubingh and E. I. Haskal, in *Organic Light-Emitting Materials and Devices V*, SPIE, 2002, vol. 4464, p. 59.
89 C. Stow and M. Hadfield, *Proc. R. Soc. London, Ser. A*, 1981, **373**, 419–441.
90 H. Abdolmaleki, P. Kidmose and S. Agarwala, *Adv. Mater.*, 2021, **33**, 2006792.
91 N. J. Wilkinson, M. A. A. Smith, R. W. Kay and R. A. Harris, *Int. J. Adv. Manuf. Technol.*, 2019, **105**, 4599–4619.
92 A. Mahajan, C. D. Frisbie and L. F. Francis, *ACS Appl. Mater. Interfaces*, 2013, **5**, 4856–4864.
93 B. Avvaru, M. N. Patil, P. R. Gogate and A. B. Pandit, *Ultrasonics*, 2006, **44**, 146–158.
94 R. J. Lang, *J. Acoust. Soc. Am.*, 1962, **34**, 6–8.
95 R. Bellman and R. H. Pennington, *Q. Appl. Math.*, 1954, **12**, 151–162.
96 A. Dalmoro, A. A. Barba and M. D'Amore, *Sci. World J.*, 2013, **2013**, 482910.

97 A. A. Barba, M. d'Amore, S. Cascone, G. Lamberti and G. Titomanlio, *Chem. Eng. Process.*, 2009, **48**, 1477–1483.
98 K. A. Ramisetty, A. B. Pandit and P. R. Gogate, *Ultrason. Sonochem.*, 2013, **20**, 254–264.
99 Q. Huang and Y. Zhu, *Adv. Mater. Technol.*, 2019, **4**, 1800546.
100 R. Kumar and K. S. L. Prasad, *Ind. Eng. Chem. Process Des. Dev.*, 1971, **10**, 357–365.
101 L. Juslin, O. Antikainen, P. Merkku and J. Yliruusi, *Int. J. Pharm.*, 1995, **123**, 257–264.
102 J. U. Park, M. Hardy, S. J. Kang, K. Barton, K. Adair, D. K. Mukhopadhyay, C. Y. Lee, M. S. Strano, A. G. Alleyne, J. G. Georgiadis, P. M. Ferreira and J. A. Rogers, *Nat. Mater.*, 2007, **6**, 782–789.
103 Y. Han and J. Dong, *J. Micro Nano-Manuf.*, 2018, **6**, 040802.
104 C. Song, J. A. Rogers, J. M. Kim and H. Ahn, *Macromol. Res.*, 2015, **23**, 118–123.
105 J. Fernández de la Mora, *Annu. Rev. Fluid Mech.*, 2007, **39**, 217–243.
106 Z. Yin, Y. Huang, Y. Duan and H. Zhang, in *Electrohydrodynamic Direct-Writing for Flexible Electronic Manufacturing*, Springer Singapore, Singapore, 2018, pp. 89–116.
107 L. Mu, C. Jiang, J. Wang, H. Zheng, L. Ying, M. Xu, J. Wang, J. Peng and Y. Cao, *SID Symp. Dig. Tech. Pap.*, 2020, **51**, 485–488.
108 D. R. Chen and D. Y. H. Pui, *Aerosol Sci. Technol.*, 1997, **27**, 367–380.
109 A. M. Gañan-Calvo, *J. Aerosol Sci.*, 1994, **25**, 309–310.
110 J. Fernandez De La Mora, J. Navascues, F. Fernandez and J. Rosell-Llompart, *J. Aerosol Sci.*, 1990, **21**, S673–S676.
111 J. Bae, J. Lee and S. H. Kim, *J. Appl. Polym. Sci.*, 2017, **134**, 45044.
112 K. Tang and A. Gomez, *J. Colloid Interface Sci.*, 1996, **184**, 500–511.
113 J. Zeleny, *Proc. Cambridge Philos. Soc.*, 1915, 71–83.
114 S. N. Jayasinghe and M. J. Edirisinghe, *J. Aerosol Sci.*, 2002, **33**, 1379–1388.
115 M. Yu, K. H. Ahn and S. J. Lee, *Mater. Des.*, 2016, **89**, 109–115.
116 M. Cloupeau and B. Prunet-Foch, *J. Electrost.*, 1989, **22**, 135–159.
117 S. N. Jayasinghe and M. J. Edirisinghe, *Appl. Phys. Lett.*, 2004, **85**, 4243–4245.
118 A. Lee, H. Jin, H. W. Dang, K. H. Choi and K. H. Ahn, *Langmuir*, 2013, **29**, 13630–13639.
119 S. D. Hoath, W.-K. Hsiao and S. Jung, in *NIP & Digital Fabrication Conference*, Cambridge, MA, USA, 2014, pp. 299–303.
120 J. Ding, P. J. Tracey, W. Li, G. Peng, P. G. Whitten, J. Ding, P. Tracey, W. Li, G. Peng, P. G. Whitten and G. G. Wallace, *Text. Light Ind. Sci. Technol.*, 2013, **2**, 161–173.
121 S. Gürgen, M. C. Kuşhan and W. Li, *Prog. Polym. Sci.*, 2017, **75**, 48–72.
122 S. Naficy, R. Jalili, S. H. Aboutalebi, R. A. Gorkin, K. Konstantinov, P. C. Innis, G. M. Spinks, P. Poulin and G. G. Wallace, *Mater. Horiz.*, 2014, **1**, 326–331.
123 C. Vallés, R. J. Young, D. J. Lomax and I. A. Kinloch, *J. Mater. Sci.*, 2014, **49**, 6311–6320.
124 C. L. Barrie, P. C. Griffiths, R. J. Abbott, I. Grillo, E. Kudryashov and C. Smyth, *J. Colloid Interface Sci.*, 2004, **272**, 210–217.
125 L. Dybowska-Sarapuk, K. Kielbasinski, A. Arazna, K. Futera, A. Skalski, D. Janczak, M. Sloma and M. Jakubowska, *Nanomaterials*, 2018, **8**, 602.
126 K. Fu, Y. Wang, C. Yan, Y. Yao, Y. Chen, J. Dai, S. Lacey, Y. Wang, J. Wan, T. Li, Z. Wang, Y. Xu and L. Hu, *Adv. Mater.*, 2016, **28**, 2587–2594.
127 Y. Liu, Q. Zhang and R. Liu, *Rheol. Acta*, 2021, **60**, 763–774.
128 Z. An, Y. Zhang, Q. Li, H. Wang, Z. Guo and J. Zhu, *Powder Technol.*, 2018, **328**, 199–206.
129 S. T. Knauert, J. F. Douglas and F. W. Starr, *J. Polym. Sci., Part B: Polym. Phys.*, 2007, **45**, 1882–1897.
130 A. N. Omrani, E. Esmaeilzadeh, M. Jafari and A. Behzadmehr, *Diamond Relat. Mater.*, 2019, **93**, 96–104.
131 T. Yokozeki, S. C. Schulz, S. T. Buschhorn and K. Schulte, *Eur. Polym. J.*, 2012, **48**, 1042–1049.
132 P. Pötschke, T. D. Fornes and D. R. Paul, *Polymer*, 2002, **43**, 3247–3255.
133 A. Y. Malkin, S. O. Ilyin, M. P. Arinina and V. G. Kulichikhin, *Colloid Polym. Sci.*, 2017, **295**, 555–563.
134 K. Sun, T.-S. Wei, B. Y. Ahn, J. Y. Seo, S. J. Dillon and J. A. Lewis, *Adv. Mater.*, 2013, **25**, 4539–4543.
135 Y. Rho, K.-T. Kang and D. Lee, *Nanoscale*, 2016, **8**, 8976–8985.
136 L. Alves, E. Ferraz, A. F. Lourenço, P. J. Ferreira, M. G. Rasteiro and J. A. F. Gamelas, *Carbohydr. Polym.*, 2020, **237**, 116109.
137 R. Karyappa and M. Hashimoto, *Sci. Rep.*, 2019, **9**, 14178.
138 P. Lopez-Sanchez, J. Nijsse, H. C. G. Blonk, L. Bialek, S. Schumm and M. Langton, *J. Sci. Food Agric.*, 2011, **91**, 207–217.
139 J. Moon, J. E. Grau, V. Knezevic, M. J. Cima and E. M. Sachs, *J. Am. Ceram. Soc.*, 2002, **85**, 755–762.
140 R. P. Tortorich and J. W. Choi, *Nanomaterials*, 2013, **3**, 453–468.
141 M. H. U. Bhuiyan, R. Saidur, M. A. Amalina, R. M. Mostafizur and A. K. M. S. Islam, in *Procedia Engineering*, Elsevier Ltd, 2015, vol. 105, pp. 431–437.
142 S. Tanvir and L. Qiao, *Nanoscale Res. Lett.*, 2012, **7**, 226.
143 S. S. Khaleduzzaman, I. M. Mahbubul, I. M. Shahrul and R. Saidur, *Int. Commun. Heat Mass Transfer*, 2013, **49**, 110–114.
144 S. Vafaei, A. Purkayastha, A. Jain, G. Ramanath and T. Borca-Tasciuc, *Nanotechnology*, 2009, **20**, 185702.
145 L. Jiang, S. Li, W. Yu, J. Wang, Q. Sun and Z. Li, *Colloids Surf., A*, 2016, **488**, 20–27.
146 W. Sempels, R. de Dier, H. Mizuno, J. Hofkens and J. Vermant, *Nat. Commun.*, 2013, **4**, 1757.

147 L. Sun, K. Yang, Z. Lin, X. Zhou, Y. Zhang and T. Guo, *Ceram. Int.*, 2018, **44**, 10735–10743.
148 J. Yan, G. Zou, A. Wu, J. Ren, A. Hu and Y. N. Zhou, *J. Electron. Mater.*, 2012, **41**, 1924–1930.
149 Z. Huang, Y. Tang, H. Guo, X. Feng, T. Zhang, P. Li, B. Qian and Y. Xie, *Ceram. Int.*, 2020, **46**, 10096–10104.
150 J. Vaithilingam, E. Saleh, L. Körner, R. D. Wildman, R. J. M. Hague, R. K. Leach and C. J. Tuck, *Mater. Des.*, 2018, **139**, 81–88.
151 Y. Zhang, X. Chen, F. Liu, L. Li, J. Dai and T. Liu, *Adv. Condens. Matter Phys.*, 2018, **2018**, 1–9.
152 R. Dou and B. Derby, *Langmuir*, 2012, **28**, 5331–5338.
153 D. Mampallil and H. B. Eral, *Adv. Colloid Interface Sci.*, 2018, **252**, 38–54.
154 L. Cui, J. Zhang, X. Zhang, Y. Li, Z. Wang, H. Gao, T. Wang, S. Zhu, H. Yu and B. Yang, *Soft Matter*, 2012, **8**, 10448.
155 D. Mampallil, J. Reboud, R. Wilson, D. Wylie, D. R. Klug and J. M. Cooper, *Soft Matter*, 2015, **11**, 7207–7213.
156 V. D. Ta, R. M. Carter, E. Esenturk, C. Connaughton, T. J. Wasley, J. Li, R. W. Kay, J. Stringer, P. J. Smith and J. D. Shephard, *Soft Matter*, 2016, **12**, 4530–4536.
157 Y. Oh, J. Kim, Y. J. Yoon, H. Kim, H. G. Yoon, S. N. Lee and J. Kim, *Curr. Appl. Phys.*, 2011, **11**, S359–S363.
158 P. J. Yunker, T. Still, M. A. Lohr and A. G. Yodh, *Nature*, 2011, **476**, 308–311.
159 J. Li, M. C. Lemme and M. Östling, *ChemPhysChem*, 2014, **15**, 3427–3434.
160 X. Shen, C. M. Ho and T. S. Wong, *J. Phys. Chem. B*, 2010, **114**, 5269–5274.
161 Z. Zhan, J. An, Y. Wei, V. T. Tran and H. Du, *Nanoscale*, 2017, **9**, 965–993.
162 M. Mionić, K. Pataky, R. Gaal, A. Magrez, J. Brugger and L. Forró, *J. Mater. Chem.*, 2012, **22**, 14030–14034.
163 T. Kajiya, W. Kobayashi, T. Okuzono and M. Doi, *Langmuir*, 2010, **26**, 10429–10432.
164 B. J. Perelaer, A. W. M. de Laat, C. E. Hendriks and U. S. Schubert, *J. Mater. Chem.*, 2008, **18**, 3209.
165 M. Zenou, O. Ermak, A. Saar and Z. Kotler, *J. Phys. D: Appl. Phys.*, 2014, **47**, 025501.
166 J. Chung, N. R. Bieri, S. Ko, C. P. Grigoropoulos and D. Poulikakos, *Appl. Phys. A: Mater. Sci. Process.*, 2004, **79**, 1259–1261, Springer Verlag.
167 S. Hong, J. Yeo, G. Kim, D. Kim, H. Lee, J. Kwon, H. Lee, P. Lee and S. H. Ko, *ACS Nano*, 2013, **7**, 5024–5031.
168 O. A. Yeshchenko, I. M. Dmitruk, A. A. Alexeenko and A. v. Kotko, *Nanotechnology*, 2010, **21**, 045203.
169 X. Yang, W. He, S. Wang, G. Zhou, Y. Tang and J. Yang, *J. Mater. Sci.: Mater. Electron.*, 2012, **23**, 1980–1986.
170 K. J. Rao, B. Vaidhyanathan, M. Ganguli and P. A. Ramakrishnan, *Chem. Mater.*, 1999, **11**, 882–895.
171 F. M. Wolf, J. Perelaer, S. Stumpf, D. Bollen, F. Kriebel and U. S. Schubert, *J. Mater. Res.*, 2013, **28**, 1254–1261.
172 M. L. Allen, M. Aronniemi, T. Mattila, A. Alastalo, K. Ojanperä, M. Suhonen and H. Seppä, *Nanotechnology*, 2008, **19**, 175201.
173 L. Hu, D. S. Hecht and G. Grüner, *Chem. Rev.*, 2010, **110**, 5790–5844.
174 B. Chen, Y. Jiang, X. Tang, Y. Pan and S. Hu, *ACS Appl. Mater. Interfaces*, 2017, **9**, 28433–28440.
175 Y. Li, T. Gao, Z. Yang, C. Chen, W. Luo, J. Song, E. Hitz, C. Jia, Y. Zhou, B. Liu, B. Yang and L. Hu, *Adv. Mater.*, 2017, **29**, 1700981.
176 V. Kuzmenko, E. Karabulut, E. Pernevik, P. Enoksson and P. Gatenholm, *Carbohydr. Polym.*, 2018, **189**, 22–30.
177 G. Spinelli, P. Lamberti, V. Tucci, R. Kotsilkova, S. Tabakova, R. Ivanova, P. Angelova, V. Angelov, E. Ivanov, R. di Maio, C. Silvestre, D. Meisak, A. Paddubskaya and P. Kuzhir, *Materials*, 2018, **11**, 2256.
178 L. Chen, H. Xie, W. Yu and Y. Li, *J. Dispersion Sci. Technol.*, 2011, **32**, 550–554.
179 B. Ruan and A. M. Jacobi, *Nanoscale Res. Lett.*, 2012, **7**, 127.
180 J. Zhao, Y. Yu, B. Weng, W. Zhang, A. T. Harris, A. I. Minett, Z. Yue, X.-F. Huang and J. Chen, *Electrochem. Commun.*, 2013, **37**, 32–35.
181 M. S. Arnold, A. A. Green, J. F. Hulvat, S. I. Stupp and M. C. Hersam, *Nat. Nanotechnol.*, 2006, **1**, 60–65.
182 M. S. Ata and I. Zhitomirsky, *J. Colloid Interface Sci.*, 2015, **454**, 27–34.
183 W. Wenseleers, I. L. Vlasov, E. Goovaerts, E. D. Obraztsova, A. S. Lobach and A. Bouwen, *Adv. Funct. Mater.*, 2004, **14**, 1105–1112.
184 Y. Su and I. Zhitomirsky, *J. Colloid Interface Sci.*, 2013, **399**, 46–53.
185 S. S. Chen, H. R. Zhang and I. Todd, *Scr. Mater.*, 2014, **72–73**, 47–50.
186 S. Wang, T. Song, H. Qi and Z. Xiang, *Chem. Eng. J.*, 2021, **419**, 129602.
187 B. Dan, G. C. Irvin and M. Pasquali, *ACS Nano*, 2009, **3**, 835–843.
188 S. R. Raghavan, G. Fritz and E. W. Kaler, *Langmuir*, 2002, **18**, 3797–3803.
189 Z. Lin, J. J. Cai, L. E. Scriven and H. T. Davis, *J. Phys. Chem.*, 1994, **98**, 5984–5993.
190 H. Menon, R. Aiswarya and K. P. Surendran, *RSC Adv.*, 2017, **7**, 44076–44081.
191 X. Liang, H. Li, J. Dou, Q. Wang, W. He, C. Wang, D. Li, J. Lin and Y. Zhang, *Adv. Mater.*, 2020, **32**, 2000165.
192 J. N. Israelachvili, *Intermolecular and surface forces*, Academic Press, 3rd edn, 2011.
193 O. v. Kharissova, B. I. Kharisov and E. G. de Casas Ortiz, *RSC Adv.*, 2013, **3**, 24812.
194 L. Lavagna, R. Nisticò, S. Musso and M. Pavese, *Mater. Today Chem.*, 2021, **20**, 100477.
195 S. Giordani, S. D. Bergin, V. Nicolosi, S. Lebedkin, M. M. Kappes, W. J. Blau and J. N. Coleman, *J. Phys. Chem. B*, 2006, **110**, 15708–15718.
196 M. W. Forney and J. C. Poler, *J. Phys. Chem. C*, 2011, **115**, 10531–10536.
197 K. D. Ausman, R. Piner, O. Lourie, R. S. Ruoff and M. Korobov, *J. Phys. Chem. B*, 2000, **104**, 8911–8915.

198 V. A. Davis, L. M. Ericson, A. N. G. Parra-Vasquez, H. Fan, Y. Wang, V. Prieto, J. A. Longoria, S. Ramesh, R. K. Saini, C. Kittrell, W. E. Billups, W. W. Adams, R. H. Hauge, R. E. Smalley and M. Pasquali, *Macromolecules*, 2004, **37**, 154–160.
199 S. Ramesh, L. M. Ericson, V. A. Davis, R. K. Saini, C. Kittrell, M. Pasquali, W. E. Billups, W. W. Adams, R. H. Hauge and R. E. Smalley, *J. Phys. Chem. B*, 2004, **108**, 8794–8798.
200 S. D. Bergin, Z. Sun, P. Streich, J. Hamilton and J. N. Coleman, *J. Phys. Chem. C*, 2010, **114**, 231–237.
201 Z. Sun, V. Nicolosi, D. Rickard, S. D. Bergin, D. Aherne and J. N. Coleman, *J. Phys. Chem. C*, 2008, **112**, 10692–10699.
202 J. Lee, D. R. Hwang, J. Hong, D. Jung and S. E. Shim, *J. Dispersion Sci. Technol.*, 2010, **31**, 1230–1235.
203 P. S. Goh, A. F. Ismail, M. Aziz, M. Rusop and T. Soga, in *AIP Conference Proceedings*, AIP, 2009, pp. 224–228.
204 Y. Kwon, B. Yim, J. Kim and J. Kim, *Microelectron. Reliab.*, 2011, **51**, 812–818.
205 D. Yan, F. Wang, Y. Zhao, J. Liu, J. Wang, L. Zhang, K. C. Park and M. Endo, *Mater. Lett.*, 2009, **63**, 171–173.
206 H. Li, J. C. Nie and S. Kunsági-Máté, *Chem. Phys. Lett.*, 2010, **492**, 258–262.
207 S. Roh, J. Lee, M. Jang, M. Shin, J. Ahn, T. Park and W. Yi, *J. Nanomater.*, 2010, **2010**, 1–6.
208 P.-C. Ma, S.-Y. Mo, B.-Z. Tang and J.-K. Kim, *Carbon*, 2010, **48**, 1824–1834.
209 P. Yadav, S. M. Gupta and S. K. Sharma, *J. Therm. Anal. Calorim.*, 2022, **147**, 6537–6561.
210 Y. Xu, X. Wang, R. Tian, S. Li, L. Wan, M. Li, H. You, Q. Li and S. Wang, *Appl. Surf. Sci.*, 2008, **254**, 2431–2435.
211 M. E. Sullivan, D. Klosterman and G. R. Palmese, *Nucl. Instrum. Methods Phys. Res., Sect. B*, 2007, **265**, 352–355.
212 C.-H. Tseng, C.-C. Wang and C.-Y. Chen, *Chem. Mater.*, 2007, **19**, 308–315.
213 C.-H. Jung, D.-K. Kim and J.-H. Choi, *Curr. Appl. Phys.*, 2009, **9**, S85–S87.
214 L. Lin, H. Peng and G. Ding, *Appl. Therm. Eng.*, 2015, **91**, 163–171.
215 I. W. Almanassra, A. D. Manasrah, U. A. Al-Mubaiyedh, T. Al-Ansari, Z. O. Malaibari and M. A. Atieh, *J. Mol. Liq.*, 2020, **304**, 111025.
216 A. Uthaman, H. M. Lal, C. Li, G. Xian and S. Thomas, *Nanomaterials*, 2021, **11**, 1234.
217 R. Rastogi, R. Kaushal, S. K. Tripathi, A. L. Sharma, I. Kaur and L. M. Bharadwaj, *J. Colloid Interface Sci.*, 2008, **328**, 421–428.
218 K. A. S. Fernando, Y. Lin, W. Wang, S. Kumar, B. Zhou, S.-Y. Xie, L. T. Cureton and Y.-P. Sun, *J. Am. Chem. Soc.*, 2004, **126**, 38.
219 C.-Y. Hu, Y.-J. Xu, S.-W. Duo, R.-F. Zhang and M.-S. Li, *J. Chin. Chem. Soc.*, 2009, **56**, 234–239.
220 S. Meuer, L. Braun, T. Schilling and R. Zentel, *Polymer*, 2009, **50**, 154–160.
221 M. Kühnast, C. Tschierske and J. Lagerwall, *Chem. Commun.*, 2010, **46**, 6989–6991.
222 C. Lechner and A. F. Sax, *Appl. Surf. Sci.*, 2017, **420**, 606–617.
223 B. I. Kharisov, O. v. Kharissova and A. V. Dimas, *RSC Adv.*, 2016, **6**, 68760–68787.
224 E. E. Tkalya, M. Ghislandi, G. de With and C. E. Koning, *Curr. Opin. Colloid Interface Sci.*, 2012, **17**, 225–232.
225 S. M. Fatemi and M. Foroutan, *J. Iran. Chem. Soc.*, 2015, **12**, 1905–1913.
226 Y. Bai, D. Lin, F. Wu, Z. Wang and B. Xing, *Chemosphere*, 2010, **79**, 362–367.
227 P. Randhawa, J.-S. Park, S. Sharma, P. Kumar, M.-S. Shin and S. S. Sekhon, *J. Nanoelectron. Optoelectron.*, 2012, **7**, 279–286.
228 H. van Nguyen, N. M. Tun and E. G. Rakov, *Russ. J. Inorg. Chem.*, 2015, **60**, 536–540.
229 C. Biswas, K. K. Kim, H. Z. Geng, H. K. Park, S. C. Lim, S. J. Chae, S. M. Kim, Y. H. Lee, M. Nayhouse and M. Yun, *J. Phys. Chem. C*, 2009, **113**, 10044–10051.
230 X. Li, Y. Zhang, L. Jing and X. He, *Chem. Eng. J.*, 2016, **292**, 326–339.
231 E. Karpushkin, A. Berkovich and V. Sergeyev, *Macromol. Symp.*, 2015, **348**, 63–67.
232 S. A. Ntim, O. Sae-Khow, F. A. Witzmann and S. Mitra, *J. Colloid Interface Sci.*, 2011, **355**, 383–388.
233 J. Liu, O. Bibari, P. Mailley, J. Dijon, E. Rouvière, F. Sauter-Starace, P. Caillat, F. Vinet and G. Marchand, *New J. Chem.*, 2009, **33**, 1017–1024.
234 M. Horie, M. Stowe, M. Tabei, H. Kato, A. Nakamura, S. Endoh, Y. Morimoto and K. Fujita, *Toxicol. Mech. Methods*, 2013, **23**, 315–322.
235 H. Y. Lee and B. S. Kim, *Biosens. Bioelectron.*, 2009, **25**, 587–591.
236 L. Vaisman, H. D. Wagner and G. Marom, *Adv. Colloid Interface Sci.*, 2006, **128–130**, 37–46.
237 G. Ciofani, V. Raffa, V. Pensabene, A. Menciassi and P. Dario, *Fullerenes, Nanotubes, Carbon Nanostruct.*, 2009, **17**, 11–25.
238 J. Pang, G. Xu, Y. Tan and F. He, *Colloid Polym. Sci.*, 2010, **288**, 1665–1675.
239 P. Keinänen, S. Siljander, M. Koivula, J. Sethi, E. Sarlin, J. Vuorinen and M. Kanerva, *Heliyon*, 2018, **4**, e00787.
240 A. J. Blanch, C. E. Lenehan and J. S. Quinton, *J. Phys. Chem. B*, 2010, **114**, 9805–9811.
241 M. Zhang, L. Su and L. Mao, *Carbon*, 2006, **44**, 276–283.
242 K. Singh, S. K. Sharma and S. M. Gupta, *Integr. Ferroelectr.*, 2020, **204**, 11–22.
243 W. H. Duan, Q. Wang and F. Collins, *Chem. Sci.*, 2011, **2**, 1407.
244 Babita, S. K. Sharma and S. M. Gupta, *Mater. Res. Express*, 2018, **5**, 055511.
245 M. Youssry, M. Al-Ruwaidhi, M. Zakeri and M. Zakeri, *Emergent Mater.*, 2020, **3**, 25–32.
246 K. Yang, Z. Yi, Q. Jing, R. Yue, W. Jiang and D. Lin, *Chin. Sci. Bull.*, 2013, **58**, 2082–2090.

247 M. Abedi, R. Fangueiro and A. G. Correia, *J. Nanomater.*, 2020, **2020**, 1–20.
248 M. F. Islam, E. Rojas, D. M. Bergey, A. T. Johnson and A. G. Yodh, *Nano Lett.*, 2003, **3**, 269–273.
249 B. Han and X. Yu, *Front. Mater.*, 2014, **1**, 27.
250 H. K. F. Cheng, Y. Pan, N. G. Sahoo, K. Chong, L. Li, S. H. Chan and J. Zhao, *J. Appl. Polym. Sci.*, 2012, **124**, 1117–1127.
251 H. Jung, J. S. Yu, H. P. Lee, J. M. Kim, J. Y. Park and D. Kim, *Carbon*, 2013, **52**, 259–266.
252 H.-S. Kim, W.-I. Park, M. Kang and H.-J. Jin, *J. Phys. Chem. Solids*, 2008, **69**, 1209–1212.
253 M. Calvaresi, M. Dallavalle and F. Zerbetto, *Small*, 2009, **5**, 2191–2198.
254 X. Zhang, H.-J. Sue and R. Nishimura, *Carbon*, 2013, **56**, 374–382.
255 Kim and H. Li, in *Carbon Nanotubes - From Research to Applications*, InTech, 2011.
256 L. Dong, K. L. Joseph, C. M. Witkowski and M. M. Craig, *Nanotechnology*, 2008, **19**, 255702.
257 S. M. Fatemi and M. Foroutan, *J. Nanostruct. Chem.*, 2016, **6**, 29–40.
258 B. Suárez, B. M. Simonet, S. Cárdenas and M. Valcárcel, *Electrophoresis*, 2007, **28**, 1714–1722.
259 N. Poorgholami-Bejarpasi and B. Sohrabi, *Fluid Phase Equilib.*, 2015, **394**, 19–28.
260 P. Castell, M. Cano, W. K. Maser and A. M. Benito, *Compos. Sci. Technol.*, 2013, **80**, 101–107.
261 M. Miao, in *Carbon Nanotube Fibers and Yarns*, Elsevier, 2020, pp. 61–69.
262 B. K. Ryglowski, R. D. Pollak and Y. W. Kwon, in *ASME 2010 Pressure Vessels and Piping Conference: Volume 9*, ASMEDC, 2010, pp. 221–230.
263 J. Wang and Y. Li, *J. Am. Chem. Soc.*, 2009, **131**, 5364–5365.
264 C. Li, A. Schäffer, H. Vereecken, M. Heggen, R. Ji and E. Klumpp, *J. Environ. Sci.*, 2013, **25**, 466–472.
265 Y. Bai, I. S. Park, S. J. Lee, T. S. Bae, F. Watari, M. Uo and M. H. Lee, *Carbon*, 2011, **49**, 3663–3671.
266 A. Yadav, N. Bagotia, S. Yadav, A. K. Sharma and S. Kumar, *Sep. Purif. Technol.*, 2022, **284**, 120262.
267 Q. Wang, Y. Han, Y. Wang, Y. Qin and Z.-X. Guo, *J. Phys. Chem. B*, 2008, **112**, 7227–7233.
268 I. Madni, C.-Y. Hwang, S.-D. Park, Y.-H. Choa and H.-T. Kim, *Colloids Surf., A*, 2010, **358**, 101–107.
269 R. M. F. Fernandes, B. Abreu, B. Claro, M. Buzaglo, O. Regev, I. Furó and E. F. Marques, *Langmuir*, 2015, **31**, 10955–10965.
270 A. Yousefi, S. Javadian, M. Sharifi, N. Dalir and A. Motaee, *J. Bio-, Tribo-Corros.*, 2019, **5**, 82.
271 F. Lu, S. Zhang and L. Zheng, *J. Mol. Liq.*, 2012, **173**, 42–46.
272 H. Kim, H.-S. Kim, H. S. Lee, I.-J. Chin and H.-J. Jin, *J. Nanosci. Nanotechnol.*, 2008, **8**, 5543–5546.
273 M. Kang and H.-J. Jin, *Colloid Polym. Sci.*, 2007, **285**, 1163–1167.
274 J. Ren, Y. Liu, D. L. Kaplan and S. Ling, *MRS Bull.*, 2019, **44**, 53–58.
275 M. Ohadi, P. Rezaei, M. Mehrabani, B. Behnam and M. Ansari, *J. Cluster Sci.*, 2022, **33**, 975–984.
276 K. N. H. Priya, C. S. Meghana, K. R. Neha, S. P. Shilpa, M. R. Yashaswini and C. Manjunatha, *ECS Trans.*, 2022, **107**, 11261–11275.
277 J. Zhao, Z. Wang, H. Mashayekhi, P. Mayer, B. Chefetz and B. Xing, *Environ. Sci. Technol.*, 2012, **46**, 5369–5377.
278 K. Shah, D. Vasileva, A. Karadaghy and S. P. Zustiak, *J. Mater. Chem. B*, 2015, **3**, 7950–7962.
279 Z. Lin, T. Le, X. Song, Y. Yao, Z. Li, K. Moon, M. M. Tentzeris and C. Wong, *J. Electron. Packag.*, 2013, **135**, 011001.
280 N. Berrada, S. Hamze, A. Desforges, J. Ghanbaja, J. Gleize, T. Maré, B. Vigolo and P. Estellé, *J. Mol. Liq.*, 2019, **293**, 111473.
281 Z. Abbas, C. Labbez, S. Nordholm and E. Ahlberg, *J. Phys. Chem. C*, 2008, **112**, 5715–5723.
282 M. Das, M. Sarkar, A. Datta and A. K. Santra, *Fuel*, 2018, **220**, 769–779.
283 N. Sinha and J. K. Singh, *J. Mol. Liq.*, 2017, **246**, 244–250.
284 B. Hajra, M. Kumar, A. K. Pathak and C. Guria, *Fuel*, 2016, **166**, 130–142.
285 D. Mei, Y. Fang, Z. Zhang, D. Guo, Z. Chen and C. Sun, *Powder Technol.*, 2021, **388**, 526–536.
286 B. Zhao, V. S. Sivasankar, A. Dasgupta and S. Das, *ACS Appl. Mater. Interfaces*, 2021, **13**, 10257–10270.
287 Y. Zhang, Y. Cui, S. Wang, X. Zhao, F. Wang and G. Wu, *Mater. Lett.*, 2020, **267**, 127547.
288 F. Qi, N. Chen and Q. Wang, *Mater. Des.*, 2018, **143**, 72–80.
289 B. Duan, Y. Zhou, D. Wang and Y. Zhao, *J. Alloys Compd.*, 2019, **771**, 498–504.
290 S. C. Zhang, W. G. Fahrenholtz, G. E. Hilmas and E. J. Yadlowsky, *J. Eur. Ceram. Soc.*, 2010, **30**, 1373–1380.
291 S. Yuan, J. Bai, C. K. Chua, J. Wei and K. Zhou, *Polymers*, 2016, **8**, 370.
292 A. Denneulin, J. Bras, F. Carcone, C. Neuman and A. Blayo, *Carbon*, 2011, **49**, 2603–2614.
293 D. Soltman and V. Subramanian, *Langmuir*, 2008, **24**, 2224–2231.
294 H. Hu and R. G. Larson, *Langmuir*, 2005, **21**, 3963–3971.
295 H. Hu and R. G. Larson, *Langmuir*, 2005, **21**, 3972–3980.
296 H. Hu and R. G. Larson, *J. Phys. Chem. B*, 2006, **110**, 7090–7094.
297 S. Pegel, P. Pötschke, G. Petzold, I. Alig, S. M. Dudkin and D. Lellinger, *Polymer*, 2008, **49**, 974–984.
298 S. W. Kim, T. Kim, Y. S. Kim, H. S. Choi, H. J. Lim, S. J. Yang and C. R. Park, *Carbon*, 2012, **50**, 3–33.
299 K. K. Kim, S. M. Yoon, J. Y. Choi, J. Lee, B. K. Kim, J. M. Kim, J. H. Lee, U. Paik, M. H. Park, C. W. Yang,

K. H. An, Y. Chung and Y. H. Lee, *Adv. Funct. Mater.*, 2007, **17**, 1775–1783.
300 C. Richard, F. Balavoine, P. Schultz, T. W. Ebbesen and C. Mioskowski, *Science*, 2003, **300**, 775–778.
301 O. Matarredona, H. Rhoads, Z. Li, J. H. Harwell, L. Balzano and D. E. Resasco, *J. Phys. Chem. B*, 2003, **107**, 13357–13367.
302 S. C. Lim, D. S. Lee, K. K. Kim, Y. C. Choi, H. S. Kim, J. H. Lee, U. Paik and Y. H. Lee, *Jpn. J. Appl. Phys.*, 2009, **48**, 111601.
303 T. Mori and K. Tanaka, *Acta Metall.*, 1973, **21**, 571–574.
304 N. de Jonge and F. M. Ross, *Nat. Nanotechnol.*, 2011, **6**, 695–704.